JPL Quarterly Technical Review

Volume 2 January 1973 Number 4

Papers on:

Bioengineering
Chemistry
Civil Systems
Computer Applications
Electronics
Environmental Sciences
Industrial Processes
Optics
Pyrotechnics
Telecommunications

Abstracts of:

Technical Reports
Technical Memorandums
JPL Quarterly Technical Review
Open Literature Reporting

Jet Propulsion Laboratory/California Institute of Technology

JPL Quarterly Technical Review
Volume 2, Number 4

Jet Propulsion Laboratory
California Institute of Technology
4800 Oak Grove Drive
Pasadena, California 91103

Prepared Under Contract NAS 7-100
National Aeronautics and Space Administration

First Class
Permit No. 2376
Pasadena, Ca.

Business Reply Mail No Postage Necessary If Mailed In U.S.A.

Postage Will Be Paid By

JET PROPULSION LABORATORY
CALIFORNIA INSTITUTE OF TECHNOLOGY
4800 Oak Grove Drive
Pasadena, California 91103

Attention: Manager, Technical Information and
Documentation Division Support Section 651

JPL Quarterly Technical Review

Volume 2 January 1973 Number 4

THIS CARD MAY BE USED TO ORDER (1) A REPRINT OF AN ARTICLE PUBLISHED IN THE "PAPERS" SECTION, OR (2) A COPY OF A JPL-PUBLISHED DOCUMENT REFERENCED IN THE "ABSTRACTS" SECTION. THE OPEN LITERATURE (e.g., JOURNAL) REPORTING REFERENCED IN THE ABSTRACTS SECTION IS NOT AVAILABLE FROM JPL AND IS THEREFORE NOT LISTED ON THIS CARD.

TO ORDER, ENCIRCLE THE APPROPRIATE PAGE OR ENTRY NUMBERS AND SUPPLY THE FOLLOWING INFORMATION:

NAME: _____

ORGANIZATION: _____

ADDRESS: _____
STREET

_____
CITY STATE ZIP

FROM THE "PAPERS" SECTION

pp. 1-6
pp. 7-17
pp. 18-28
pp. 29-37
pp. 38-43
pp. 44-52
pp. 53-61
pp. 62-71
pp. 72-86
pp. 87-92

FROM THE "ABSTRACTS" SECTION (BIBLIOGRAPHY OF CURRENT REPORTING)

A02	E01	H01	L08	M16	R09	W06
A03	E02	H03	L09	M17	R10	Y01
A04	E04	H04	L10	M18	R11	Y03
A05	E05	H08	L11	M19	S08	Z02
B03	E07	H09	L12	M22	S09	
B04	F01	H12	L13	M25	S10	
B05	F03	H13	L15	N01	S14	
B06	F06	J01	L16	O04	S16	
B07	F08	K01	L19	P01	S18	
B13	F11	K02	M01	P03	S21	
C04	G01	K05	M05	R02	S24	
C05	G02	K08	M07	R03	T01	
C07	G05	L04	M10	R04	V01	
D01	G08	L05	M11	R05	V02	
D02	G09	L06	M13	R06	W04	
D03	G11	L07	M14	R08	W05	

JPL Quarterly Technical Review

Volume 2 January 1973 Number 4

Contents

1 **Lipid-Absorbing Polymers**

H. E. Marsh, Jr., and C. J. Wallace

7 **Unified Approach to the Biomechanics of Dental Implantology**

D. E. Grenoble and A. C. Knoell

18 **Thermoluminescence: Potential Applications in Forensic Science**

J. D. Ingham and D. D. Lawson

29 **A High-Efficiency, Small, Solid-State Laser for Pyrotechnic Ignition**

L. C. Yang and V. J. Menichelli

38 **Generation of Narrow High Current Pulses**

V. J. Menichelli and L. A. Rosenthal

44 **Development of a Thick-Film Silicon Ribbon Growth Technique for Application to Large-Area Solar Cells and Arrays**

P. A. Berman

53 **Information Management System for the California State Water Resources Control Board (SWRCB)**

T. C. Heald and G. H. Redmann

62 **On the Feasibility of Efficient Multiamplitude Communication**

J. G. Smith

72 **Helicopter Visual Aid System**

R. L. Baisley

87 **The Mesa Arizona Pupil Tracking System**

D. L. Wright

Bibliography of Current Reporting

94 **Author Index With Abstracts**

170 **Subject Index**

184 **Publication Index**

JPL Quarterly Technical Review Volume 2 Number 4 January 1973

Index: biology, chemistry

Lipid-Absorbing Polymers

H. E. Marsh, Jr. and C. J. Wallace

Propulsion Division

Present medicinal approaches to cholesterol reduction are indirect. They employ ion exchange to bind bile acids (which are derived from cholesterol by the liver) so that they will be eliminated instead of assimilated.

New polymers have been made that have the unusual property of being capable of absorbing both water and oils. As a result of this property, they are able to absorb lipids from micellar solutions. Lipid absorptions from model bile solution as high as 10% (based on dry polymer weight) in 5 min and 59% at equilibrium have been measured. The presence of significant amounts of cholesterol, as well as of bile acid, in the absorbed lipids has been confirmed by thin layer chromatography.

Introduction

Present medicinal approaches to reducing serum and tissue cholesterol levels in man are indirect. Intestinal reabsorption of bile acids, which are liver-produced derivatives of cholesterol, is reduced by administration of nonabsorbable bile acid-binding polymers. The binding is accomplished by means of ion exchange on polymers bearing amine groups. For example, materials under study include various primary, secondary, and tertiary ethylamine adducts of cellulose and other polysaccharides (Refs. 1,2), a copolymer of tetraethylene pentamine and epichlorohydrin (Ref. 3), and a quaternary ammonium styrene-divinylbenzene copolymer. The last polymer, known as Cholestyramine, has been in use medically for a number of years.

The approach of the JPL work is different in two ways. It aims at removing not only bile acids but also cholesterol itself. The operating mechanism is absorption instead of ion exchange.

An isotropic micellar solution of bile lipids[1] was employed for in vitro measurements of the absorption capacities and absorption rate capabilities of polymers. Henceforth, this solution will be called model bile.

The first polymers tested were representative of those shown in previous work (Ref. 4) to have high capacities for absorbing hydrocarbon materials, including some lipids. All were composed of lightly crosslinked, amorphous hydrocarbon chains from which the sol fraction had previously been extracted. Although the data were unsystematically variable, a result found later to be caused by incomplete removal of the sol (or nonnetwork) fraction from polymer samples, there was sufficient evidence for the conclusion that these hydrocarbon polymers were incapable of absorbing significant amounts of bile lipids from micellar solutions. In addition, it was found that the model bile solution could extract lipids from polymers.

Micelle-Polymer Interaction

The failure of oleophilic polymers as absorbers for lipids from micellar solutions led to the proposition that a successful polymer must be composed of a mixture of both oleophilic and hydrophilic chains. The basis for this theory is the higher affinity of lipid polar groups for water, as demonstrated in these experiments, over that of their larger aliphatic parts for the hydrocarbon polymer chains. High polar group-water affinity is the force also that makes possible the solution of high concentrations of properly proportioned lipids in water. In such solutions water is the continuous phase, and all of the lipid molecules are in micelles that are submicroscopic clusters arranged so that the large hydrocarbon tails of the molecules are surrounded by a sheath composed of their polar groups.

The interaction between micelles and hydrocarbon polymers that might be expected on the basis of the above discussion would be limited to the polymer surface. Lipid molecules coming into close contact with polymer chains will be unable to diffuse into the polymer because of the force retaining the polar groups in the aqueous phase. At equilibrium a polymer particle probably would resemble a very large micelle, a hydrocarbon body surrounded by a polar sheath. Therefore, for a polymer to be able to absorb larger amounts of bile lipids, it must be able to absorb water, as well as oils, so as to attract both parts of lipid molecules.

Polymer Preparation and Composition

The general scheme for preparing oil-absorbing urethane-cured polymers described previously (Ref. 4) was used. Formulations were calculated to

[1] In human bile, the lipids, bile salt, lecithin, and cholesterol in proportions ranging around 60.7%, 33.7%, and 5.6%, occur as 8.9% total lipids in water. The model bile solutions used in this work contained 45.5% total lipids distributed as 54.9% sodium cholate, 44% crude egg lecithin, and 1.1% cholesterol. This departure in composition was necessary for the preparation of stable, homogeneous, isotropic micellar solutions using available ingredients. Lack of lecithin purity is believed to be the cause of the impossibility of obtaining stable representative compositions. Cholesterol concentration, based on total solution, is the same, however.

yield low levels of crosslinking. Prepolymers and other ingredients were dissolved, in formulated proportions, in a solvent. The mixtures were cured by heat. After cure, sol (or nonnetwork) fractions were removed by repetitive extraction. To obtain accurate lipid absorption capacity measurements, it was found necessary to approximately double the number of fresh extractions. Thin layer chromatography (TLC) was adopted as a measure of extraction effectiveness.

Because of their high water solubility and their suitability for use in urethane systems, hydroxyl-terminated polyethylene oxide (PEO) prepolymers were selected to contribute hydrophilic chains in polymeric mixtures with the previously used oleophilic polybutadiene (PB) prepolymers. Dioxane was found to be an appropriate solvent for dissolving the prepolymers and in which to produce cured, homogeneous, mixed-chain polymers. Polymers were prepared with several weight ratios of the two kinds of prepolymers: parts PEO to parts PB of 100/0, 90/10, 75/25, and 0/100, each with appropriate amounts of curing ingredients.

Measurement of Lipid Absorption

Polymer samples were used in two particle size classes for lipid absorption tests: chunk (about 6 mm) and ground (about 1 mm). Contact times for polymer samples with model bile ranged from 5 min to 220 h. Samples were weighed before contact, after contact, and after subsequent removal of absorbed water by vacuum drying.

Results

The maximum absorptions that were measured were obtained with polymer No. 806, which is composed of 75 parts PEO and 25 parts PB plus curing ingredients. Total absorption (water plus lipids) at equilibrium measured on a number of samples of this type of polymer ranged from 305 to 309%, based on original polymer weight. Lipid absorption (measured after removal of absorbed water) measured from 57 to 59.4%. These measurements were made after from 140 to 150 h of contact. After 5 min, the corresponding values were 54.2 to 59.8% total and 4.1 to 10.8% lipids.

The particle size effects on absorption rate expected from diffusion considerations were observed in all comparisons between chunk and ground samples. Chunk absorption was slower. Rate measurements also indicated that in the earlier time periods water absorption leads lipid absorption. The water and lipid absorption rates in ground polymer No. 806 (75/25 PEO/PB) are illustrated in Fig. 1.

Absorbates extracted from representative samples that had absorbed significant amounts of lipids were shown by thin layer chromatography (TLC) to contain all three lipids: cholesterol, sodium cholate, and lecithin. No quantitative measurement of the relative concentrations of these three compounds were made; however, qualitative examination of the TLC

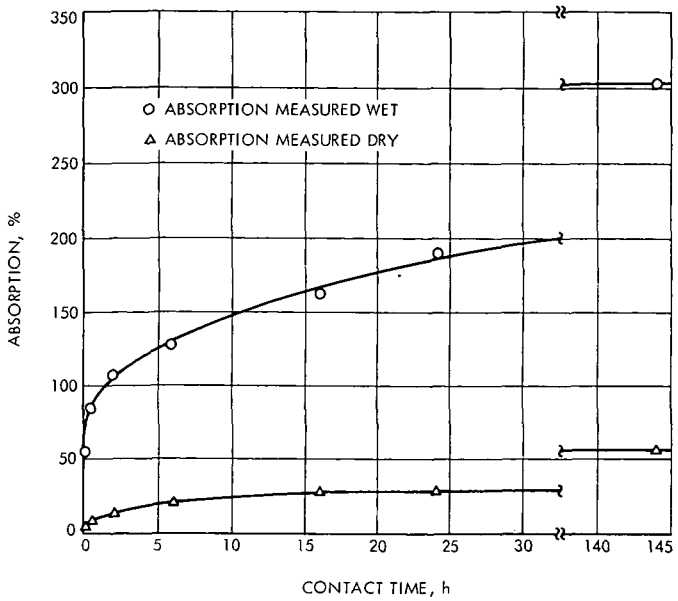

Fig. 1. Rate of absorption of model bile by ground polymer No. 806

records indicate that they are probably in about the same proportions as they were in the model bile solutions. A TLC record confirming cholesterol absorption in polymer No. 806 (75/25 PEO/PB) is shown compared with a standard in Fig. 2.

The absorption capacity of polymers for lipids from micellar solutions is highly dependent upon polymer structure. This result is illustrated in Fig. 3. In 147 h, polymer No. 720 (100/0 PEO/PB) absorbed 271% total material, but, after the water was removed, only 0.3% lipid residue remained. In 144 h, polymer No. 800 (0/100 PEO/PB) absorbed only 3% total, 2/3 of which was lipid. In corresponding contact times, polymers with intermediate compositions, No. 734 (90/10) and No. 806 (75/25), absorbed much more lipid, 9.5% and 59% respectively. Reliable data are not available for polymers whose compositions lie between PEO/PB ratios of 75/25 and 0/100 because of difficulties in grinding these more rubbery materials in the laboratory. This obstacle will be eliminated in future work, and it can be expected from the data in Fig. 3 that higher absorption capacities will be measured.

Conclusions

The results of these experiments permit the following conclusions:

(1) While crosslinked polyethylene oxide (PEO) polymers will absorb water and crosslinked polybutadiene (PB) polymers will absorb lipids, neither polymer will absorb appreciable amounts of lipids from micellar solutions of lipids in water.

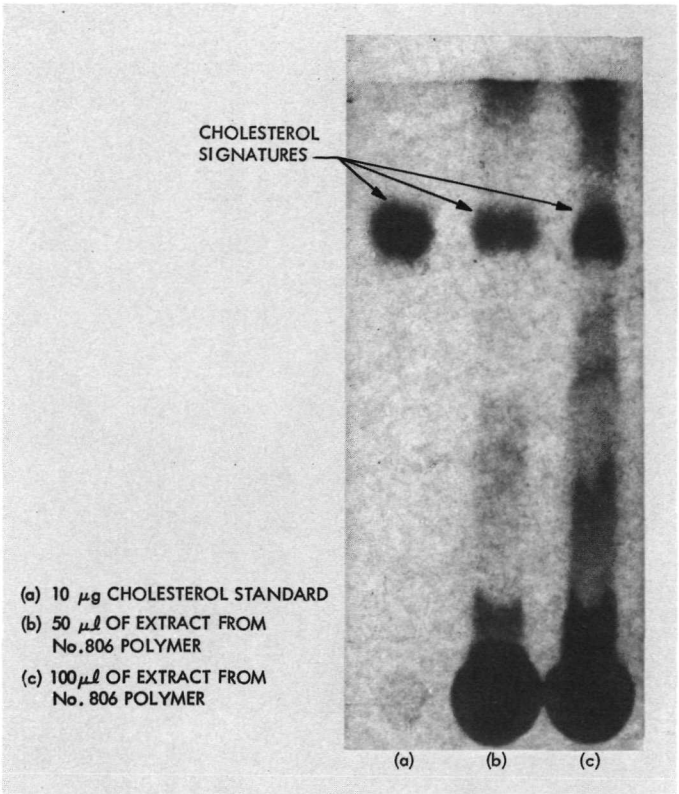

Fig. 2. Thin layer (TLC) chromatograph showing cholesterol in absorbate from polymer No. 806

(2) Crosslinked, amorphous polymers composed of homogeneous mixtures of PEO and PB chains will absorb significant amounts of lipids from micellar solutions.

(3) The lipid absorption capability of mixed chain polymers is markedly dependent on the relative proportions of oleophilic and hydrophilic chains in the polymer. Whereas the highest absorption measured was 59.4% lipid (based on original polymer weight) in a 75/25 PEO/PB polymer, trends in the data indicate the probability that higher capacities will be found in compositions between 75/25 and 0/100 PEO/PB.

(4) Short-term absorption capacity can be improved by reduction in polymer particle size. Almost 24 h were required for a 75/25 PEO/PB polymer in chunk form (~6 mm) to absorb the 10% achieved in 5 min by the same polymer ground to ~1 mm size.

(5) All three lipids used to make the micellar test solutions, cholesterol, sodium cholate, and lecithin, were found in absorbates. There was no evidence of selectivity related to lipid structure.

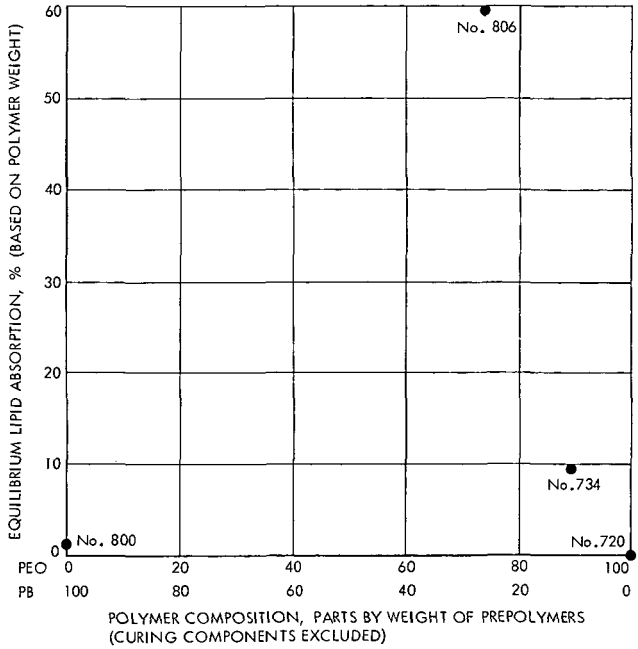

Fig. 3. Relationship between polymer structure and micellar lipid absorption

References

1. Bitman, J., et al., "Effects of DEAE-Sephadex, a Cellulose Anion Exchanger, on Lipids of Rats and Cows," *J. Dairy Sci.*, Vol. 54, p. 768, 1971.

2. Parkinson, T. M., "Hypolipidemic Effects of Orally Administered Dextran and Cellulose Anion Exchangers in Cockerels and Dogs", *J. Lipid Res.* Vol. 8, p. 24, 1967.

3. Parkinson, T. M., Gunderson, K., and Nelson, A., "Effects of Colestipol (U-26, 5974 Å), a New Bile Acid Sequesterant, on Serum Lipids in Experimental Animals and Man," *Atherosclerosis*, Vol. 11, p. 531, 1970.

4. Marsh, H. E., Jr., "Oil-Absorbing Polymers", *JPL Quarterly Technical Review*, Vol. 1, No. 1, p. 49, 1971.

JPL Quarterly Technical Review Volume 2, Number 4 January 1973

Index: bioengineering

Unified Approach to the Biomechanics of Dental Implantology

D. E. Grenoble

University of Southern California

A. C. Knoell

Applied Mechanics Division

The human need for safe and effective dental implants is well-recognized. Although many implant designs have been tested and are in use today, a large number have resulted in clinical failure. These failures appear to be due to biomechanical effects, as well as biocompatibility and surgical factors.

This article proposes a unified approach, using multidisciplinary systems technology, for the study of the biomechanical interactions between dental implants and host tissues. The approach progresses from biomechanical modeling and analysis, supported by experimental investigations, through implant design development, clinical verification, and education of the dental practitioner.

The result of the biomechanical modeling, analysis, and experimental phases would be the development of scientific design criteria for implants. Implant designs meeting these criteria would be generated, fabricated, and tested in animals. After design acceptance, these implants would be tested in humans, using efficient and safe surgical and restorative procedures. Finally, educational media and instructional courses would be developed for training dental practitioners in the use of the resulting implants.

Introduction

The development and application of safe and effective dental implants as replacements for natural teeth has long been the main goal of implant dentistry. The clinical significance for such development and application is obvious. In the United States alone, there are approximately 56,000,000 teeth extracted annually, and there are over 850,000,000 missing teeth in our population (Ref. 1). People who are partially or fully edentulous would be materially aided through the use of functional, long-lasting implants that prevented resorption of the alveolar bone while preserving normal oral function.

Yet, as great as the need appears to be, safe and effective human implants are still not available. Many designs and devices have been attempted, but most have resulted in clinical failure. These failures appear to be due as much to the lack of consideration of biomechanical factors as to anatomical, biological, and surgical requirements. Implant designs have been developed on a trial-and-error basis largely without consideration of the design requirements for proper mechanical stimulation of the alveolar bone of the mandible or maxilla.

Dental biomechanical research efforts are under way to place the development and application of dental implants on a sound rational basis to ensure long-term clinical success. Important contributions have recently been made in many areas, including biomechanical modeling and analysis (Ref. 2), studies of tissue compatibility with implant biomaterials (Ref. 3), studies of biophysical properties of hard tissues (Ref. 4), and characterization of cellular response to mechanical loading (Ref. 5). However, these contributions primarily reflect the results of individual or group researchers working on specialized aspects of the dental implant problem. What is needed is a unified approach to the biomechanics of dental implants that integrates the results of these researchers and uses multidisciplinary systems technology to develop implant designs with a high probability of clinical success. Such an approach, supported by feasibility demonstration data, is described in this article.

Description of Approach

The unified approach to the biomechanics of dental implantology consists of five phases. The relationship of these phases is demonstrated in Fig. 1.

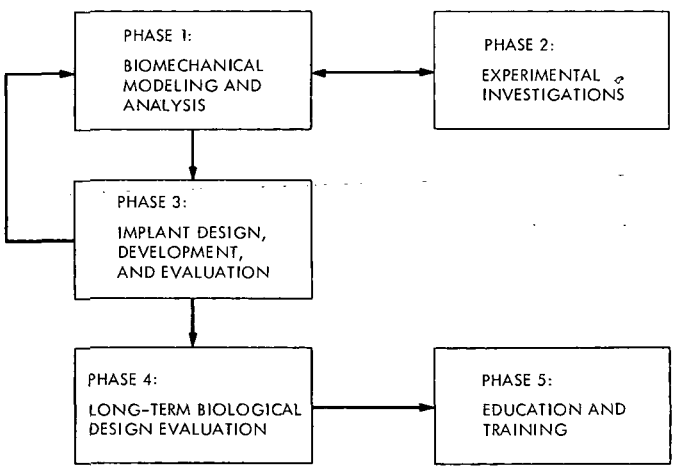

Fig. 1.–Unified approach to the biomechanics of dental implantology

Phase 1: Biomechanical Modeling and Analysis

The first phase of the approach involves the development of three-dimensional, finite-element mathematical models of the human mandible and maxilla and the analysis of these models using computerized techniques. The models require the incorporation of biological parameters such as bone bioelectricity, as well as physiological, anatomical, and mechanical features, in order to develop biomechanical relevance and clinical significance. Many of these parameters have already been defined in various research efforts reported in the literature.

The types of biomechanical models to be developed include models of the mandible and maxilla, both with and without implants. Analysis of the normal models under occlusal loading would yield baseline data on the natural biomechanical response of the mandible and maxilla. Analysis of the models containing implants would enable comparison with the normal baseline response to assess analytically the implant design function and develop biomechanical design criteria for implants.

Analysis requirements include the use of computer techniques capable of handling time variation in material properties and loading, since these are natural oral conditions. In addition, it appears necessary to develop what might be termed a biomechanical bone remodeling algorithm to predict analytically the long-term success potential associated with a given implant design. Such an algorithm has already been proposed (Ref. 6). This algorithm essentially accounts for the time variation in mandible or maxilla geometry due to bone resorption and formation in the local region of the implant. This anatomical change is caused by the applied load on the implant and is manifested by the resulting physiological alterations in the supporting bone structure (Ref. 4).

Phase 2: Experimental Investigations

In order to develop credibility in the analytical predictions, it is necessary to perform experimental investigations to verify the biomechanical models and/or determine areas of possible improvement. These investigations should be done *in vitro* and *in vivo*, preferably using non-destructive, non-contacting test techniques. Techniques of this type are needed to measure true test medium response without disturbance due to mechanical attachments or probes.

Fortunately, several test techniques satisfying these requirements are available, such as holography, electrical impedance measurement, acoustics, and radiography. (The first two techniques have been investigated for this application by the authors and will be discussed later.) Suffice it to say, however, that more work in this area is needed to gain a better understanding of mandibular and maxillary biomechanical response.

During this phase, consideration should also be given to developing short-term biological techniques that could accurately predict long-term bone response to mechanical loading of implants. These techniques, which would

be based upon cellular activity observations and verified through animal testing, would identify sets of morphological and biochemical parameters associated with the initiation of bone resorption. Application of these techniques would provide a powerful means of immediately assessing the clinical success potential of dental implants.

Phase 3: Implant Design, Development, and Evaluation

This phase of the approach utilizes the results of the previous phases and incorporates further the dental and biological considerations necessary to develop sound implant devices for human usage. Recognizing that the resulting implant designs must ultimately be converted to dental implants available to the practitioner and patient, consideration must be given to the manufacturing, processing, and cost of dental implants. Thus, this phase of activity consists of the development of implant design criteria and implant designs, the biomechanical evaluation of each design using the biomechanical bone remodeling algorithm, the fabrication and laboratory evaluation of specific implant designs, and the subsequent evaluation of these designs in short-term animal testing. The design criteria to be developed include:

(1) Biomechanical criteria, which would consist of implant configuration and physical-property requirements based upon the results and experience gained in the previous phases.

(2) Biological criteria, which would include requirements relating to tissue compatibility, systemic toxicity, and carcinogenesis.

(3) Dental criteria, which would reflect consideration of surgical and restorative procedures, bacterial invasion, epithelial attachment, and implant function.

(4) Anatomical criteria, which would include design constraints based upon implant site anatomy and intended implant usage.

(5) Production criteria, which would be based upon cost and quality-control requirements.

Implant designs would then be developed that satisfy these criteria. The design phase would include the development of new designs, as well as consideration of existing implant devices. Designs developed in this manner would automatically relate acceptable implant shape with suitable biomaterials and account for design flexibility to satisfy clinical constraints.

The implant designs would be analytically evaluated through the use of the bone remodeling algorithm. The algorithm would estimate the probable time-sequence stages of resorption and formation of alveolar bone, which take place in the mandible or maxilla in response to the presence of a design implant under specific loading conditions. Each implant design would be studied in each of the proposed modes of application under a range of loading conditions. Using this technique, it would be possible to obtain rapidly a quantitative estimate of the long-term success potential or reliability of each implant design.

Those designs that meet the design criteria will be fabricated for laboratory analysis and short-term testing *in vivo*. The fabrication considerations for the designs consist of the feasibility of mass production and the cost per unit. The main thrust would be to generate implant designs that can be produced at low cost and in large quantities, if needed, from readily available materials.

A series of laboratory tests would be performed on each implant design to determine its reliability under a given function and its probable mechanical lifetime. The types of tests would include strength and physical property characterization, corrosion resistance, and thermal and fatigue behavior.

The most promising implant designs, as determined by algorithm evaluation and laboratory screening, would be fabricated for short-term *in vivo* animal testing. These tests would be designed to demonstrate short-term implant performance and to supply information whereby probable long-term function could be estimated. Included in these tests would be the application of the previously discussed short-term biological techniques to predict long-term biomechanical response of the mandible or maxilla containing dental implants.

Those designs that, both analytically and biologically, appear to maintain the supporting alveolar bone (or at least not mechanically irritate it) and appear to allow rapid healing of the surgical site and demonstrate good clinical signs (e.g., gingival condition, sulcus depth, and plaque collection) would be tested on a long-term basis in animals and humans. Those designs that appear to stimulate rapid alveolar bone resorption would be returned to the design stage for modification of those portions of the implant configuration affecting tissue response.

Phase 4: Long-Term Biological Design Evaluation

For the animal tests, implants would be placed in both fresh extraction sites and healed edentulous sites according to their projected use. Splinting or self-immobilization techniques would be developed for each implant design as needed. The implants would be restored after a suitable healing period. The long-term effects of normal occlusion, hyperocclusion, and implants placed at an angle to occlusal loading would be studied.

Long-term clinical trials would then be conducted in humans on those designs that functioned well during the first years of long-term animal testing. A human case-study population would be developed so that biostatistically significant data could be obtained from reasonably small numbers of patients in each implant test category. Patient selection criteria would be established for the study of each implant design. These criteria would be formulated both for control of the experiment and for testing their application by the dentist in practice.

A standardized-treatment planning format would be designed for each implant configuration. When a patient is accepted, a treatment schedule would be documented. Comparison could then be made, after the treatment

of many patients, to determine how well such treatment plans can be maintained and to identify what difficulties arose and how they were resolved during each case study.

A variety of surgical procedures would be employed based upon the proposed function of the implant. In each edentulous site, the alveolar bone would be exposed to allow good visual inspection of the site for final location of the implant position, final planning of the surgical procedure, and final choice of implant size. Use of full thickness flaps or removal of a tissue plug would be dependent upon implant design.

Techniques of socket preparation would also be studied so that step-by-step procedures could be developed for each design. Socket preparation procedures would be designed to avoid penetration of the mandibular canal or maxillary sinus or perforation of the buccal or lingual plates. These procedures would be simplified so as to be within the capabilities of the general dental practitioner.

A primary focus of the human implant case studies would be to develop step-by-step procedures and guidelines for restorative procedures. Indeed, the total treatment plan; the choice of implant location, design, and size; and the surgical procedure to be used should all be determined in part by the intended function of the final restoration. Naturally, maintenance of good gingival tissue health and crestal alveolar bone will depend on the contouring of the crown and on the geometry of the restoration–implant and implant–tissue interfaces. Thus, the development of simple restorative procedures that can be taught to the average general practitioner in a logical, step-by-step manner would be of critical importance.

The human studies would also consider the forms of postoperative care required for each implant and would provide recommended steps for such care during healing and following restoration. Emergency procedures would be documented for implant removal and for site treatment following removal.

Finally, patient oral-hygiene requirements would have to be developed for proper maintenance of each implant type. This is necessary to ensure prevention of implant failure due to hygienic causes.

Phase 5: Education and Training

After standardizing the procedures to be used in applying the dental implants, a series of educational media would be prepared for use in training dental practitioners. These media would take the form of training manuals, films, video tapes, slide-tape presentations, and documentation of human case studies and animal research results. These media would present in detail all factors to be considered in the selection of patients and appropriate implants, treatment planning, surgical and restorative procedures, patient oral hygiene, and patient education.

Feasibility Demonstration

The feasibility of implementing the above approach was largely demonstrated through a pilot program (Ref. 7) and a large-scale private research project investigating the application of vitreous carbon as a dental implant biomaterial.

Mathematical Modeling and Structural Analysis of a Dried Human Mandible

In the pilot study, an integrated biomechanical modeling, analysis, and experimental program was conducted using a dried human mandible. Such a specimen was chosen because it simplified the initial exercise of each phase of the program. Although the dried mandible did not represent the *in vivo* system, this exercise did verify modeling capabilities and the experimental procedures to be used in the above approach. A finite-element, half-symmetric, structural model of the mandible was developed (Ref. 2). The model, based on a first-order approximation of the stiffness and geometry of the human mandible, is shown in Fig. 2. The model geometry was derived from measurements taken of the actual mandible specimen using horizontal sectioning techniques, and the material properties were derived from the literature.

Loading on the occlusal surface of the first bicuspid was used to study the analytical response of the mathematical model. This tooth was selected

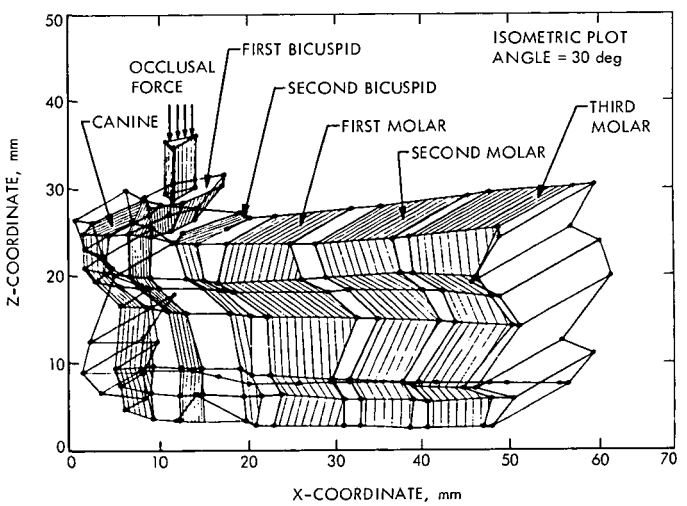

Fig. 2. Three-dimensional view of half-symmetry mathematical model of mandible

because of its clinical significance and ease of modeling. Nodal stresses and the deformation of the model under the applied load were generated using the general-purpose computer program ELAS (Ref. 8). As a check on model accuracy, predicted deformations were compared with test results obtained using holographic interferometry applied to a human mandible in the dried state. The holographic technique was chosen because it offered the advantage of non-contact mapping of the extremely small displacements occurring in the deformation field of a mandible specimen.

A qualitative comparison of analysis and test displacement contours (Fig. 3) indicates that good agreement between test and theory was achieved. The direction of the numerical contour slopes predicted analytically is consistent with that of the fringe slopes obtained holographically. In general, slopes are negative in the mesial direction and positive in the distal direction relative to the loaded first mandibular bicuspid.

Specific investigation of the holographic data also shows a condition of looping fringes between teeth in the local area of loading. Stiffness variation between regions of high (dentin) and low (alveolar bone) elastic modulus is apparently the cause. This effect appears to have been predicted analytically, as is evidenced in the low left-hand region of the numerical contours.

Clearly, model extension and improvement to represent the clinical human condition will require the incorporation of biological parameters, as discussed above. Experimental verification of improved biomechanical models using non-contacting techniques such as holography will also be required.

Detection of Bioelectric Responses in a Dried Human Mandible

Fig. 4 shows the apparatus used to detect bioelectric responses in the dried human mandible under loading conditions similar to those used in the

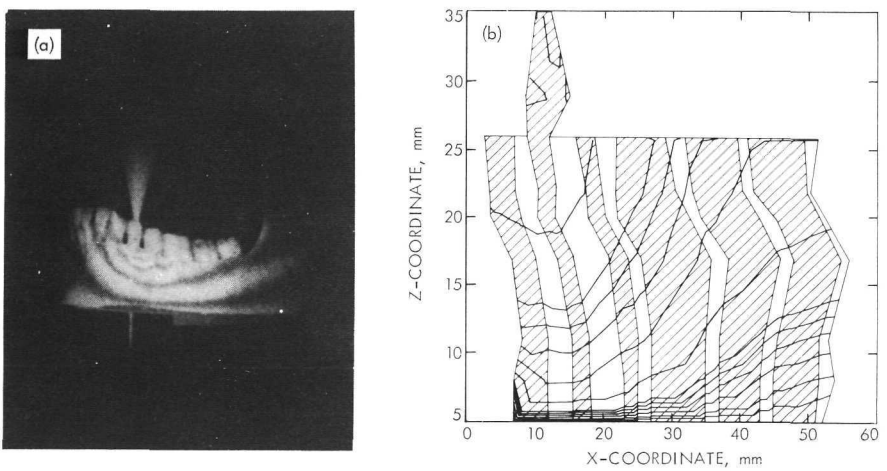

Fig. 3. Comparison of displacement contours: (a) hologram and (b) computer predictions

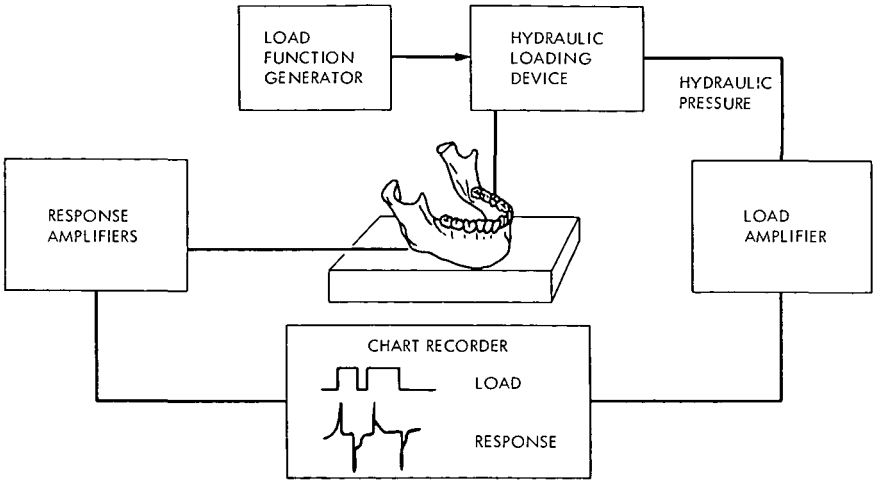

Fig. 4. Bioelectric response experimental apparatus

model and holographic studies. This experiment was undertaken as a prelude to determining the bioelectric material properties of the *in vivo* mandible and maxilla. These properties are necessary to biologically characterize improved biomechanical models in order to relate mechanically induced deformation to bone remodeling response (Refs. 4 and 5).

A static load was applied to the first bicuspid of a dried human mandible that was supported on a block of epoxy resin and loaded through an epoxy rod. The epoxy block and rod served to insulate electrically the mandible from the loading apparatus in order to prevent grounding of the bioelectric signals. Bioelectric surface signals resulting from mandible loading were amplified and recorded on a strip chart recorder.

The experimental apparatus worked satisfactorily, and analysis of the data obtained is in progress. The results achieved thus far, coupled with the results reported by others (Refs. 9 and 10) in determining the bioelectric response of bone, strongly attest to the feasibility of characterizing the *in vivo* bioelectric response of the human mandible. It is clear, however, that a technique to map rapidly the bioelectric surface response of hard tissues would facilitate experimental procedure and improve data accuracy.

Investigation of Cellular Activities Involved in Bone Resorption

Studies have been conducted on the changes in cellular activities and metabolism of hard tissues after stimulation of bone resorption by hormonal and drug stimuli. During these studies, a number of testing procedures, including tissue biopsy techniques, were developed and evaluated. (Details of some results of these studies are presented in Ref. 11.) At a minimum, these studies have served to establish the feasibility of using cellular activity parameters as short-term markers for bone resorption.

Design and Development of an Endosteal Implant

A large-scale research program has been undertaken to develop and test an endosteal implant made from vitreous carbon. Short-term animal histological studies designed to evaluate material biocompatibility and epithelial attachment to the implant have been completed. Long-term work is in progress to evaluate systemic toxicological and carcinogenic effects due to the implant biomaterial.

In the course of these studies, surgical and restorative procedures associated with the implant designs, which were initially empirically evolved, have been developed. These procedures were designed to allow the implants to function both in free-standing situations and as abutments for fixed prostheses.

A series of educational aids has been developed for use in training dental practitioners in the proper procedural use of the carbon endosteal implant. These aids include a film, training manual, and laboratory exercise, as well as formal continuing-education courses.

The experience obtained in this program has demonstrated the need for implant design development using an integrated scientific and clinical approach such as described above.

References

1. Dummett, C. O., "Year 2000 Community Dentistry," *J. Amer. Dent. Assoc.*, Vol. 82, 1971.

2. Gupta, K., Knoell, A., and Grenoble, D., "Mathematical Modeling and Structural Analysis of the Mandible," *J. Biomed. Mater., Med. Devices, Artificial Organs*, Vol. 1, No. 2 (In press).

3. *Oral Implantology*. A. N. Cranin, Editor. Charles C. Thomas, Publisher, Springfield, Ill., 1970.

4. Bassett, C. A., *The Biochemistry and Physiology of Bone*, Second Edition, Vol. III. Academic Press, N. Y., 1971.

5. Frost, H. M., *The Laws of Bone Structure*. Charles C. Thomas, Publisher, Springfield, Ill., 1964.

6. Gupta, K., Knoell, A., and Grenoble, D., *A Biomechanical Bone Remodeling Algorithm*, submitted for presentation at the 8th AMMI Meeting, Washington, D.C., March 1973.

7. *Biomechanics of Dental Implants*, California Institute of Technology President's Fund Task, Grant No. PF-036, February 1972.

8. Utku, S., and Akyuz, F., *ELAS — A General-Purpose Computer Program for the Equilibrium Problems of Linear Structures*, Technical Report 32-1240. Jet Propulsion Laboratory, Pasadena, Calif., February 1968.

9. McElhaney, J. H., et al., "Mechanical Properties of Cranial Bone," *J. Biomechan.*, Vol. 3, 1970.

10. Fukada, E., "Mechanical Deformation and Electrical Polarization in Biological Substances," *Biorheology*, Vol. 5, No. 199, 1968.

11. Mills, B. G., et al., "Bone Cell Response to Serum Calcium Altering Drugs," *Clinical Orthopaedics*, Vol. 78, No. 56, 1971.

Index: chemistry, scientific instruments, soil sciences, solid-state physics

Thermoluminescence: Potential Applications in Forensic Science

J. D. Ingham and D. D. Lawson

Propulsion Division

In crime laboratories one of the most difficult operations is to determine unequivocally whether or not two samples of evidence of the same type were originally part of the same thing or were from the same source. It has been found that high temperature thermoluminescence (room temperature to 723 K) can be used for comparisons of this type, although work to date indicates that there is generally a finite probability for coincidental matching of glass or soil samples. Further work is required to determine and attempt to minimize these probabilities for different types of materials, and to define more clearly the scope of applicability of thermoluminescence to actual forensic situations.

Introduction

The criminalistics operation in the investigative process is to identify, evaluate, and interpret potential evidence or physical materials associated with crime situations. These materials frequently offer the most convincing means of relating a suspect to an act or a scene, or of showing that a person has been incorrectly suspected.

Methods that may be available to criminalists and that have been applied to evidence materials include conventional chemical analysis, optical microscopy, gas chromatography, spectrometry, and measurements of physical properties such as refractive index and density. When applying these techniques the criminalist usually compares the physical materials found at the scene of a crime, or known to be related to a crime, with those known to be related to the suspect. He then attempts to demonstrate convincing relationships, either negative or positive, from the results.

Because of practical limitations it is very often not possible to say unequivocally that two materials were derived from the same source, since no two things are exactly alike. In such cases the criminalist must examine all information available and then make an accurate estimate of the situation based on his past experience. Except for such evidence as clear fingerprints,

very characteristic bullet rifling patterns, or other special cases, most evidence materials fall in the category described above. That is, the criminalist requires all the information that he can obtain to effectively compare and evaluate evidence materials.

Therefore, there is a critical need for new methods and instruments that can be used for the accurate interpretation of physical evidence, not to replace those techniques already in use, but to extend and enlarge the capabilities of forensic practitioners to individualize or convincingly assess the source relationships of evidence materials.

From the work carried out at JPL, it appears that thermoluminescence (TL) is one of the more discriminating methods available for differentiating between specific samples of several type of materials, including glass, soils, safe insulation, salts, and other nonmetallic solids. It was recently pointed out that a national survey of criminalists has indicated that improved methods are needed most for glass, hair, paint, soil, fibers, and blood, in that order (Ref. 1); therefore, it is believed that the application of TL methods would be of significant value for the investigation of a number of important types of evidence materials.

Thermoluminescence: Technical

Thermoluminescence (TL) is the emission of light that may occur when a material is heated to temperatures below incandescence (Ref. 2). The primary cause of these light emissions is previous exposure of the material to natural or laboratory ionizing radiation at or below the temperature at which heating is started. The radiant energy displaces some electrons in the solid; these electrons are trapped in imperfections and vacancies in the crystal lattice and escape with the emission of light when the temperature is raised to supply the required amount of kinetic energy. The color or wave length distribution of the light may vary over the entire visible spectrum and appears at different temperatures depending on the basic crystal structure, the presence of impurities or trace components, and the radiation, thermal, and pressure histories of the material.

For high temperature TL, which is the subject of this work, the temperature range is from room temperature to 723 K (450° C). TL response is recorded in about two minutes as temperature vs light intensity to give a TL curve. Since the responses, even for relatively pure materials, depend on several subtle variable factors such as concentrations of minor components and environmental history, the shapes of the TL curves often depend on the source of the particular material. For applications to criminalistics, TL response for a specific material is compared with the curve obtained under the same conditions for another sample of the same substance of known origin. If the curves are essentially identical, a common source is indicated for the two materials being compared.

Thermoluminescence: Literature

TL was probably first described in the last half of the seventeenth century by Robert Boyle. In 1928 the coloration of glass by radioactivity followed by heating to bleach the color and evolve light was described by Lind (Ref. 3). Also in the twenties, the TL responses of fluorite and carbonate minerals were observed (Refs. 4 and 5). It was noted that after once being heated these materials would not again emit light on heating, but that TL could be regenerated by exposure to X-rays or radium. Urbach (Ref. 6) and Randall and Wilkins (Ref. 7) recorded glow curves and interpreted them theoretically.

Between 1948 and 1959, F. Daniels and others carried out a large amount of work on potential applications of TL (Ref. 8). These included applications to uranium prospecting, radiation damage and dosimetry, geological age determinations of minerals and rocks, stratigraphy, catalysis, and identification and control of ceramic materials. Good results have been obtained by TL for archeological dating of pottery (Refs. 9 and 10). Since the intensity of TL of a sample depends on the extent of high temperature drainage, it has been used as a paleoclimatological tool to determine the time for glaciation of antarctic regions and to estimate microclimatic effects (Refs. 11 and 12). Although most TL investigations have been concerned with fairly well-defined minerals and materials, Nishita and Hamilton have studied a number of soil samples, especially from the point of view of using soils as radiation dosimeters (Ref. 13), and a limited study of the stratigraphy of lunar samples by TL has been carried out (Ref. 14). At JPL over 100 antarctic dry valley soil samples have been investigated by TL mainly to attempt to correlate microclimate and soil properties with TL responses, which were then related to microbial abundances. (Refs. 15 and 16).

Although there appear to be no previous investigations directed toward applications of TL to criminalistics, theoretical considerations and much of the work described in the literature indicate that TL responses are characteristic and may depend on the source of a particular material. For example, four samples of potassium bromide from different sources gave decidedly different glow curves (Ref. 17). Differences characteristic of the source have also been observed for glass, clay, soils, seashore sand, and calcite (Refs. 2, 18 and 19).

Results and Discussion

The scope of applications of TL to forensic investigations has not yet been fully defined. Therefore, this is essentially a progress report, with emphasis on the status of current methodology for high temperature TL (room temperature to 723 K (450° C)) as applied to materials such as glass and soil samples.

The samples were prepared by mild crushing or grinding, sieved to reasonably uniform particle size and exposed to laboratory irradiation. All samples to be compared were exposed to the same dose of ionizing radiation

from a Cs 137 or Co 60 source. The TL curves were then recorded by heating each sample (~7 mg) at a rapid rate (~9 K/s) and measuring the light evolved vs temperature using a TL photometer (Fig. 1). The light intensity range covered four decades from about 0.01 to 10 μ/m, but was expressed in arbitrary units. A view of the current sample cup and resistance heated support ribbon is shown in Fig. 2. The samples were volumetrically loaded into the cup by means of a microspoon. If the curves were exactly the same, or very different, they could be compared visually (cf Figs. 3 and 4). However, for curves that were questionably similar, or for comparisons of all combinations of more than two or three curves, a statistical method was used (Ref. 20).

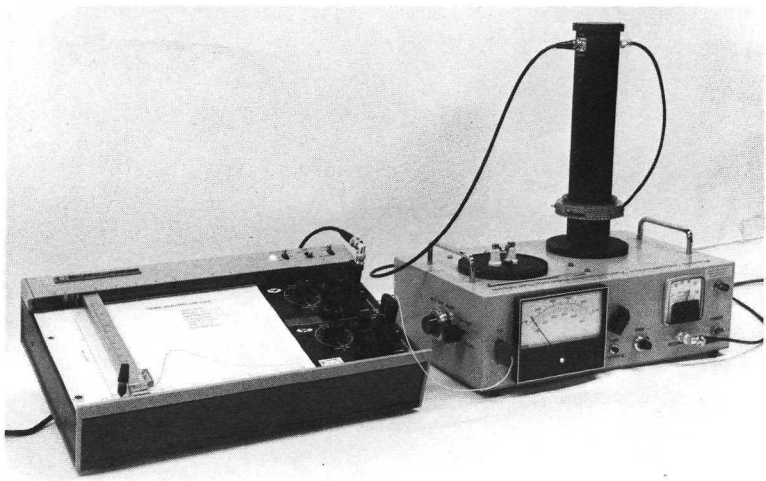

Fig. 1. Thermoluminescence photometer

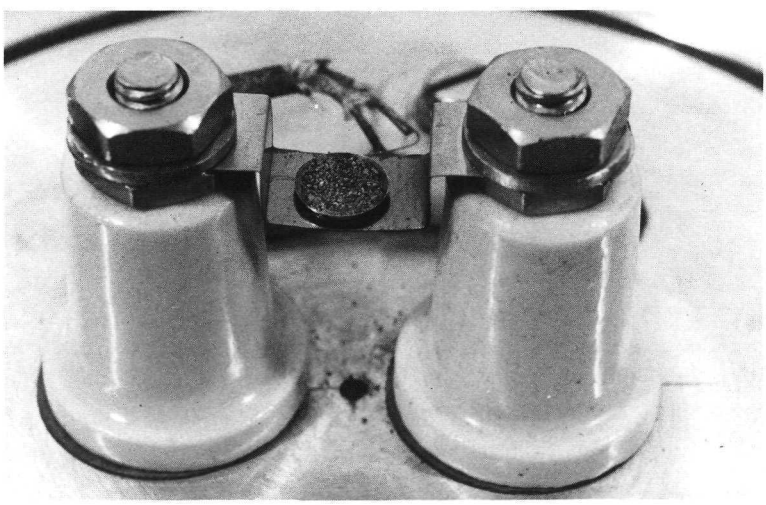

Fig. 2. Thermoluminescence sample cup and heater

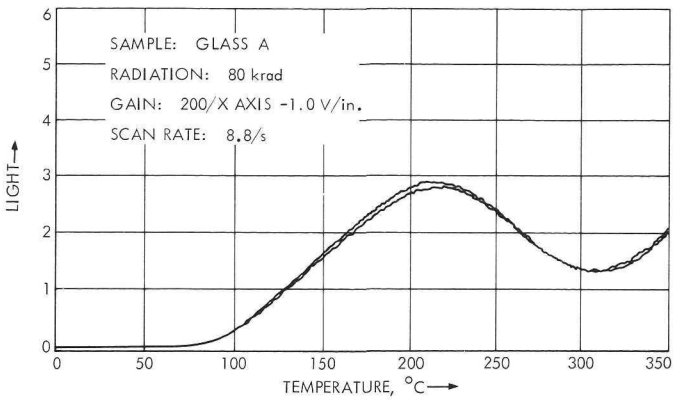

Fig. 3. Thermoluminescence curve for glass sample (A)

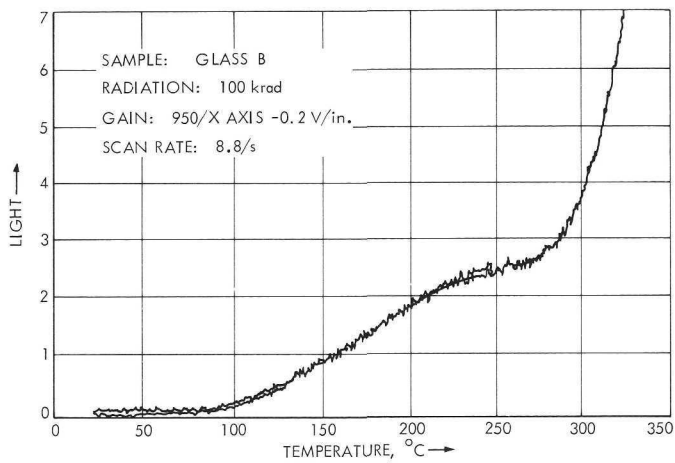

Fig. 4. Thermoluminescence curve for glass sample (B)

For an initial estimate of the utility of TL in forensic situations, data for ten auto headlamp lenses were obtained and compared by the χ^2 method (Ref. 20). The threshold value of χ^2 was determined from only one headlamp, designated AC No. 4201.

The values of χ^2 are used to compare curves; each χ^2 value represents the magnitude of the absolute differences in areas between the two TL curves being compared. These values are calculated from:

$$\chi^2 = \sum \frac{(E - O)^2}{E} \qquad (1)$$

in which E and O are the expected and observed events, respectively. The two curves to be compared are divided into 33 equal parts at 10 K intervals. The differences in light intensities at each interval are then measured from the chart to give 33 values of E - O. Since there is no rationale for defining which curve represents expected events or which represents observed events, E and O are interchanged in Eq. (1) to calculate two χ^2 values for each comparison of two curves. It is obvious that the larger the χ^2 values, the greater the difference between the two curves, and, if the curves are the same, χ^2 equals 0. Comparison of curves obtained from several measurements on samples from the same source results in χ^2 values that are low, and reflect the reproducibility of the TL method.

A series of χ^2 values calculated from TL measurements on four different glass samples taken from different parts of the same AC No. 4201 lens are shown in the matrix below.

	(2)	(3)	(4)
(1)	0.101 0.096	0.429 0.597	0.472 0.421
(2)		0.494 0.366	0.151 0.165
(3)			0.871 0.587

Samples (1), (2), (3), and (4) were taken from the central, right, left, and lower parts of the lens, respectively. For comparisons among four curves, χ^2 values have been calculated from all possible combinations of the four, to give six pairs of values (that is, n(n - 1)/2 equals 6.) By using probability paper, the mean (X) and standard deviation (S) were found to be 0.42 and 0.28, respectively. These could have been directly calculated with slightly more accuracy, but the probability plot was convenient and showed that the data could be reasonably well represented as a normal distribution. The threshold value of χ^2 was used as a criterion for curve matching. Thus, if χ^2 for a comparison of two curves for different lens glasses was less than the threshold value of χ^2, a match of the two curves was indicated. In the example above, the threshold value was χ^2 equals 1.26, obtained by adding three times the standard deviation to the mean. Three S was added to the mean because it has been found that for a normal distribution about 99.7% of the measurements fall in the range of X $\pm$3S; thus, using only the four TL curves nearly all TL curves for lens AC No. 4201 should have χ^2 values of less than 1.26 when compared with a lens sample known to be from this lens. However, it has been shown by Ojena, et al. (Ref. 21), that variations in refractive index for the same auto headlamp lenses occur, probably because of differences in the annealing schedule at different positions of the lens. In agreement with their work, it was found that the χ^2 value for a sample taken from the edge of lens AC No. 4201 was greater than 1.26 in two comparisons with the four AC No. 4201 samples discussed above. If this TL curve was

included in the calculation of the threshold χ^2, the value was found to be 2.41. Since there is no reason to exclude this last sample, the larger threshold value was used for the comparisons of headlamp glasses shown in Table 1. It can be seen that sample 1 matches 2 and 6; 2 matches 6; and 3 matches 5 and 6, which represents 89% success in differentiating among auto headlamp samples.

Table 1. Matrix of χ^2 values for different headlight lens samples[a]

Sample No.	Identification	χ^2 value by sample No.									
		(2)	(3)	(4)	(5)	(6)	(7)	(8)	(9)	(10)	
1	Tungsol 4001, new	1.59 1.95	7.54 11.53	25.76 70.06	13.90 26.29	1.99 2.42	7.29 4.94	5735 115	66.64 4509	6.77 5.11	(1)
2	GE 4012, new		5.71 8.56	21.81 52.60	10.60 18.00	2.02 2.61	18.43 10.76	8206 121	62.20 4587	13.00 8.25	(2)
3	AG 4201 (center section), new			8.54 15.89	1.85 2.46	2.89 2.27	27.73 13.09	5633 139	44.40 1931	41.71 21.21	(3)
4	AC 4201, 3 years old; removed from auto				5.27 3.51	37.63 16.37	127 31.63	(16451) 168	24.77 756	156 44.47	(4)
5	Tungsol 4413, new					10.73 6.71	54.94 20.11	7879 151	36.06 1563	72.73 30.03	(5)
6	Chevrolet 1948 headlamp, auto salvage yard, El Monte, Calif.						12.53 6.85	5536 127	55.06 3102	19.07 12.04	(6)
7	Ford 1956 headlamp, auto salvage yard, El Mónte, Calif.							106 1807	71.75 3665	11.88 7.92	(7)
8	Italian headlamp, auto salvage yard, El Monte, Calif.								213 9775	98.62 3532	(8)
9	English Lucas headlamp, from MG-TD									7216 87.97	(9)
10	Japan Toshiba headlamp, auto salvage yard, Monrovia, Calif.										

[a]Exposed to 1 Mrad of Co 60.

The above results clearly show that TL response is not a unique characteristic of auto headlamp samples at the present stage of development, and that the probability of coincidental matching can be quite high. If a threshold of X + 3S is used it appears that TL can only be used for exclusionary evidence, i.e., where the TL curves obviously do not match, or for preliminary investigations that might lead to further substantial evidence.

However, in the context of actual cases, it may be practical to decrease the threshold value. For example, when a threshold value of X + S equals 1.31 was used for the headlamp lens data in Table 1, no coincidental matches were observed in the 45 comparisons. But this procedure would result in the observation of about 16% negative comparison results for samples obtained from the same material. Thus, by using a lower threshold value, existing data indicate that coincidental positives can be greatly decreased, but that about one of six true positives would incorrectly appear to be negative. At least in those cases where positive matching would be incriminating, the assignment of a lower threshold value may be justified, since the loss of some evidence is not as serious as the application of invalid evidence.

In six comparisons of windshield glasses, the χ^2 values for one comparison were 0.69, 1.72, which is a true coincidental match even if the threshold was substantially less than 2.4. Similarly, for three comparisons of auto door glass there was one coincidental match (χ^2 equals 0.75, 1.12). Also for 21 comparisons of vodka bottles (all of the same vodka brand), there were 5 χ^2 values less than 1.3, or 24% of the comparisons were coincidental matches. In this example, there were no χ^2 values between 1.3 and 2.4; therefore, either threshold would give the same results.

A threshold value of 1.8 was determined for building window glass and the χ^2 values were calculated for two samples. All three comparisons resulted in χ^2s that were well above the threshold values. Four additional samples all required different levels of irradiation to induce thermoluminescence, indicating there were no matches among these other four samples. These results show that TL may be more satisfactory for applications to building glass than for auto glass, but a larger statistical sample will be required for confirmation.

The situation is much more favorable for soil samples. Out of 630 comparisons involving 36 samples, there were only 15 (2.38%) coincidental matches, and these were obtained using a predetermined relatively high threshold χ^2 value of 3.30. Furthermore, after making the comparisons it was found that only 6 of the 15 matching comparisons were purely coincidental: two of the remaining samples were taken from the same location, and the other matching pairs were taken from slightly different depths at the same location; thus the true coincidental matches involved only ~1% of the total number of comparisons. There were only four totally coincidental positive comparisons if the threshold χ^2 value was taken as X + S = 2.52. Since all of these samples were collected from one northern California county, these results should not be applied universally without

further confirmation. For example, it is possible that surface samples taken from a relatively large, rolling dune or desert area may give TL curves that are much more alike than the above results would predict.

Conclusions

Thermoluminescence appears to be a useful technique for the interpretation and evaluation of certain types of physical evidence materials. The degree of discrimination among soils is greater than for glass samples, which probably arises because of the standardization and quality control applied in the manufacture of glass, and its more constant composition. Preliminary work indicates that for most other materials, such as salts, relatively pure minerals and safe insulation, the overall differences in TL curves for each type of material are intermediate between glass and soils.

There are a number of things that should be done to further define the scope of applications and improve the methodology of TL. For example, the amount of data should be greatly increased to provide greater reliability in the statistical evaluation of results for different types of samples, preferably by criminalists who would be more familiar with potential forensic situations. There are also some instrumental and procedural modifications that may be warranted. These include examination of the effects of prior sample annealing, simple modifications of the sample pan to facilitate uniform loading, and inclusion of measurements of spectral distribution of TL light to greatly decrease the probability for coincidental matching of unrelated samples. These spectral measurements are feasible, either by obtaining a series of TL curves for each sample with different filters between the sample pan and detector, or by using a more elaborate TL photometer that records a series of spectra at small temperature intervals between room temperature and 723 K.

References

1. Kingston, C. R., *Report to the Criminalistics Subcommittee of ASTM Committee E-30 on Forensic Science*, Phoenix, Arizona, Feb. 22, 1971.
2. Daniels, F., Boyd, C. A., and Saunders, D. F., "Thermoluminescence as a Research Tool", *Science*, Vol. 117, pp. 343-349, 1953.
3. Lind, S. C., *The Chemical Effects of Alpha Particles and Electrons*, p. 29, Reinhold's, New York, 1928.
4. Wick, F. G., *Phys. Rev.*, Vol. 25, p. 588, 1925.
5. Wick, F. G., *J. Opt. Soc. Am.*, Vol. 21, p. 223, 1931.
6. Urbach, F., *Aksd. Wiss. Wein. Ber.*, Vol. 139, No. 20, p. 354, 1930.
7. Randall, J. T., and Wilkins, M. E. F., *Proc. R. Soc.*, Vol. A184, p. 366, 1945.

8. Daniels, F., "Early Studies of Thermoluminescence in Geology", in *Thermoluminescence of Geological Materials*. Edited by D. J. McDougall, pp. 3-12, Academic Press, New York, 1968.

9. Mazess, R. B., and Zimmerman, D. W., "Thermoluminescence Dating of Some Peruvian Pottery", in *Thermoluminescence of Geologic Materials*. Edited by D.J. McDougall, pp. 445-448, Academic Press, New York, 1968.

10. Ralph, E. K., and Han, M. C., "Dating of Pottery by Thermoluminescence", *Nature*, Vol. 210, pp. 245-247, 1966.

11. Ronca, L. B., "Thermoluminescence as a Paleo-Climatological Tool", in *Thermoluminescence of Geological Materials*. Edited by D. J. McDougall, pp. 495-506, Academic Press, New York, 1968.

12. Zeller, A. N., "The Influence of Microclimate Upon the Thermoluminescence of Rock", in *Thermoluminescence of Geologic Materials*. Edited by D.J. McDougall, pp. 507-518, Academic Press, New York, 1968.

13. Nishita, H., and Hamilton, M., "Spurious Thermoluminescence of Soils", *Soil Science*, Vol. 110, pp. 371-378, 1970.

14. Doell, R. R., and Dalrymple, G. B., "Thermoluminescence of Apollo 12 Lunar Samples", *Earth and Planetary Science Letters*, Vol. 10, pp. 357-360 1971.

15. Cameron, R. E., and Benoit, R. E., "Microbial and Ecological Investigations in Victoria Dry Valley, Southern Victoria Land, Antarctica", Antarctic Research Series, American Geophysical Union, *Antarctic Terrestial Biology*, in press.

16. Ingham, J. D., Cameron, R. E., and Lawson, D. D., "Microbial Abundance and Thermoluminescence of Antarctic Dry Valley Soils", *Soil Science*, in press.

17. Fieschi, R., and Scaramelli, P., "Photostimulated Thermoluminescence in Alkali Halide Crystals", in *Thermoluminescence of Geological Materials*. Edited by D. J. McDougall, pp. 291-308, Academic Press, New York, 1968.

18. Mejdahl, V., "Thermoluminescence in Seashore Sand", in *Thermoluminescence of Geological Materials*. Edited by D. J. McDougall, pp. 453-462, Academic Press, New York, 1968.

19. Medlin, W. L., "Thermoluminescence Growth Curves in Calcite", in *Thermoluminescence of Geologic Materials*. Edited by D. J. McDougall, pp. 91-101, Academic Press, New York, 1968.

20. Lawson, D. D., and Framan, E. P., "Numerical Correlation and Evaluation in the Comparison of Evidentiary Materials," *J. Forensic Sci.*, in press.

21. Ojena, S. M., DeForest, P. R., and Crim, D., "A Study of Refractive Index Variations Within and Between Sealed Beam Headlights Using a Precise Method", *J. Forensic Sci.*, Vol. 17, No. 3, pp. 409-425, 1972.

JPL Quarterly Technical Review Volume 2, Number 4 January 1973

Index: electronic components and circuits, masers and lasers, optics, pyrotechnics

A High-Efficiency, Small, Solid-State Laser for Pyrotechnic Ignition

L. C. Yang and V. J. Menichelli

Propulsion Division

A completely self-contained, small, neodymium laser has been designed and demonstrated for use in a pyrotechnic ignition system. A nominal 16 J of laser energy (1.06-μm wavelength, 1-ms duration) was achieved in a rectangular 10.5- × 15.1- × 25.4-cm package weighing 5.14 kg. This high energy-to-weight ratio is encouraging for laser applications in which specific energy efficiency (energy per unit weight or volume) is important. The laser design concepts are described, and some results on pyrotechnic ignition are given. Some details on a laser currently under construction, which will be 1/8 the size of the above laser, are included.

Introduction

The use of a pulsed solid-state laser in aerospace work and other applications such as ranging and communication depends largely on its specific efficiency, i.e., laser energy per unit volume or weight. In the early days of laser development, there was considerable enthusiasm to achieve higher-energy output per unit volume. However, today with less severe restrictions on size, laser energies have reached self-destruction limits on the lasing materials. The design of a highly efficient, portable, solid-state laser is still a most interesting challenge. The problems imposed under the restrictions of weight and size are essentially dependent upon the total efficiency of each link in the chain of laser generation, including the power supply, high-voltage circuitry, capacitor bank, flash lamp, pumping configuration, laser rod, and cooling method. Weight and volume restrictions have fundamental impacts on the efficient design, because a good uniform discharge, such as in a pulse-forming network or even a resistive–inductive–capacitive (R–L–C) circuit, is difficult to miniaturize, being limited by the large size of the choke.

Laser Head

The laser rod (1.27-cm diameter, 15.24-cm length) was made from fused silica doped with 3% by weight of Nd_2O_3 with flat-ends configuration. The rough lateral surface (~0.3-μm roughness) combined with an absorption coefficient $\alpha = 0.18$ cm^{-1} (corresponding to the doping level and the effective pumping band of 5700 to 6000 Å) provide a very uniform pumping of the rod; therefore, the optical gain and energy output are quite homogeneous over the cross section of the rod (Ref. 1). The rod is also doped with cerium oxide for anti-solarization purposes, so a UV shield between the flash lamp and the rod is unnecessary. The laser mirrors have a reflectivity of 70 and 100% at 1.06 μm. The mirrors are multi-layer ZnS and $ThOF_2$ films vacuum-deposited on the ends of the rod, which have a 1/20 wavelength (at 1.06 μm) flatness and are parallel to each other within 0.5 seconds of arc.

A helical flash lamp was made from 5-mm ID × 7-mm OD quartz tubing. The length of the lamp was 12.7 cm, with an ID of 1.3 cm to closely fit the laser rod. Twelve helical turns spaced 3 mm apart were chosen to obtain a homogeneous light irradiance on the surface of the rod. The anode and cathode electrodes were made of tungsten and stainless steel, respectively, and the xenon gas was filled at 4×10^4-N/m^2 pressure. The design of the laser cavity is very compact, with the void spaces between the rod and lamp as small as possible. The ratio of volume occupied by the rod to that of the cavity is purposely made as large as possible. The light generated by the flash lamp undergoes multi-reflections and refraction by the lamp walls, the rod, and the cavity reflector. This causes the light energy density inside the cavity to be quite homogeneous. Therefore, the large relative volume of the rod will allow more light to be absorbed for laser action. This is an empirical approach that has proven to be very useful, because, in a helical cavity, the determination of pumping efficiency by ray tracing as used in an elliptical cavity (Ref. 2) is virtually impossible.

In order to avoid the use of large chokes of the order of 10^2 μh, an R–C discharge was chosen to excite the flash lamp. An effective arc length of 79 cm and a quartz tubing ID of 5 mm, in conjunction with the 54-μF capacitor bank, were chosen to provide an arc resistance of 9.0 Ω at 4.9 kV. The resultant average current density of 1000 A/cm^2 corresponds to approximately 7000 K in color temperature, producing a blackbody radiation (Ref. 3) highly rich in the effective pumping band (5700 to 6000 Å) of the neodymium ions. The flash lamp reflector was made from gold-plated, finely polished, half-hard silver foil 0.12 mm thick. The thin gold film protects the silver surface from oxidizing during storage and from the strong irradiation of the flash lamp. It also offers the best spectral reflectivity for the effective pumping band (96% at 5800 Å). The foil tightly wrapped around the flash lamp is also in good contact with the inner liner.

There were several factors considered in the design and application of boron nitride for the cavity inner liner. Because of the compact design of the cavity, it is difficult to remove the heat produced by the flash lamp through air circulation. A diffusive heat sink must be used. The high voltage being

used further required a material with high dielectric strength. It is also impossible to completely enclose the flash lamp with the metallic reflector, which means that some of the dielectric inner liner will be exposed to the flash lamp light. The high UV content of the flash lamp light has a surface burning effect on most dielectric materials such as epoxy, fiberglass, and Teflon. Use of these materials as an inner liner would produce residues that would be deposited on the surfaces of the rod and lamp, leading to laser output deterioration after a small number of operations. Boron nitride has very high thermal conductivity (0.28 W-cm/cm^2-K) and dielectric strength (3.8×10^4 V/mm). For the visible spectrum, it has a reflectivity of 82%, and its resistance to UV radiation has been tested and found to be excellent. Another advantage is its excellent machinability as compared to that of the other popular heat sink ceramics such as alumina or beryllia. Alumina also shows color changes from the irradiation of a xenon flash lamp. Beryllia is not attractive because of its health hazard.

Electronics

The high-voltage energy bank shown in Fig. 1 contains two 5-kV, cylindrical, aluminum–Mylar-foil-type, high-energy density capacitors (44 and 10 μF) made by the Maxwell Laboratory, Inc. The 5-kV-rated series was chosen because it provides the maximum electrical energy storage per unit volume and weight, and it will have a life usage of over 10,000 discharges. Operational levels up to 5.5 kV have shown it to be quite safe, with breakdown occurring beyond 6 kV. The 44-μF capacitor is 10.2 cm in diameter, is 16.5-cm in length and weighs 2.27 kg, while the 10-μF capacitor is 5.1 cm in diameter, is 16.5 cm in length, and weighs 0.68 kg.

The dimensions of the dc-to-dc high-voltage converter are $8.25 \times 8.25 \times 6.35$ cm, and its weight is 1.6 kg. It consists of a regulated 2.7-kHz oscillator, a 11.8-dB amplifier, a $\times 54$ voltage step-up transformer, and rectifiers. The input requires 24 to 28 V dc and a 9-A peak current. The output is adjustable from 3 to 6 kV at 25-mA average current level via a 10-kΩ potentiometer. The charging time for the 54 μF to 4.9 kV is about 8 s, and the overall electrical power efficiency is about 80%. The weight consists mainly of insulation and a thick aluminum case shielding, which can be reduced if desired.

The flash lamp discharge was initiated by a 20-kV, 6.0-μs triggering pulse delivered between the lamp reflector and the ground electrode of the lamp. It was generated by discharging the energy stored in an 8-μF capacitor at 300 V dc through the primary of an EG&G model TR180 cylindrical triggering transformer of 2.62- $\times$ 4.0-cm size, 28.4-g weight, and 112:1 turn ratio. The capacitor was charged with a small dc-to-dc converter ($3.5 \times 3.5 \times 2.5$ cm in size and 85 g in weight).

The high-current-rated dc input was provided by a battery-pack measuring $5.6 \times 8.4 \times 12.7$ cm and weighing about 0.9 kg. The pack consisted of 19

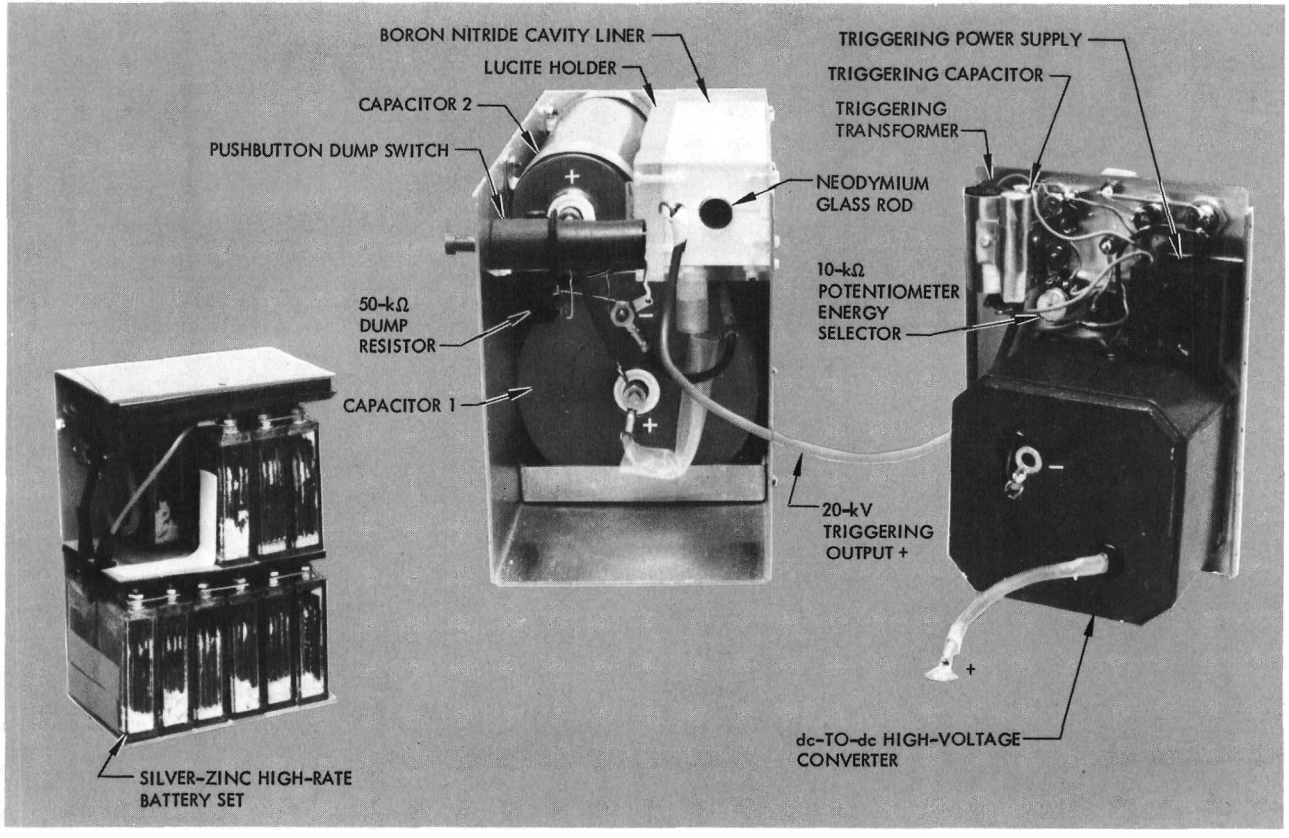

Fig. 1. Interior of laser and battery package, showing electronic components

Yardney HR, 1.5-V, silver–zinc, high-efficiency batteries. At a 9-A discharging rate, it provides 28 V dc with about 1.5-A-hr life, which is sufficient for 50 laser operations at highest laser output levels.

The high-voltage safety factor was designed to be about 20, based on 1.2 $\times$ 10^4-V/mm insulation strength. A pushbutton dump switch is provided to allow the high-voltage energy to be bypassed and discharged through a 10-W 50-kΩ power resistor.

Laser Performance

Figs. 2a and 2b are oscillograms showing the xenon flash lamp discharge. Voltage and current agreed quite well with the design estimates. Fig. 2c shows the lamp light output at 4.9-kV discharge, as seen by a Korad S-1 vacuum photodiode. Fig. 2d shows the corresponding laser output of 16 J via a MgO reflector and the same diode in the characteristic relaxation manner modulated by the flash lamp light output shape. The lower triggering limit of the flash lamp was about 3.4 kV of bank voltage, which gave a laser output of 4.5 J. The slope efficiency is therefore about 3% and the absolute efficiency is 2.5%, which are fairly close to the maximum yellow-light-band efficiency produced by an xenon flash lamp (Ref. 4). After approximately 300 operations, the maximum laser energy output remained at a constant value of 16 J, even during short-term continuous pulsing (10 shots in series). The interior of the laser head showed no sign of deterioration, which was encouraging with respect to the reliability of the laser.

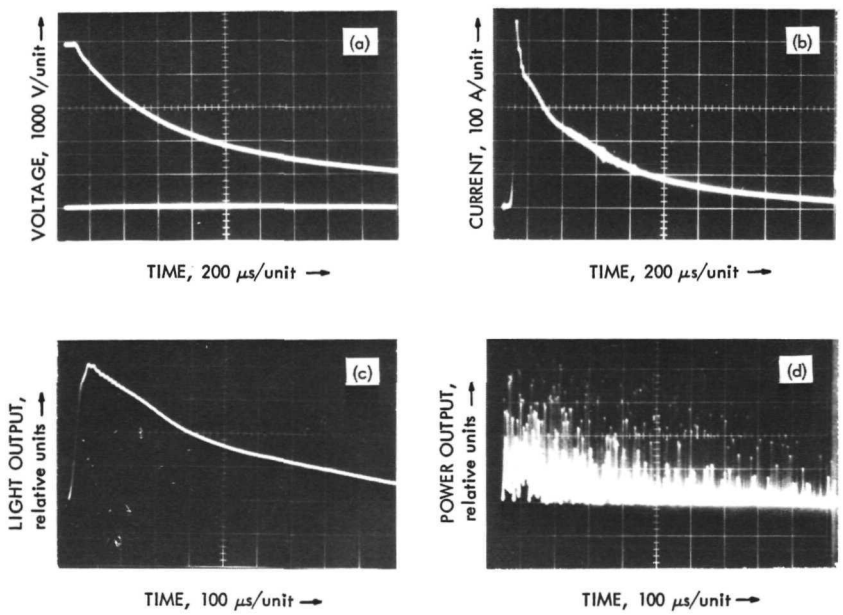

Fig. 2. Laser performance characteristics at 4.9-kV discharge: (a) flash lamp voltage, (b) flash lamp current, (c) flash lamp light intensity output, and (d) laser power output (16 J)

Since both the high-voltage converter and the capacitors have a maximum capability of 6 kV, it is safe to operate the system at a 5.5-kV level. The projected laser energy would then be approximately 20 J. There is space available in the laser package to allow the installation of a passive Q-switch unit. Assuming a 20% Q-switch efficiency, the system is therefore capable of producing more than 3 J of Q-switched output.

Pyrotechnic Ignition

A laser pyrotechnic ignition system consisting of a laser, pyrotechnic devices, and fiber optics has been assembled and is shown in Fig. 3. Fig. 4 shows the laser pyrotechnic ignition device. It has the same external dimensions as the SBASI (single-bridgewire Apollo standard initiator), but the electrical connector has been modified to accept a fiber-optics bundle. The bridgewire/header has been replaced with a glass-to-metal sealed window designed to withstand at least 3.5×10^8 N/m^2 of pressure. The pyrotechnic mixture is NH_4ClO_4/Zr (50/50). The high light absorption of zirconium in the visible and near IR, combined with the diffusive internal light scattering of NH_4ClO_4 crystals, resulted in an 85% absorbability for the mix in this spectrum range. The laser sensitivity of the device was 0.77 J/cm^2 when pressed under 3.45×10^7 N/m^2 of pressure against the glass window.

Glass was chosen for the fiber optics rather than plastic, because glass has better transmission at 1.06 μm and better resistance to deterioration under

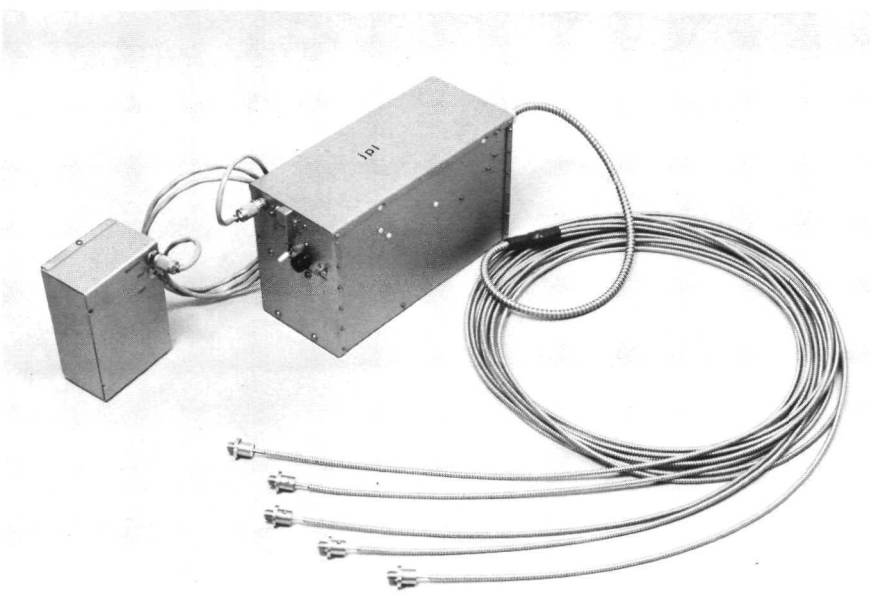

Fig. 3. Laser pyrotechnic ignition system

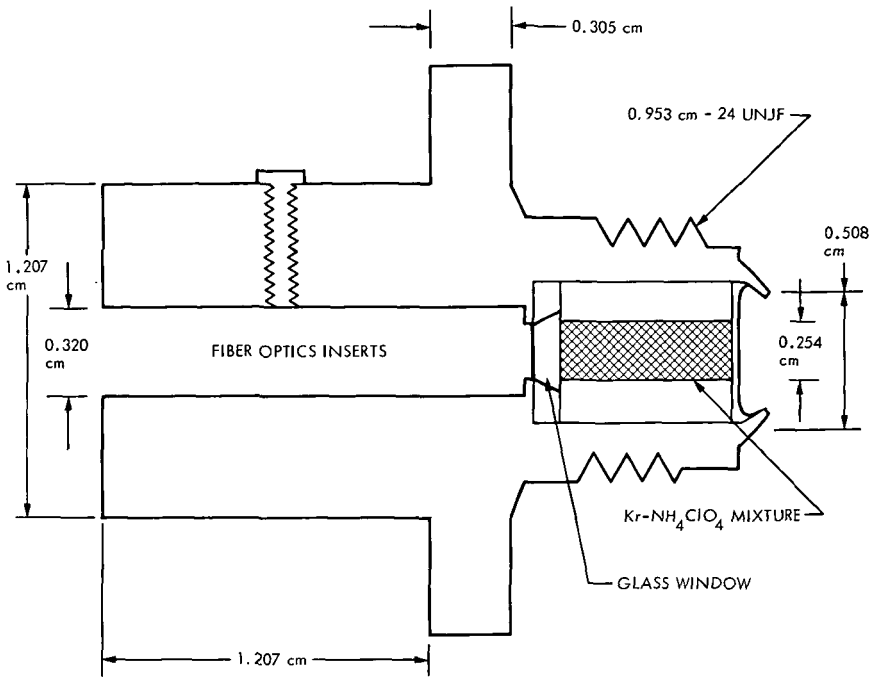

Fig. 4. Laser pyrotechnic ignition device

the intense focused neodymium laser beam. For commercially available glass fiber-optics bundles made from 70-μm-diameter individual fibers, the light transmission at 1.06 μm can be expressed as $I/I_0 = e^{-\alpha x}$, with α typically of the order of 0.4/m.

A test was conducted to demonstrate the simultaneous initiation of five pyrotechnic devices. The fiber optics for this particular test was fabricated to have a single input that branched into five identical output fiber optics. The total length to each pyrotechnic device was 3.7 m. Randomization of the individual fibers resulted in equal light splitting within ±5% at each output and independent of the light input distribution. The gas pressure generated by the burning pyrotechnic material was monitored by the same method as that used for spacecraft electroexplosive devices. The system consists of a 1-cm^3 pressure bomb, a Kistler 607A pressure transducer, and a Kistler 504A (or 504, 503) charge amplifier. The results of the test at 16-J laser output energy, as recorded by two oscilloscopes, are shown in Fig. 5. The sharp-rise peak pressure in each channel was reached within approximately 0.2 ms after the start of the laser pulse. This time can be associated with the burning time through the 0.25-cm-long pyrotechnic column. In other words, due to the high laser energy used in the experiment, the pyrotechnic starts to react in tens of microseconds upon receiving the laser pulse. This type of ignition characteristic is very desirable for the functioning of pyrotechnic devices.

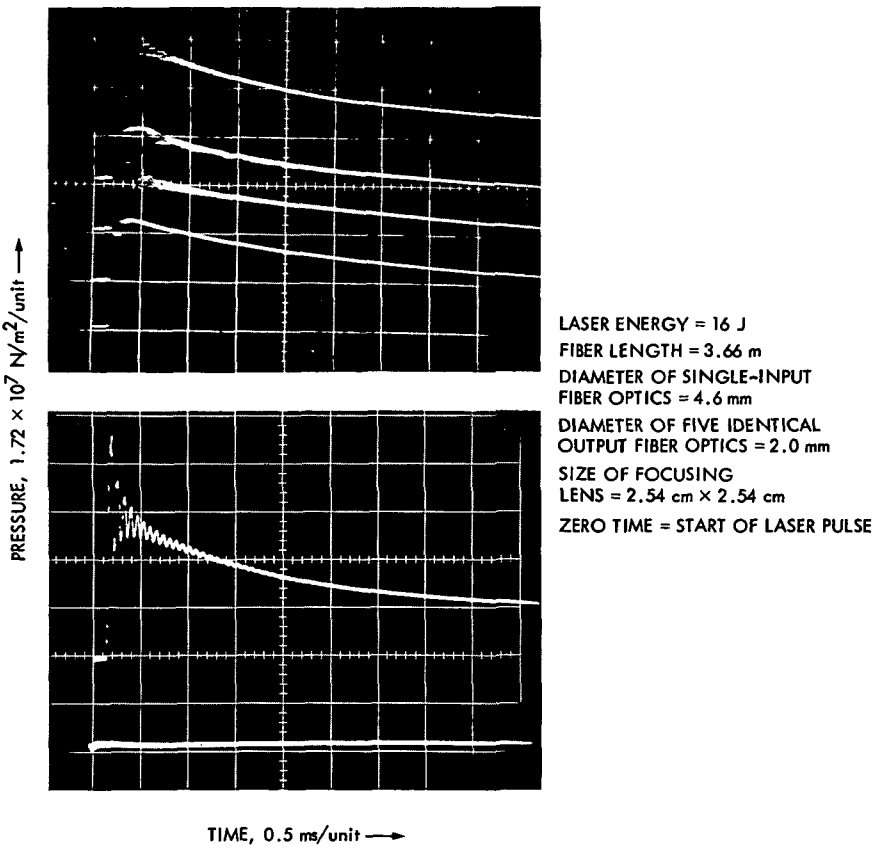

Fig. 5. Test record of simultaneous initiation of laser explosive devices by laser energy

Some Bruceton-type tests are planned in order to establish all fire and no-fire laser energy limits. The 16-J laser energy available in the system is capable of initiating as many as 20 devices simultaneously through a 3-m-long fiber optics or a single device through an 18-m-long fiber optics.

Work in Progress

In view of the progress made, especially in the achievement of high laser efficiency, plans have been made to build a smaller laser pyrotechnic ignition system suitable for spacecraft applications. A laser ignition system of 5.1- × 7.6- × 12.7-cm size, less than 0.7-kg weight, and approximately 2.0-J output will be sufficient to actuate four pyrotechnic devices simultaneously at a distance of 3.0 m (through fiber optics). This would satisfy the requirements of, e.g., the Viking lander separation mechanism. At first glance, it appears to involve a scaling down of the present laser; however, analyses have indicated that some fundamental changes in the design concept have to be adopted. For example, in order to achieve energy storage efficiency and flash lamp spectral efficiency, a linear or annular lamp

should be used instead of the helical lamp. Also, a low-voltage (500-V) capacitor with high capacitance (800 to 1100 μF) should be used. The only types of capacitors that satisfy the size and weight requirements are specially made electrolytic capacitors. Other components such as the triggering transformer have to be further miniaturized. Because of the lower pumping level (~100 J electrical), the laser output depends critically on the size of the laser rod and the reflectivity of the output mirror. Therefore, more caution has to be taken in the development. The development is proceeding on schedule and is expected to be finished by the end of fiscal year 1973. A parallel effort exploring the feasibility of adopting better fiber optics is also under way. The latest developments in this area are fused-end glass fiber optics, continuous reflection index clading fiber, and low-attenuation fiber waveguides.

Acknowledgement

The authors wish to acknowledge the assistance of Lloyd H. Swanson of the JPL Propulsion Division in performing the pyrotechnic tests and Fred J. Cairo of the JPL Fabrication Services Division in helping fabricate the laser.

References

1. *Investigation of Laser Beam Profile Uniformity*, Final Technical Report, NASA Contract No. NAS 7-744. Owens Illinois Co., Toledo, Ohio, March 1970.

2. Schuldt, S. B., and Aagard, R. L., *Appl. Opt.* Vol. 2, p. 509, 1963.

3. Gonoz, John H., *J. Appl. Phys.*, Vol. 36, p. 742, 1965.

4. Gonoz, John H. and Newell, P. Bruce, *J. Opt. Soc. Am.*, Vol. 56, p. 87, 1966.

JPL Quarterly Technical Review Volume 2, Number 4 January 1973

Index: electronic components and circuits, pyrotechnics

Generation of Narrow High Current Pulses

V. J. Menichelli and L. A. Rosenthal

Propulsion Division

Many of the fundamental factors affecting the initiation of electroexplosive devices have not been satisfactorily explained. A description of a narrow, high current pulse generator capable of pulses 4 microseconds wide and 94 amperes is given which will be useful in the study of the initiation mechanism.

Introduction

The most critical area of an electroexplosive device (EED) is the bridgewire/header/explosive interface. The bridgewire acts as an electrothermal transducer accepting electrical energy and converting it to heat, consequently causing ignition of the explosive. The behavior of the bridgewire with various forms of electrical input energies and its coupling to the explosive material are of basic interest because many fundamental factors affecting the initiation of EEDs have not yet been satisfactorily explained. Increased reliability in EEDs can be realized from a thorough understanding of the initiation process.

Initiation of EEDs is presently categorized in at least three ignition regimes. These regimes are best illustrated in the conventional sensitive EEDs (military type) requiring less than 5 A to initiate; the less sensitive 1-W, 1-A, no-fire EEDs requiring 3 to 20 A to initiate (used primarily in aerospace); and the 20- to 100-A input where the EED no longer obeys the simple current vs time-to-fire relationship but may be entering the regime of exploding bridgewires. Considerable data has been accumulated from conventional firings but little is known about the initiation process. It is felt that above 50-A input for 1-W, 1-A, no-fire EEDs, the bridgewire burns out electrically and subsequent electrical arcing is responsible for initiation. Arcing may also occur in the more sensitive military type EEDs at lower current inputs. Little is known about this mechanism and latest data indicate that another current vs time-to-fire relationship may exist.

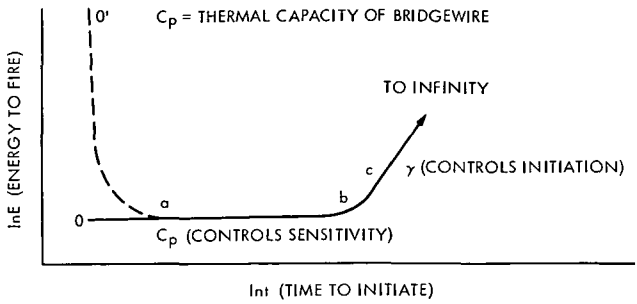

A plot of energy required as a function of initiation time (time from application of energy to first sign of light output) is given below. The plot indicates a region where anomalous behaviour is possible.

The region b to c is controlled by the heat loss of the EED (γ) and for constant current firing or long times the energy can increase to infinity or no fire. The region a to b corresponds to adiabatic firing or constant energy input. For extremely narrow pulses, it has been observed that the energy increases and a possible explanation is the inability to deliver energy rapidly in a typical electrical firing system. The region a to 0, theoretically predicted, may follow a to 0'. There is some speculation that for very fast energy delivery, degradation of heat transfer to the explosive at the bridgewire interface may be responsible. A method for delivering large current pulses for times less than 10 μs would be required to study this firing region.

Pulse Generator

The half-sine wave pulser has the capability of these rapid deliveries. A large amount of energy in a short time corresponds to a high "power" pulse. For the sine wave pulse,

$$\text{energy/time} = I^2 R t_w / 2t_w = I^2 R/2$$

$$\text{power} = \frac{V^2 C}{L} \times R/2$$

Since $Q = \sqrt{\frac{L/C}{R}}$ and must be 5 or greater for good half-sine waveform, the power follows as:

$$\text{power} = \frac{V^2}{Q^2 2R}$$

where R is the EED + circuit losses. As a conclusion, the only independent way to generate high power pulses is to go to higher operating voltages.

A system operating at voltages of nominally 1000 V with a Krytron as a discharge switch proved to be the most efficient mode of generation. A Krytron is a cold cathode gaseous discharge device of proven reliability from exploding bridgewire systems. It can operate at currents of 30 to 1200 A at voltage levels up to 5000 V. Early experiments proved that it would turn-off or commutate with a reverse oscillation, characteristic of the half-sine wave ring.

The circuit of Fig. 1 shows the essential components. Power supplies are not shown and most of the testing was performed on a +1000 V, +300 V supply. For energy control, the high voltage supply was made variable. Switch S1 is a mercury-wetted switch, normally closed. Upon opening, a +300 V trigger pulse is injected to the Krytron. This same pulse can be used for scope triggering and should not be excessively long compared to t_w or the Krytron will not commutate. The EED or load shown as R was a 1-Ω resistor in the tests to be described. An assortment of L-C combinations were evaluated.

Figure 2a shows the pulses generated by a 70-μH inductor for two capacitor sizes. The capacitors were mica RF varieties rated at 2000 V and the largest energy corresponded to 66 A peak at a t_w = 10 μs or 22 mJ. In

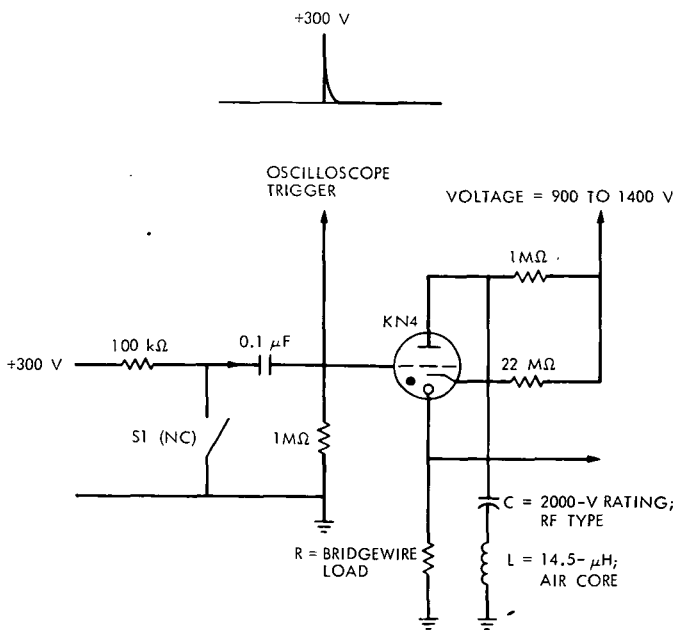

Fig. 1. Pulse generating circuit

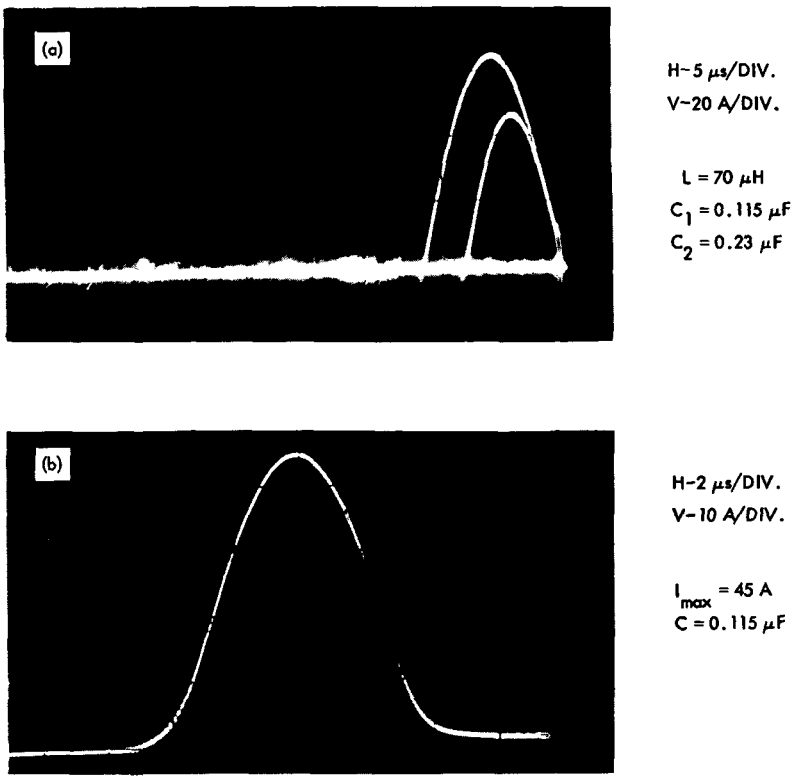

Fig. 2. Several half-sine pulse waveforms: (a) half-sine wave pulses generated in a 1-Ω resistor; (b) pulse generated employing a ferrite core

Fig. 2b, a "pulse" reactor employing a ferrite core produced a "sine-squared" type of pulse with I_{max} 45 A at t_w = 7 μs. The delay in the pulse rise is attributable to the nonlinear flux linkages (λ) characteristic.

In Fig. 3, a transmission line was explored as a means of obtaining a more rectangular pulse waveform. A cable of approximately 300 m in length replaced the L-C circuit. Since the characteristic impedance (Z_0) of the cable limits the discharge current to V/Z_o the maximum current was 20 A. Attenuation in the cable produced tilt in the waveform and at the rapid start and termination of the pulse, a large shock excitation oscillation was apparent. This confirms the concept that discontinuous (i.e., rectangular) pulses cannot be properly delivered to a load. A smooth sine wave pulse is generally superior. The pulse width was 2.8 μs corresponding to two delay times for the transmission line.

Figure 4 shows an acceptable pulse waveform generated with an inductor of 14.5 μH. At 1000 V the amplitude was 90 A at t_w = 4 μs, and 4 shots were superimposed to indicate the absence of jitter in the proposed circuit. The energy was 16.2 mJ, but by increasing the supply voltage to 2000 V, 64

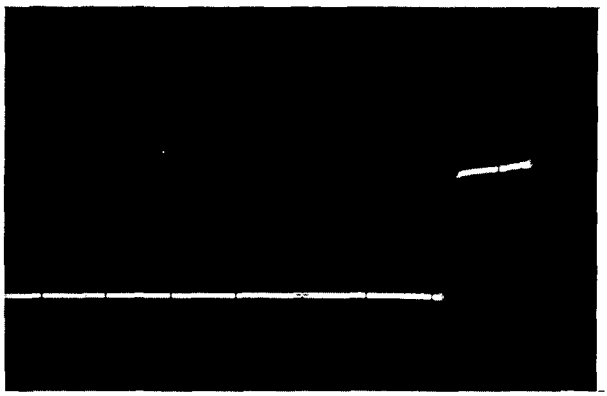

Fig. 3. Pulse waveform generated from an approximately 300-m cable

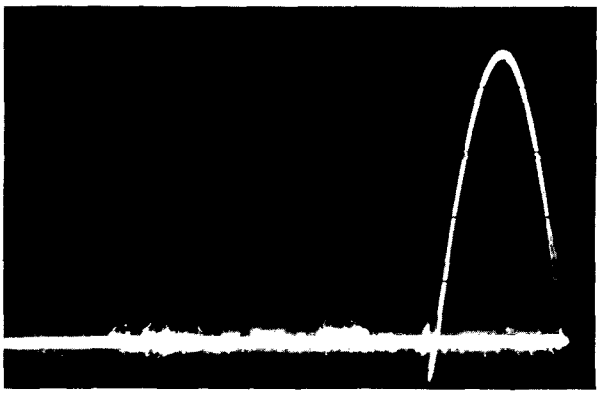

Fig. 4. Acceptable pulse waveform generated with an inductor of 14.5 μH

mJ could be obtained. The upper limit of the circuit was not explored and but for the inability of the Krytron to self-commutate, there is no reason to expect any problem. The substitution of a higher power Thyratron (3C45) as an alternate solution is possible. The capacitor size could be doubled to increase the energy by $2^{3/2}$. With C = 0.23 μf, a pulse width of 6 μs and peak current of 120 A was obtained with good waveform symmetry.

A compact instrument for delivering the required energy pulses can be built. The power supply should be adjustable up to 5000 V and two or more capacitors with a tapped inductor would offer pulse width and energy (coarse) control.

Applications

The pulse generator will allow the study of explosive initiation in the three regimes indicated above and in particular the transition between regimes. Other areas of interest resulting from this study will be the behavior of I^2t or "action" that theoretically should be a constant. The data will give a greater scope in the design of firing circuits (through relief of present electrical restrictions), which can be lighter and more compact. Also, skin effects and efficiency of energy transfer can be studied.

Index: environmental sciences, industrial processes and equipment, power sources

Development of a Thick-Film Silicon Ribbon Growth Technique for Application to Large-Area Solar Cells and Arrays

P. A. Berman

Guidance and Control Division

A new technique is described for growth of large-area silicon ribbons. This technique is an edge-defined, film-fed growth process by which single crystals can be grown having a shape controlled by the *outside* dimensions of a shaping die, growth taking place from an extremely thin film of liquid fed by capillary action from a crucible below. The material from which the die is fabricated is very critical to the process. The die must be wet by the silicon, but adverse impurities must not be introduced into the silicon, and the die must not become degraded by the molten silicon. A breakthrough in die fabrication that has allowed the growth of silicon ribbons having dimensions of 1 cm by 30 cm with a thickness of 0.7 mm is described. The implications of this significant advancement with respect to development of photovoltaic solar arrays for wide-scale terrestrial solar-to-electric energy conversion systems are discussed.

Introduction

The phenomenal growth of electrical power consumption has been well documented as has the environmental impact associated with satisfying these growth requirements. Public concern is being expressed in increasingly intense terms with respect not only to the obvious pollution caused by fossil-fuel-burning electrical power generators, but also to electrical power generation by nuclear reactor systems because of their inherent problems in safety, waste disposal, fuel, and thermal pollution. Solar photovoltaics, on the other hand, represents a very benign method of electrical power generation because the conversion process is totally nonpolluting, has no moving parts, does not consume fuel of any kind, and does not require heat (in fact, heat decreases the conversion efficiency). Photovoltaic solar arrays, which have successfully operated in the environment of space to provide electrical power for almost all unmanned spacecraft, are at the present time far too expensive for wide-scale use for terrestrial electrical power generation. This is primarily due to the high costs of ultrapure, single-crystal

silicon, of processing of the silicon into photovoltaic converters, and of fabrication of the photovoltaic converters into solar arrays (Refs. 1 and 2). For solar photovoltaic arrays to become economically feasible producers of electrical energy for wide-scale terrestrial use, these costs must be reduced by a factor of about one thousand over those costs presently experienced in the space program. It appears that significant progress towards these ends can be achieved through development of a thick-film silicon ribbon growth process for reasons outlined below.

Background

Silicon is the material from which space-type photovoltaic devices (solar cells) are fabricated because it is the most well understood semiconductor material from a device viewpoint (due to the research and development funded primarily by the semiconductor industry), and because it is capable of yielding solar cells having reasonable conversion efficiency (11 to 13%) and stability. Furthermore, it is a readily available semiconducting material, and although costly on an absolute basis, it is presently still the most economical material for photovoltaic converters on a dollar-per-watt basis.

To be economically attractive for wide-scale electrical power generation, however, solar cell costs must be decreased by approximately three orders of magnitude. A significant portion of these cell costs are associated with the use of ultrapure, single-crystal silicon, which presently costs on the order of $.30 per gram (Refs. 2 and 3), and which, in ingot form, the only configuration presently available, results in wastage of greater than 75% of the silicon by the time it is cut into rectangular blanks having a thickness of approximately 0.3 mm. Moreover, with respect to solar cell and array fabrication, a considerable fraction of the cost is involved in processing, handling, interconnecting, and attachment of large numbers of relatively small (the most common size having a 4 cm^2 area) solar cells and solar cell blanks (Refs. 1 and 2).

The use of large-area cells presents an overall cost advantage in array fabrication if the cells on a unit-area basis are no more expensive than the small-area cells. This is because the cell laydown and interconnection of fewer numbers of large-area cells should be significantly less expensive than for similar operations performed on a greater number of small-area cells. Similarly, the use of large-area blanks should result in a cost advantage in cell fabrication, with appropriate process modifications, because fewer pieces must be handled to fabricate a given total cell area (i.e., power generating capacity).

Large-area cells can be achieved by cutting the silicon ingot into large disc-shaped blanks (Refs. 4 and 5), rather than rectangular blanks as is presently the case, thus making use of the natural cylindrical geometry of the ingot, which can be grown with diameters as large as 7.5 cm. These cells, however, have a poor panel packing factor compared with rectangular cells and thus the power density of the array is compromised. Large rectangular cells can be obtained by a second method, namely by slicing the ingot so that

the major axis of the rectangle is parallel to the ingot growth axis, thus making use of the length of the ingot rather than the width (which is of smaller dimension). This latter method, however, necessitates a tradeoff between the maximum size of the blank as against ingot utilization due to the geometric constraints involved in cutting rectangles from cylinders.

One of the major systems proposed for large-scale solar photovoltaic energy converters is a Satellite Solar Power Station (SSPS) (Refs. 6 and 7), a large central electrical power generating station located in synchronous orbit, which, even using silicon cells having a thickness of 0.05 mm as contrasted with Mariner-type solar cells having a thickness of 0.4 mm, has a proposed system weight of 18- to 45-million kg (40- to 100-million lb). Slicing the silicon ingot to provide blanks of 0.05-mm thickness will result in even greater silicon wastage due to the increased number of saw cuts and lapping required per ingot (i.e., while the number of blanks per ingot is increased, the number of saw cuts is proportionally increased. Moreover, each blank must be lapped and etched, similar to thicker cells, so that the total silicon wastage per ingot is greater for 0.05-mm thick blanks than for 0.4-mm blanks). With respect to the cutting of thin silicon cell blanks, there must be a compromise between the maximum-area dimensions and the minimum-thickness dimension due to breakage factors associated with the relatively brittle silicon material. Hence it appears that ultrathin 0.05-mm-thick cells will be difficult to achieve for areas much greater than the commonly used 4 cm^2, if one is constrained to cut the blanks from an ingot as is presently done.

In addition, over and above the material wastage and breakage problems, the cutting operations induce defects in the silicon, which are to some extent removed by lapping and etching, but which still remain significant, adversely affecting the resultant cell performance.

Motivated by the need for large-area, highly efficient, lightweight (i.e., thin) solar cells, the Jet Propulsion Laboratory solicited proposals from industry pertaining to the development of thick-film silicon growth techniques. The effort as delineated by the JPL Statement of Work was to be directed toward a program "to develop a technique for producing P-type silicon films of quality, thickness, and area requisite to the production of low-cost, high-efficiency (sic), large-area solar cells." Thus the goal would be a process whereby silicon can be grown in the form of a large or continuous area "blank," requiring no lapping, sawing, or etching, making maximum use of the silicon material, and allowing the fabrication of very-large-area, thin solar cells. The effort defined by the JPL Statement of Work includes determination of process control requirements (e.g., thermal, mechanical, and operator control requirements, as well as in-process evaluation requirements), determination of maximum-area dimension capability, determination of film-thickness capability, determination and optimization of film dimensions, determination and optimization of consistency of film crystalline properties (such as resistivity, dislocation density, and impurity density), determination and optimization of film growth, determination of

stability of equipment used in processes, determination of in-process replenishment requirements of silicon and dopants, submission of 20 sample state-of-the-art silicon films having an area of 1 cm by 2 cm and a thickness of 0.1 mm, and submission of 10 sample state-of-the-art silicon films having an area of 20 cm^2 and a thickness of 0.1 mm.

On the basis of the responses received, JPL selected Tyco Laboratories, Inc. to perform this effort under JPL Contract No. 953365 (initiated February 1972) using the Edge-Defined Film Growth (EFG) process developed by Tyco for growth of sapphire ribbons, filaments, and tubes.

Description of the EFG Process

Edge Defined Film Growth is a process by which single crystals can be grown having a shape controlled by the *outside* dimensions of a die, growth taking place from an extremely thin film of liquid fed by capillary action from a crucible below (Ref. 8). This method appears to be more stable than other methods of shaped growth and shows great promise for being an industrially feasible process for the formation of single-crystal silicon ribbon directly and continuously from the melt.

A quartz crucible is used to contain silicon heated above the silicon melt point. The bottom surface of the die is immersed into the molten silicon such that the molten silicon is able to enter capillary slots or tubes located within the die; these slots are perpendicular to the top and bottom die faces. If the contact angle between the molten silicon and the die material is less than 90°, and the geometry of the capillary slots or tubes is properly designed, the molten silicon rises by capillary action to the upper surface of the die. The contact angle Θ is defined as the angle between the tangent of the molten silicon at the point of contact to the die material and the surface of the die at point of contact; that is to say, complete wetting corresponds to $\Theta = 0°$ and no wetting whatsoever corresponds to $\Theta = 180°$. A small diameter silicon seed having the desired crystallographic orientation is inserted into the capillary seed slot in the upper face of the die and the temperature adjusted so that the silicon solidifies onto it. By proper control of temperature and seed withdrawal rate, the molten silicon begins to spread across the die surface until it reaches the edges of the die, at which point the liquid spreading is halted because of the 90° change in effective contact angle at the outer perimeter. With proper adjustment of temperature and pull rate, the crystal will then continue to grow with a cross-sectional area and shape determined by the outside perimeter of the die. The physics of this process are such that it is self-stabilizing over a relatively wide range of power input fluctuations by means of changes in the thickness of molten film. Furthermore, the growth interface is effectively decoupled from the bulk melt surface, permitting continuous replenishment of the melt during growth. This is of great importance in establishing a low-cost process with maximum equipment utilization since the machine does not have to be shut down to replace the silicon charge and this is a considerable advantage of the EFG process over other methods of silicon growth. Another distinct

advantage is to be found with respect to consistency of chemical composition (i.e., impurity distribution). Because of the fast growth rate and the faster linear motion rate of the liquid supply, segregation effects are negligible and hence the solidified silicon crystal has the same chemical composition as the bulk liquid.

In the past, a significant research effort was expended by the Air Force on a webbed dendrite technique of ribbon growth, but the technique was not found to be economically feasible because of the very stringent controls required. For example, it was found necessary to maintain growth temperatures constant to within ±0.02°C, which not only imposed excruciatingly difficult control requirements but also rendered crucible replenishment practically impossible.

Because of the inherent characteristics of the EFG process, such stringent controls are not required. EFG-grown sapphire ribbon is routinely grown with minimum operator control at the Tyco facility. The contractor is commercially producing sapphire ribbons, cylindrical rods, and other complex shapes using the EFG technique.

The major problems to be overcome in the growth of silicon ribbons by the EFG technique are associated with the growth-die: specifically, the geometry of the die and the material from which the die is made. The die must be wet by the silicon, but adverse impurities must not be introduced into the silicon, and the die must not become degraded by the molten silicon. Because of the reactivity of silicon at growth temperatures (about 1400°C), these conditions are not easily satisfied; however, a significant number of options exist (Refs. 9 and 10).

The major advantages of the EFG technique are: production of accurately controlled cross sections, self-stabilization over relatively wide ranges of power input fluctuation by means of changes in the thickness in the molten film, growth rates limited only by latent heat removal from the solid-liquid interface, decoupling of the growth interface from the bulk melt surface permitting continuous replenishment of the melt during growth, arbitrary choice of crystalline orientation, minimization of segregation effects due to the fast growth rate and linear motion rate of the liquid supply, and high crystalline perfection.

Status of the Program

A number of techniques for fabricating the growth die are being investigated (Refs. 9 and 10). Dies made of the following materials are being evaluated: silicon carbide obtained by conversion of high purity graphite (for example Dow Corning Pyrobond), quartz-silicon combinations, quartz-silicon carbide combinations, graphite, and beryllium oxide. In conjunction with this, studies on the die configuration (geometry) are also being made along with methods of temperature control across the die surface. Thus, the approach is to investigate various materials as well as configuration of the die and methods of temperature control, including heat shielding, in an

attempt to mitigate the degradation of die materials. With respect to die configuration and temperature control, it appears advantageous to have the ends of the orifice receive less heat than the middle, and the configuration and shielding modifications are being made to achieve this end. A very brief description of the status of the die material investigations is given below.

Coatings of Silicon Dioxide on Refractory Metals and Silicon Carbide

These coatings were obtained by pyrolysis of silane in the presence of oxygen. The quartz films were too thin and/or too porous to resist molten silicon. This, coupled with a slow deposition rate, led to the abandonment of this technique.

Hot Pressed Silicon Dioxide/Silicon

Orifices were fabricated from hot pressed mixtures of SiO_2/Si in ratios of 5, 10, and 30% Si. These orifices were all unsuccessful because of the low strength of the mixtures. Tests of the wettability of these materials by silicon showed a tendency for the silicon within the structure to run out when molten and for the material to warp when it was in pieces the thickness of typical orifices. This technique has been abandoned.

Silicon Dioxide/Silicon Carbide

A slice of hot-pressed 80% quartz/20% silicon carbide with a small silicon chip was heated to approximately 1650°C, which is the typical temperature used to prewet orifices, for 10 min then cooled approximately to 1,450°C, typical of operating growth temperatures. The samples were held for 50 min at the 1,450°C temperature before cooling to room temperature. The silicon was found to wet the surface of the slice completely, stopping at only a few mils of penetration of the silicon into the bulk of the slice. In addition, the surface of the solid silicon left was very clean, without the ordinary haze of tiny reprecipitated silicon carbide crystals found when a similar experiment was done on silicon carbide material. Orifices of this material are currently being fabricated and evaluated.

Beryllium Oxide

The use of beryllium oxide will represent the first effort in evaluating entirely new die materials. It has been reported that beryllium dopes silicon P-type, so that if beryllium does tend to leach out into the silicon, it will at least be doping it in the proper direction. Experiments in this material have not yet been initiated but will be begun in the near future.

Silicon Carbide

The first attempts to grow silicon ribbon on this program were made utilizing pressed and sintered silicon carbide as the die material with quartz as the crucible material. Silicon carbide was wet by the silicon, and little difficulty was encountered in obtaining the initial capillary rise required for

a growth initiation. This was found to be especially facilitated when the silicon carbide was "pretinned" with liquid silicon before assembling into the shaping-die configuration. The resistivity of these initial ribbons was low, of the order of 0.1 Ω-cm, possibly due to either the leaching of impurities from the silicon carbide or from dissolution of the silicon carbide itself, the latter being observed upon inspection of the shaping-die after growth.

Initial dies fabricated from silicon carbide appeared to undergo severe degradation during the growth process and formed inclusions in the grown silicon ribbon. Also the resistivity of the resultant silicon was very low indicating contamination of the silicon by the die material. More recently, samples of various silicon carbide materials made by the conversion of graphite were evaluated by melting silicon on a piece of the material and holding it at a temperature typical of growth conditions. One material was clearly superior to the others in that it appeared to be very dense, and the wetting of molten silicon was confined to the surface.

Graphite

The most recent very positive results, of the nature of a breakthrough, have been obtained by utilizing a die fabricated from high-density, small-grain-size graphite material. Using this die in conjunction with a thicker molybdenum cover plate for increased thermal stability, ribbons having dimensions of 1 cm wide by 30 cm long with a thickness of about 0.7 mm have been grown. Cursory examination of the die indicated essentially no deterioration. This was further evidenced by measurement of 2- to 3-Ω-cm resistivity at several points along the ribbon, indicating that at least there was no gross contamination of the silicon by the die. More extensive evaluation of the crystalline properties of these ribbons will be undertaken in the near future; however, the success of the silicon ribbon program to date is encouraging.

Conclusions

A breakthrough in the growth of thick-film silicon ribbons by means of the EFG process has been achieved through improvement of thermal and mechanical growth system stability and through development of a shaping die fabricated from high-density, small-grain-size graphite material. Ribbons having dimensions of 1 cm wide by 30 cm long, and a thickness of approximately 0.7 mm have recently been grown as a result of these improvements. The suitability of these ribbons for solar cell materials still has to be evaluated.

This development program, if successful, could have an impact solar array fabrication technology, resulting in improved array fabrication techniques. The solar cells fabricated from large-area films, grown by means of the technique discussed, potentially can result in significant improvements in power density, weight, and economics. Furthermore, rather than fabricating an array from a large number of relatively small (4 cm^2 is the most commonly used size) solar cells and interconnecting them together, the array

could possibly be made of a far fewer number of cells, each having lengths of 20 cm, 30 cm, or even more.

If successfully developed, the described ribbon cell could be used to produce large-area, highly efficient, lightweight, economical solar arrays, and therefore would be particularly advantageous where these characteristics are of prime importance. The improved economics that could be realized through solar cell and array fabrication processes geared to take advantage of the large-area silicon ribbons would also enhance the feasibility of wide-scale, Earth-based solar photovoltaic electrical power generating systems (e.g., solar farms and rooftop solar-electric generators).

References

1. Berman, P. A., *Considerations with Respect to the Design of Solar Photovoltaic Power Systems for Terrestrial Applications*, Technical Report 32-1556. Jet Propulsion Laboratory, Pasadena, Calif., June 15, 1972.

2. Berman, P. A., *Photovoltaic Solar Array Technology Required for Three Wide-Scale Generating Systems for Terrestrial Applications: Rooftop, Solar Farm, and Satellite*, Technical Report 32-1573. Jet Propulsion Laboratory, Pasadena, Calif., October 1972.

3. Ralph, E. L., "Large Scale Solar Electrical Power Generation," presented at the Solar Energy Society Conference, NASA Goddard Space Flight Center, Greenbelt Md., May 1971.

4. Berman, P. A., *High Efficiency Silicon Solar Cells*, Report No. VIII, Final Report. Contract No. DA 36-039-SC-907, covering period from June 1962 to July 1964. U.S. Army Electronics Laboratories, Fort Monmouth, N.J.

5. Berman, P. A., "Design of Solar Cells for Terrestrial Use," presented at the Solar Energy Conference, Boston, Mass., March 1966. Published in *Solar Energy*, Vol. 11, Nos. 3 and 4, 1967.

6. Glaser, P. E., "Power from the Sun," *Mech. Eng.*, Vol. 91, No. 3, March 1969.

7. Ralph, E. L., and Benning, F., "The Role of Solar Cell Technology in the Satellite Solar Power Station," in *Conference Record of the Ninth IEEE Photovoltaic Specialists Conference, Silver Springs, Md., May 1972.*

8. Bates, H. E., Cocks, F. H., Mlavsky, A. I., "The Edge-Defined, Film-Fed Growth (EFG) of Silicon Single Crystal Ribbon for Solar Cell Applications," in *Conference Record of the Ninth IEEE Photovoltaic Specialists Conference, Silver Springs, Maryland, May 1972.*

9. Bates, H. E., Cocks, F. H., Mlavsky, A. I., *Thick Film Silicon Growth Techniques: First Quarterly Progress Report*, JPL Contract 953365,

covering period February-May 1972. Tyco Laboratories, Waltham, Mass.

10. Bates, H. E., et al., *Thick Film Silicon Growth Techniques: Second Quarterly Progress Report,* JPL Contract 953365, covering period June-August 1972. Tyco Laboratories, Waltham, Mass.

Index: environmental sciences, information distribution and display, management systems

Information Management System for the California State Water Resources Control Board (SWRCB)

T. C. Heald and G. H. Redmann

Data Systems Division

A study was made to establish the requirements for an integrated state-wide information management system for water quality control and water quality rights for the State of California. The data sources and end requirements were analyzed for the data collected and used by the numerous agencies, both State and Federal, as well as the nine Regional Boards under the jurisdiction of the State Board. The report details the data interfaces and outlines the system design. A program plan and statement of work for implementation of the project is included.

Introduction

The extraordinary growth in population, resulting in increased industry, irrigated agriculture, and the ever-growing demands for water-oriented recreation has increased water use at a tremendous rate. Unless new and better ways of reducing pollution and managing water resources are found, the nation not only faces the potential of having a water-limited economy but also complete crisis of the water environment.

In California, the State Water Resources Control Board (SWRCB) is designated as the State Water Pollution Control Agency for all purposes stated in the Federal Water Pollution Control Act. The State Water Quality Control Act states that "The health, safety, and welfare of the people requires (sic) there be a statewide program for the control of the quality of all waters in the state."

To meet this requirement, the SWRCB entered into an agreement with JPL to perform a joint study to formulate the State Board's data management needs for an information system and to outline the system design, including the development of cost estimates and an implementation plan/schedule.

Study Constraints

In keeping with the desire to implement the data management system as early as possible and with maximum use of existing hardware, the following constraints were applied:

1. Use the STORET system of computer programs operated and controlled by the Environmental Protection Agency (EPA), Office of Water Quality (OWQ).
2. Use the existing California Department of Water Resources (DWR) computer system.
3. Use a combination of both systems.

Approach

The formulation of a data system for the SWRCB required the gathering of information from numerous sources. Many types of data generated, collected, and stored in separate agency offices are important in conducting a comprehensive analysis of water quality within the State. Representatives from all major offices and agencies having responsibility and/or a vested interest in water quality management were interviewed and the information obtained from these offices was compiled and analyzed. From this information the basis for this integrated data system was developed.

Existing Information Flow

Discussions with the agencies and departments concerned revealed that a wealth of data is being gathered by the different organizations. Several groups are gathering data on water quality, and there is a considerable amount of data on related matters such as flow rates, land use, and withdrawal rate. Although individual organizations have responsibilities relating to the reporting of the data that they gather, the capability for interpretation and use of data would be greatly enhanced if the data were correlated with similar data gathered from other agencies. The exchange of data between agencies is essential to the comprehensive analysis of water quality. Figure 1 represents the collection of data by various agencies. It can be seen that all such data are a measure of water quality.

Proposed Information System

A central data processing system, utilizing a high-speed computer with data storage on magnetic tape and disk, could provide rapid access to most of the information that is being collected. Such a computerized system also would have the capability for processing the data to provide statistical summaries of water quality trends and would provide alarms when pollution increased to dangerous levels or decreasing flow rates were imminent. Figure 2 displays the way data can be gathered and distributed from a central system.

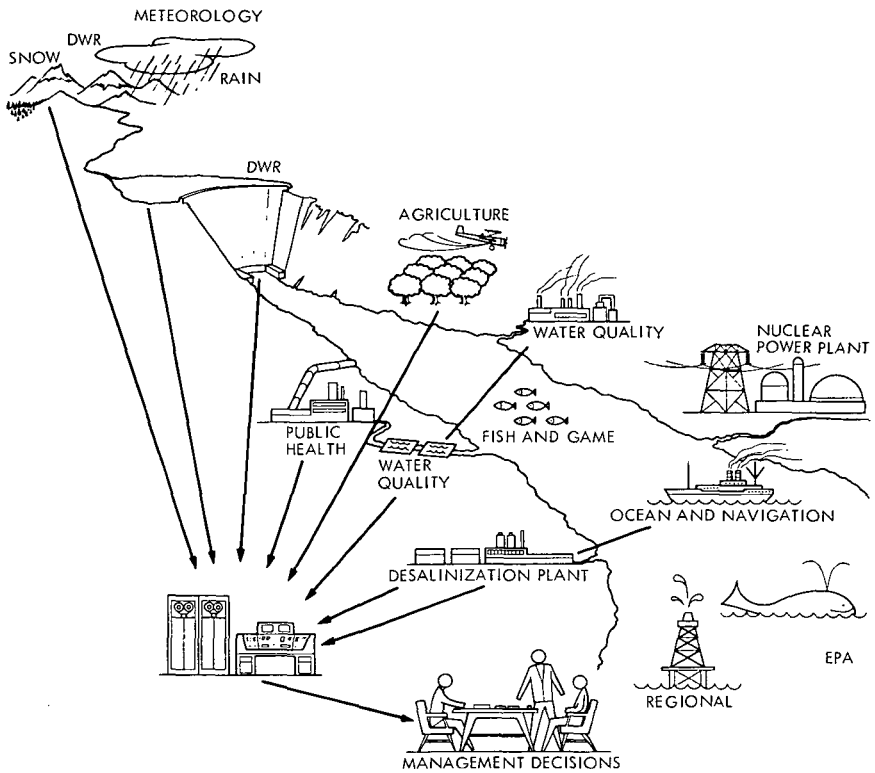

Fig. 1. Data network

Data System Development

An information management system must have as its foundation a stored data base, consisting of several files, containing all of the data required to analyze a particular subject. It is not necessary that all of the files be accessible to an instant inquiry on an interactive basis, although it is necessary that all files be available to the interactive portion of the data base. The overhead involved in a complete information system is great in storage and core requirements; therefore, only the central and most pertinent data files should be stored and retrieved with an interactive system, while the rest of the data base is accessible by batch programming methods.

The proposed data system relates directly to the needs of the State and Regional Boards. The system should interface automatically with the DWR data base to form one large bank of data bases containing all the information necessary for management decisions.

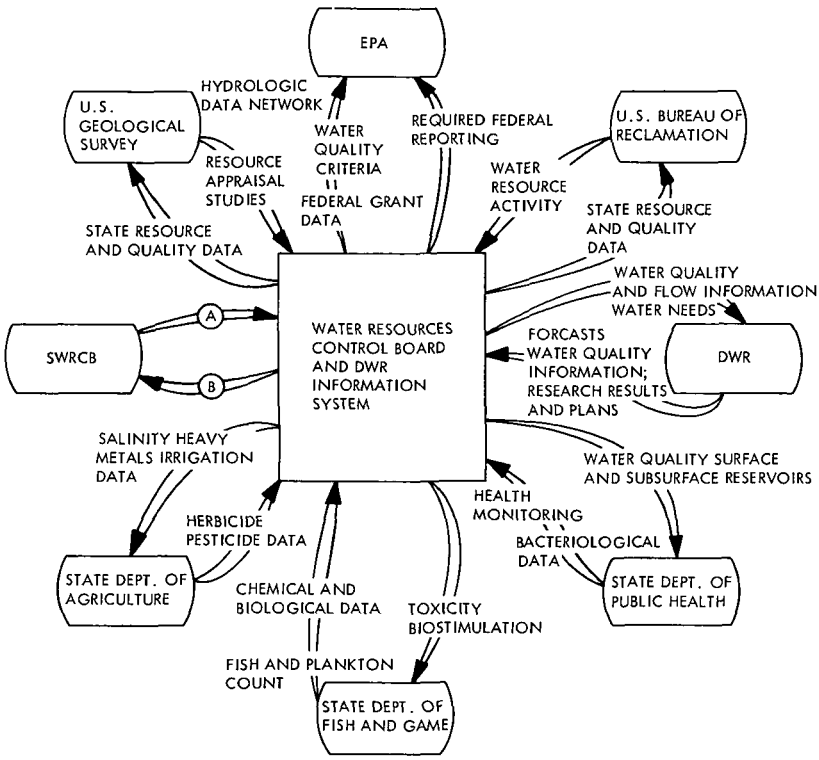

(A) WATER RESOURCES CONTROL BOARD

PLANNING AND RESEARCH
INFORMATION REQUESTS, SYSTEM PLANS, QUALITY GUIDELINES, AND RESEARCH RESULTS

REGION 2 BOARD
SELF-MONITORING DATA AND COMPLIANCE, CONTINOUS MONITORING OF BAY DELTA

REGION 4 BOARD
SELF-MONITORING DATA AND COMPLIANCE, CONTINOUS MONITORING OF L.A. HARBOR, BIOLOGICAL DATA

REGION 6 BOARD
SITUATION IN TAHOE

OTHER BOARDS
SELF-MONITORING DATA IS REQUIRED

WATER RIGHTS
WELL USERS AND WITHDRAWALS, FORECASTS OF GROUND WATER SUPPLIES

PUBLIC EDUCATION
REQUESTS FOR INFORMATION

WATER QUALITY CONTROL MODELING
FORECASTS

GRANTS ADMINISTRATION
REPORTING AND CONSTRUCTION STANDARDS

(B) WATER RESOURCES CONTROL BOARD

PLANNING AND RESEARCH
WATER QUALITY DATA, FORECASTS, TREATMENT PLANT PROGRESS

REGION 2 BOARD
QUALITY STRANDARDS, FORECASTS

REGION 4 BOARD
QUALITY STANDARDS, FORECASTS

REGION 6 BOARD
LAND USE INFORMATION AND RELATED SITUATION FORECASTS

OTHER BOARDS
QUALITY STANDARDS

WATER RIGHTS
QUALITY STANDARDS

PUBLIC EDUCATION
WATER QUALITY INFORMATION, TREATMENT PLANT PROGRESS FORECASTS

WATER QUALITY CONTROL MODELING
WATER QUALITY INFORMATION

GRANTS ADMINISTRATION
QUALITY STANDARDS

Fig. 2. Data interfaces

It is assumed that most of the terminal inquiry needs are in the Regional and State Board divisions. To satisfy these needs, the described system is structured with interactive files for terminal inquiry and batch files in combination with interactive files for analytical and statistical studies.

The files that make up the interactive portion of the data base contain the information that is most in demand by the regional offices. These files should be stored and retrieved with a data management system that allows both on-line terminal inquiry and information manipulation with conditional parameters. The requirement for a report-generating capability is important in formatting data to the terminal.

The remaining files in the data base contain all of the other information necessary for comprehensive analytical studies. These files may be stored either on tape or on direct access devices, but they must interface with the interactive portion of the data base through the use of compatible identification coding (Fig. 3).

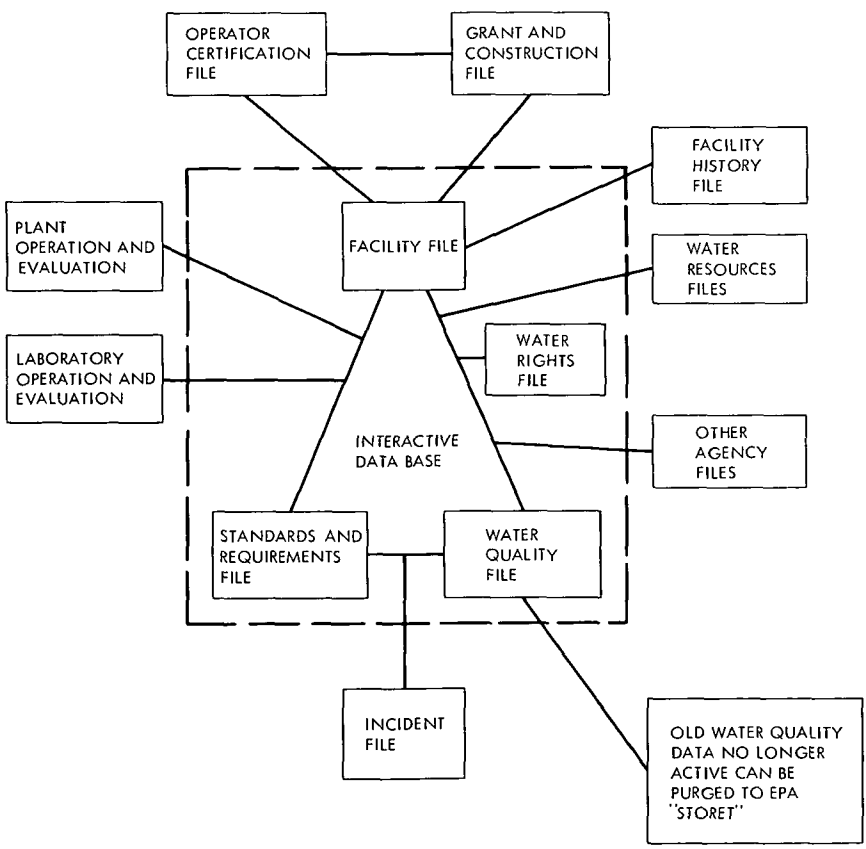

Fig. 3. Data base file structure

It is important that the detail design of the system take into consideration the expansion of data parameters on any file. The advantage of using an information system such as MARS III is that the files can be reformatted and restructured with very little impact upon the total system. Provisions should be made in the system design so that any of the information files can be made a part of the interactive portion of the data base with very little impact upon the total system.

Identification Coding

A coding structure for identification by location must be designed before any correlation of data can be made. This identification code must incorporate the present methods used by FWQA and DWR in addition to other in-depth coding. The coding should be designed so that correlation can be made by all or any combination of the identification codes. For full correlation of data, the identification coding should include, but not be limited to, the following items:

(1) Region.

(2) Basin.

(3) Sub-basin.

(4) Stream number.

(5) Mileage from mouth.

(6) Latitude.

(7) Longitude.

(8) Surface or sub-surface.

(9) Depth (if sub-surface).

(10) Station number.

(11) Discharger number.

Data Base Description

The requirements of the regional offices are so varied that rapid terminal access of data base information is a necessity. The ability to manipulate and format the data by the use of conditional parameters is a necessary requirement. The data base file structure is shown in Fig. 3.

The *Interactive Data Base* is described as follows: as the flow of data concerning water quality measurements enters the Water Quality File, the parameters can be automatically compared to the requirements for each parameter on the Standards and Requirements File and the engineering data on the Facilities File. This comparison can then establish variances from the base line and perform trend analysis and produce alarms when required. This process, over a period of time, can also perform evaluations on plant and laboratory operations.

The *Facility File* contains all of the administrative and technical descriptions of a discharge facility. This data includes process type, type of discharge, financial and manpower requirements, and compliance information.

The *Water Quality File* contains all of the quantitative and qualitative laboratory analysis data obtained from self-monitoring stations, regional test samples, and automatic monitoring devices.

The *Standards and Requirements File* contains all of the requirements and regulations established for each location. All regulated water quality data would be compared to the standards to determine compliance.

The *Water Rights File* contains data concerning regulated withdrawals from public surface and ground waters.

Output Reporting Requirements

The reporting requirements of this system are many and varied. There are requirements for detail reporting in many areas. Engineers have a need for baseline and trend reports. All offices have requirements for summary reporting capabilities. Graphic representation is required by both the State and Regional Offices. Statistical reports are required by management in all areas. The State and Regional Offices in research and special studies need modeling and simulation capabilities. The described data system provides the data necessary for all of these requirements. Some of the reports to be supplied by the system to various offices and agencies are:

(1) Periodic summary reports.

(2) Baseline and trend reports.

(3) Graphical time/performance reports.

(4) Evaluation reports on operators and laboratories.

(5) Source water quality and flow-rate reports.

(6) Statistical reporting involving history and trends.

(7) Data for quality basin modeling and simulation.

(8) Summaries of withdrawals.

(9) Prediction of downstream effects of withdrawals.

(10) Reporting required by EPA-OWQ.

(11) Special request by condition code.

(12) Land use reports and forecasts.

(13) Pesticide reporting.

(14) Incident reporting.

Future Expansion of System Capabilities

A study was performed to determine the impact of automatic sensing and monitoring upon any central system. The joint proposal submitted by Region 2 and USGS for three monitoring stations in the San Francisco Bay Region was used as a basis for the study. Each station was to be interrogated every two hours by a central station. Each station was to monitor six parameters: (1) tide gauge, (2) temperature, (3) pH, (4) dissolved oxygen, (5) turbidity, and (6) chlorides.

The study produced an alternative computer-controlled data acquisition system that could be used and could be tied to the central information system. A program would be required in the system to screen this data to store only trend and variance information. The alternative sensing and monitoring system is described in Fig. 4.

The requirements were examined from the point of view of a general purpose computer-controlled data acquisition problem rather than from a water quality sensor problem. Because the remote stations would be fixed,

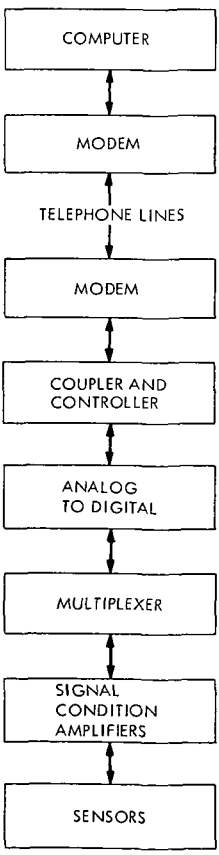

Fig. 4. Computer-controlled data acquisition system

land based, and capable of housing equipment in a protected environment, only commercial off-the-shelf data systems were considered. Additionally, due to funding constraints, communications between the remote stations and the central station were considered restricted to common-carrier switched telephone circuits.

Index: information theory, telemetry and command, wave propagation

On the Feasibility of Efficient Multiamplitude Communication

J. G. Smith

Telecommunications Division

Bandwidth constraints in Earth-satellite communication systems force consideration of uncoded M-ary modulation to obtain increased data rates. M-ary phase shift keying (MPSK) at first glance seems most promising because of the high transmitter efficiency achieved through Class C operation. Multiple phase-and-amplitude modulation candidates such as quadrature amplitude shift keying (QASK) appear less promising because the transmitter must operate at lower efficiency (in linear or multimode operation). However, initial studies indicate that QASK offers significant raw dc-power savings over MPSK, despite the reduced transmitter efficiency. For example, at S-band both solid-state and traveling wave tube (TWT) QASK transmitters can provide a 3-dB average dc-power savings over comparable 16-ary phase shift keying (PSK) for the same bit rate and error probability. The reason for this savings is that QASK requires much less average signal-to-noise ratio that 16-ary PSK for the same error rate.

Introduction

In a bandwidth-constrained communication environment, one means of achieving an increased data rate for a fixed channel bandwidth is to increase the number M of signal levels. Four-phase phase shift keying (PSK), for example, is replacing binary PSK in many such environments because of the doubled data rate at no price in band-width, power, or bit error rate. Further increases in data rates are available with M-ary phase shift keying (MPSK) in general by increasing transmitter power. Most significantly, MPSK transmitters can operate in a saturated (Class C) mode because of the constant energy nature of the signals. Thus, the relatively high transmitter efficiency of binary PSK can be maintained independent of the number of levels M.

Another form of M-ary modulation warranting consideration is quadrature amplitude shift keying (QASK), a form of multiple phase-and-amplitude modulation. QASK is inherently more efficient in terms of average transmitted power than MPSK. Variable amplitude signals, however, must

have lower transmitter operation efficiencies than those of MPSK. This is because the transmitters must be run Class A (for linear operation), or use data-rate-switched Class C final amplifiers (multimode operation). It will be shown, however, that QASK, despite the poorer transmitter efficiency, compares favorably on a raw power basis with MPSK.

In selection of a system to meet the requirements of a communication environment with specified data rate, bandwidth, noise level, and error rate, competing systems initially must be compared on the basis of the raw dc power needed to meet the communciation requirements. If the system average power-to-noise density ratio (PNR) is defined as PT/N_o, where P is the average required dc power, T is the reciprocal of the specified bandwidth, and N_o the specified noise level, then selection can be said to be made on the basis of minimum PNR.

The PNR can be written as the ratio of average signal-to-noise ratio (SNR) to average transmitter η. That is, transmitter efficiency η is S/P, where S is the average RF output power, and SNR is ST/N_o. Thus, PNR = SNR/η, and competing systems can be compared on the basis of the ratio of required SNR to transmitter efficiency η. The reason for portraying the PNR as this ratio is that even though one system has a lower transmitter efficiency than another, it may still be preferred if its SNR requirement is sufficiently low.

The aim of this article is to show that there are QASK transmitter configurations with lower PNRs than competing MPSK despite the reduced transmitter efficiency. This is possible because the required SNR of the QASK system is considerably less than that of a PSK system.

It is first shown that a particular multiple phase-and-amplitude system denoted QASK4, requires only 40% of the SNR necessary for 16-ary PSK (PSK16) with the same bandwidth, data rate, and error rate, at all error rates less than 10^{-3}. Then the transmitter efficiency of PSK16 is compared with the transmitter efficiency of two QASK4 transmitter configurations. Finally, the PNR's of the PSK16 and the QASK4 systems are compared.

The approach taken in the second and third steps is to specify four S-band PSK16 systems, with RF output powers of 1, 10, 20, and 30 W, respectively, and to compare each of these with one or more QASK4 systems of appropriately scaled average RF output power. This is to permit consideration of the transmitter efficiencies at realistic power levels and operating frequencies. Each of the four PSK16 systems are assumed appropriately sized for a communication environment of established noise level, bandwidth, and data rate. Power drains and efficiency of the S-band devices required in each transmitter configuration are based on current development technology levels.

In the next section, the QASK4 and PSK16 forms of modulation are described, and the 4-dB SNR advantage of QASK4 over PSK16 is verified. In the section, "Transmitter Configurations," transmitter configurations for achieving QASK4 are considered. Then in the section, "S-Band Device

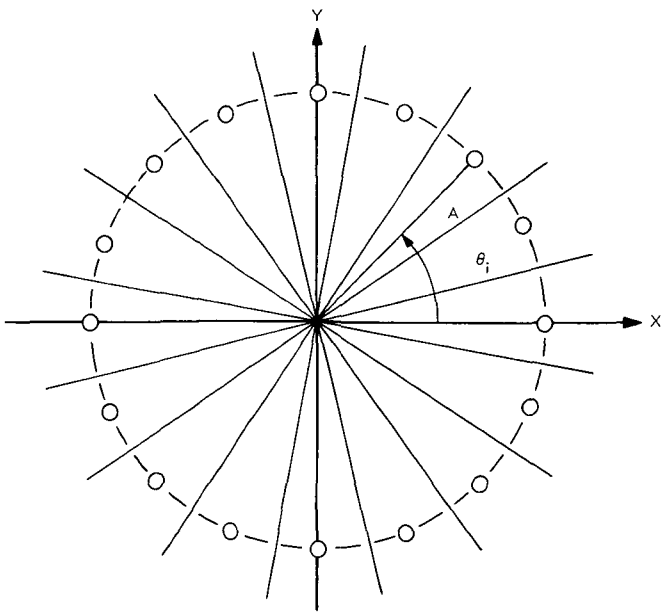

Fig. 1. PSK16 circular structure

Models," several S-band device models are specified, and finally the systems to be considered are configured and compared in the last two sections.

Two Forms of Modulation

In the PSK16 system, during each signaling time T, one of 16 signals $s_i(t)$ is sent, where

$$s_i(t) = \sqrt{2}\ A \cos [\omega_o t + \Theta_i], \quad i = 1, 2, \ldots, 16$$

frequency ω_o is S band, and the phases Θ_i are uniformly distributed around a circle, as shown in Fig. 1. The average RF signal power S is the square of the amplitude A, the bandwidth is the reciprocal of the signaling time T, and the data rate is $4/T$ bits/s. The signal $r(t)$ received during the signaling time T is $s_i(t) + n(t)$, where $n(t)$ is a sample of Gaussian white noise of two-sided noise level N_o. The probability of an M-ary symbol being correctly received is equal to the probability that the received noisy signal $r(t)$ lies in the correct detection region (the decision regions are the pie-shaped regions of Fig. 1) (Ref. 1).

In the QASK4 system, during each signaling time T, one of the 16 signals $s_i(t)$ is sent, where

$$s_i(t) = \sqrt{2}\ [X_i \cos \omega_o t + Y_i \sin \omega_o t]$$

$$= \sqrt{2}\ A_i \cos\ [\omega_o t + \Theta_i]$$

and the (X_i, Y_i) as shown in Fig. 2, form a 4 by 4 matrix of uniformly spaced points. The matrix is characterized by the signal separation parameter Δ, where $X_i = \pm\Delta, \pm 3\Delta$, $Y_i = \pm\Delta, \pm 3\Delta$.

Alternately, the signal points can be characterized in terms of power levels A_i^2 and phases θ_i as shown in Fig. 3. Note that the three power levels have relative values of 1, 5, and 9 with average power equal to the middle value. This average RF output power S is $10\Delta^2$. As with PSK16, the probability of an M-ary symbol being correctly received is equal to the probability that the received noisy signal $r(t)$ lies in its correct decision region – in this case, the rectangular regions denoted in Fig. 2.

Asymptotically, for error rates $\leq 10^{-3}$, the probability of error is largely dependent upon the minimum distance d from a signal point to a decision region boundary (Ref. 2). In PSK16, $d = A \sin \pi/16$; in QASK4, $d = \Delta$. In either case, the average probability of error is about $\exp(-d^2T/N_o)$. Thus, for PSK16, $P_e \sim \exp(-\text{SNR}/25)$ while the QASK4 $P_e \sim \exp(-\text{SNR}/10)$. A comparison of the PSK16 and QASK4 systems with equal values of T, N_o, and

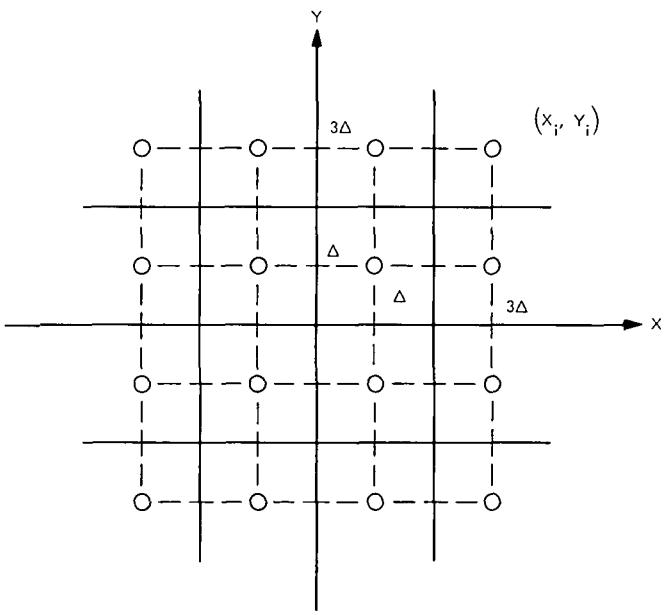

Fig. 2. QASK4 rectangular structure

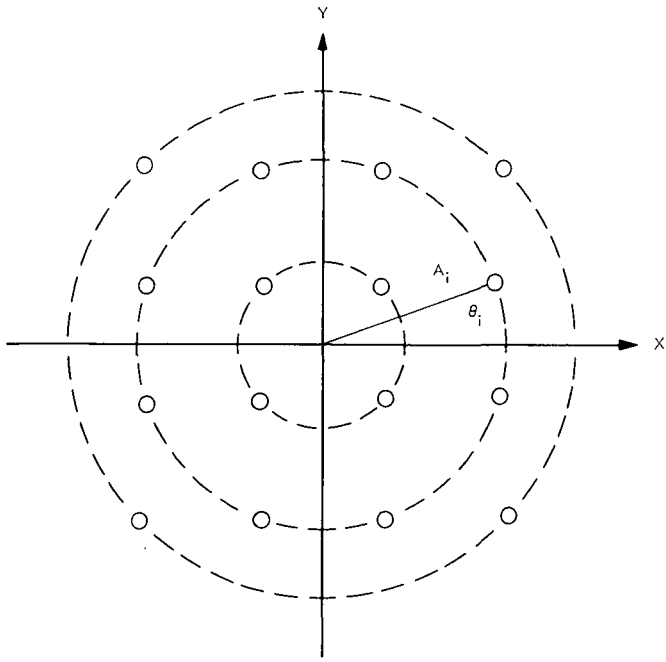

Fig. 3. QASK4 circular structure

P_e indeed verifies that the SNR requirements of QASK4 is 40% of that of PSK16, a 4-dB difference.

Transmitter Configurations

The QASK4 System can be considered in terms of envelopes and phases as indicated in Fig. 3. If linear operation is to be obtained, the exciter must be phase modulated and the driver amplitude modulated simultaneously, as shown in Fig. 4. Another (multimode) configuration utilizes data-rate-switched Class C final amplifiers as shown in Fig. 5. The switching information indicates which power level is to be switched on during a particular signaling time.

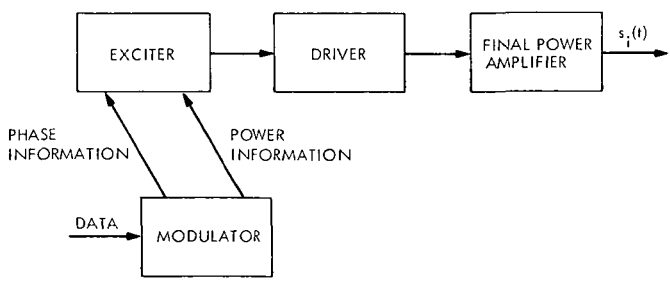

Fig. 4. QASK4 linear transmitter

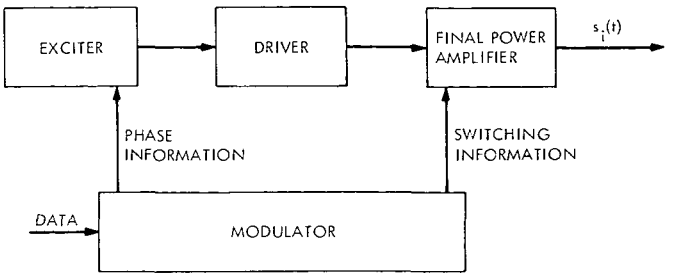

Fig. 5. QASK4 multimode transmitter

The PSK16 System by comparison is fairly straightforward, requiring simple low-level phase modulation, a driver chain, and some form of saturated final stage, as indicated in Fig. 6.

S-Band Device Models

A set of device models useful in characterizing transmitter configurations is described, based on current development technology (Ref. 3). These include exciters, Class A and Class C solid-state amplifiers, diode switches, and TWTs.

The exciter produces up to 30 mW of modulated S-band power with an input power of 1.25 W. A 33% efficient S-band Class A amplifier with 10-dB gain is typical of present technology.

At S-band below 1-W output level, 50% efficient Class C solid-state amplifiers with gains to 10 dB are not unusual. Above this power level gains of 7 dB have been obtained, also with 50% efficiency. Based on current development efforts, 10-dB gain, 50% efficient solid-state Class C amplifiers with 10-W outputs are not unreasonable projections, and are assumed here.

Recent developments in microstrip RF switches include diode switches capable of megabit switching rates of S-band power up to 50-W power levels with less than 0.25-dB insertion loss and more than 35-dB isolation. Switching power of 200 mW is required for every "on" diode. For the 2P3T

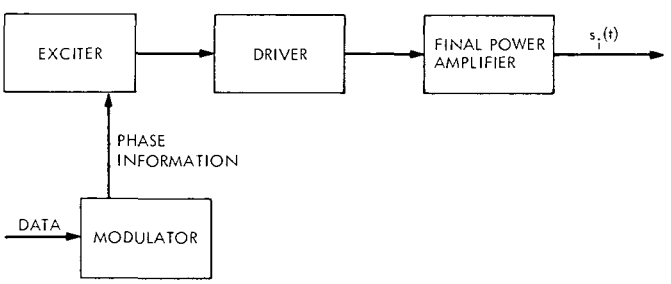

Fig. 6. PSK16 transmitter

switches considered here, this represents a constant 400-mW power drain (Ref. 4).

Traveling wave tubes designed for saturated operation at 20 or 30 W can achieve 43% and 45% efficiency, respectively. Running comparable tubes and reduced power levels, Class A, results in reduced efficiency. Recall that the QASK4 system runs at three power levels with relative values of 1, 5, and 9; that the average power is the middle value, and 4 dB below the PSK16 system compared. Thus, the QASK4 TWT competing with the 20W PSK16 TWT must run at 1.6 W, 8.0 W, and 14.4 W, while the QASK4 TWT competing with the 30 W PSK16 TWT must operate at 2.4 W, 12 W, and 21.6 W. Based on current development technology, 25%, 35%, and 45% efficiencies are assumed at each of these three relative power levels, respectively, except at 14.4 W where 40% is assumed. A 30-dB gain is assumed in each case.

System Configurations

Consider four PSK16 systems with outputs of 1, 10, 20, and 30 W. Assume the two lower power systems use Class C solid-state final stages; the higher power systems use saturated TWTs. These four systems are the first systems shown in Figs. 7a, 7b, 7c, and 7d.

A comparison is now made of several groupings of PSK16 and QASK4 configurations. First, two 400-mW average power QASK4 transmitters are compared with the 1-W PSK16 system (Fig. 7a). One of these uses unsaturated final stage operation; the other utilizes diode-switched parallel Class C finals. Both utilize solid-state final amplifiers. Secondly, two 4-W average power QASK4 systems are compared with the 10 W PSK16 (Fig. 7b). Again, both unsaturated and diode-switched, parallel saturated solid-state finals are considered. Finally, two QASK4 systems utilizing unsaturated TWT finals are compared with the higher power PSK16s as shown in Figs. 7c and 7d. Data-rate-switched parallel TWTs are either not efficient or involve tremendous energy transients, depending on whether or not the helix and beam voltages are switched; thus, they are not compared.

Comparisons of Systems

System power inputs, outputs, and efficiencies are shown in Table 1 along with dB power margins of competing systems.

For example, the input power to System No. 4 is 1.25 W for the exciter, 200 mW and 2 W for the Class C drivers, and 20 W for the final. Thus, 10 W of output power is achieved for 23.5 W of input, an efficiency of 42.5% for the PSK16 system. System No. 5 requires 15.9 W for 4 W out (25%) while System No. 6 consumes 11.7 W for 4 W out (34.0%).

At the 1-W level, savings in power (or PNR) of 1 to 1.3 dB are achieved by the QASK4 system over the PSK16. This savings is rather modest, and is limited primarily by the relatively large exciter requirements in all configurations.

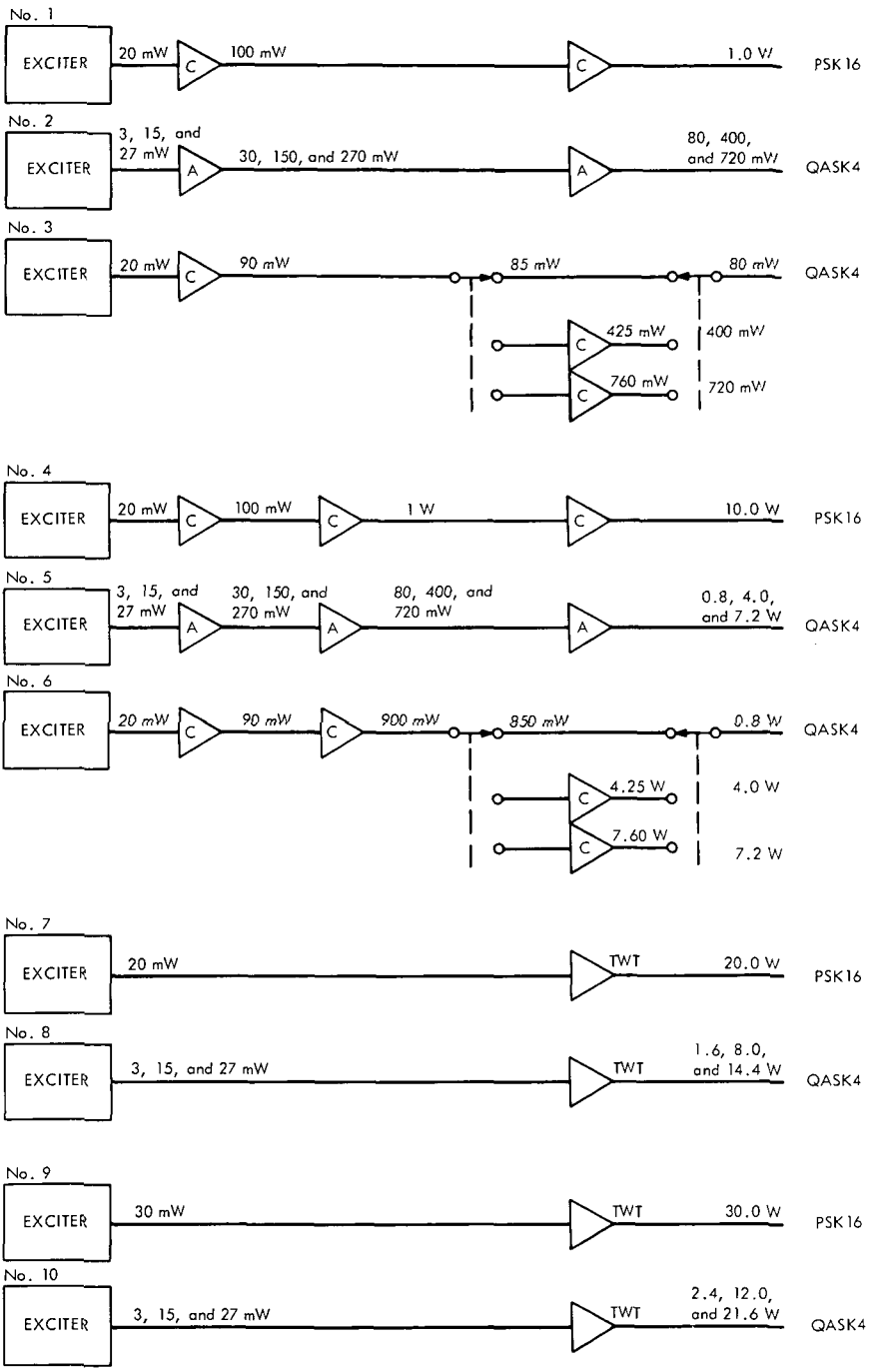

Fig. 7. Block diagrams and power levels of 10 systems: (a) 1-W equivalent systems; (b) 10-W equivalent systems; (c) 20-W equivalent systems; (d) 30-W equivalent systems

Table 1. Comparisons of candidate transmitter configurations

System No.	System description	Average output, W	Average input, W	Average PNR savings, dB	Average Efficiency, %
1	PSK16	1	3.5	0.0	29.0
2	QASK4, Class A	0.4	2.7	1.1	14.8
3	QASK4, Class C	0.4	2.6	1.3	15.4
4	PSK16	10	23.5	0.0	42.5
5	QASK4, Class A	4	15.9	1.5	25.0
6	QASK4, Class C	4	11.7	3.0	34.0
7	PSK16, W/TWT	20	47.4	0.0	42.0
8	QASK4, W/TWT	8	23.4	3.1	34.0
9	PSK16, W/TWT	30	68.0	0.0	44.0
10	QASK4, W/TWT	12	34.5	2.9	35.0

At the 10-W level, the PNR savings (QASK4 over PSK16) is 1.5 dB if QASK4 linear operation is utilized and 3 dB if QASK4-switched Class C final stages are used.

Finally, at the 20- and 30-W levels, PNR savings (QASK4 over PSK16) of about 3 dB are achieved.

Conclusions

In a bandwidth constrained environment, M-ary systems must compete on the basis of dc power required to maintain a specified error rate. This basis can be portrayed as the ratio of average RF output signal-to-noise and transmitter efficiency. It is easy to verify that QASK4 requires 4 dB less signal-to-noise than PSK16. The remaining issue is that of relative efficiencies. An attempt has been made to accurately assess the device and system efficiencies of PSK16 and QASK4 transmitter configurations based on current development technological levels. The results indicate that the losses in QASK4 transmitter efficiencies are more than offset by the decreased SNR requirements, in some cases by as much as 3 dB.

Many other factors, such as modulator complexity, modulator power drain, switch transients, dc/dc conversions, and receiver synchronization must be considered before asserting firmly that multiamplitude transmission does compete well with constant energy modulation systems; however, on the basis of this brief examination, multiamplitude communication does appear competitive.

References

1. Arthurs, E., Dym, H., "On the Optimum Detection of Digital Signals in the Presence of White Gaussian Noise," *IRE Transactions on Communication Systems,* CS-10, pp. 336-372, December 1962.

2. Gilbert, E. N., "A Comparison of Signaling Alphabets," *Bell Syst. Tech. J.,* Vol. 37, pp. 504-522, May 1952.

3. Dickinson, R. M., Detweiler, H., Choi S., of Jet Propulsion Laboratory, Pasadena, California. Private communication.

4. Choi, S., "High-Power Microstrip RF Switch," *JPL Quarterly Technical Review,* Vol. 1, No. 3, October 1971.

JPL Quarterly Technical Review Volume 2, Number 4 January 1973

Index: mechanisms, optics

Helicopter Visual Aid System

R. L. Baisley

Guidance and Control Division

The results of an evaluation of police helicopter effectiveness revealed a need for improved visual capability. A JPL program developed a method that would enhance visual observation capability for both day and night usage and demonstrated the feasibility of the adopted approach. This approach made use of remote pointable optics, a display screen, a slaved covert searchlight, and a coupled camera. The approach was proved feasible through field testing and by judgement against evaluation criteria.

Introduction

Recently, many law enforcement agencies have integrated helicopters into their patrol activities, and the trend toward their use is continuing to increase on a national scale. Experience with these aerial patrols led to recognition of the limitations of the basic observation system. The initial system was comprised of the helicopter, the observer, and sometimes minimal visual aids such as binoculars or a camera. This minimal amount of support equipment for the full range of police missions, conducted both at night and during the day, limits the potential value of the helicopter system. Many attempts have been made to adapt equipment designed for other purposes to use on police helicopter patrols. Little effort has been made, however, to design equipment specifically for the police helicopter in its performance of the patrol function.

In response to this need, the Jet Propulsion Laboratory has developed a visual aid system for helicopters that is based on a set of requirements derived from law enforcement agencies (Ref. 1).

Problem Definition and Task Objectives

The initial definition of the problem was based upon a previous civil systems task. In this task, the Los Angeles Police Department's helicopter patrol program was evaluated, with one element of this effort being the

assessment of various means by which patrol effectiveness could be increased. A major item identified was improved visual capability.

To confirm some of these observations, and to provide a broader base of understanding of the range of missions and their requirements, a nationwide survey was conducted involving 10 law enforcement organizations. This survey:

(1) Confirmed the pressing need for improved visual capability.

(2) Pointed out that the "general patrol" mission was the most appropriate one upon which to focus attention.

From this, the fundamental functional requirements for a visual aid system were established to be:

(1) It should provide an increased field of view, coupled with the capability to see at night without visible illumination. Minimum resolution should be equivalent to that of the unaided eye under conditions of daylight illumination.

(2) It should provide an improved capability to see during normal conditions of daylight illumination through an increased field of view as above and with increased resolution.

(3) It must provide evidence-gathering capability through airborne photography.

The objective of the Phase-I task was the demonstration of feasibility of the adopted approach. Key to the accomplishment of this objective were the following:

(1) Establish system requirements.

(2) Perform testing of items of critical technology.

(3) Design and fabricate a breadboard model of the system.

(4) Perform a field test of the system utilizing the support of a law enforcement agency.

System Constraints and Requirements

Physical constraints were generally bounded by the characteristics of the Bell-47 G-5 helicopter, which was chosen to be the test vehicle.

The technical requirements established for a visual aid system are outlined below.

(1) Mode of operation: daytime operation under ambient light conditions and nighttime operation using either visible illumination or nonvisible infrared illumination.

(2) Fields of view: the field of view centerline shall be pointable from the horizon to approximately 45° below the horizon and from a forward

position to 90° right azimuth. In addition, it shall be capable of variable magnfication.

(3) Visual resolution: daylight resolution capable of resolving line pairs on a 1951 Air Force resolution chart, which are separated by 50 μrad, and which have typical brightness values equal to or greater than 1000 ft-L. At night, have the capability to distinquish line pairs separated by 250 μrad and have typical brightness due to ambient illumination of 0.001 ft-L.

(4) Display characteristics: the image shall be erect and nonreverted and shall have a minimum brightness of 1 ft-L. It shall also incorporate an indicator that shows the orientation of the line of sight relative to the vehicle. A similar indicator shall be provided for the pilot.

(5) Searchlight: the searchlight shall be slaved in azimuth and elevation to the turret subassembly and shall be capable of remote control by the observer. The capability shall exist to remotely control the filter elements required for both visible and covert illumination of a target.

System Description

The breadboard Visual Aid System model consisted of five modular elements: the optical turret, the optical display, the searchlight, the control console and the auxiliary generator. Where appropriate, components were chosen from commercially available stock, although the majority were, of necessity, designed and fabricated specifically for this task.

The Visual Aid System optics and electro-optics were packaged into two separate modules: a turret module, located underneath and forward on the "chin" of the vehicle, that contained the front objective lenses and turning mirrors, and a display module, located in the helicopter cabin in front of the observer, that contained the balance of the optics. A flexible, image-carrying fiber-optics bundle connected the two modules. This connection allowed considerable freedom in location and orientation of the modules and decoupled the vibration modes between them. A description of this system, keyed to Fig. 1, is presented below.

One of the two objective lenses (3 and 4) alternatively provided a focused image upon the end of the fiber optics bundle (7), the selection depending upon the orientation of the switching mirror (6). Each of the objective lenses "looked out" through a flat glass window (1). Turning mirrors (2) were coupled to the windows in an optical scanning head. Rotation as shown about the common axis of the objective lenses represents an elevation scan. Rotation of the entire turret about the center line shown at the left of Fig. 1 represents an azimuth scan.

Objective lens (3) was a 530-mm-focal-length, 127-mm-diam, air-spaced doublet designed for this task by the JPL Fortran Optical Lens Design Program. The design was optimized for full aperture in the near infrared to correspond to nighttime use with infrared illumination.

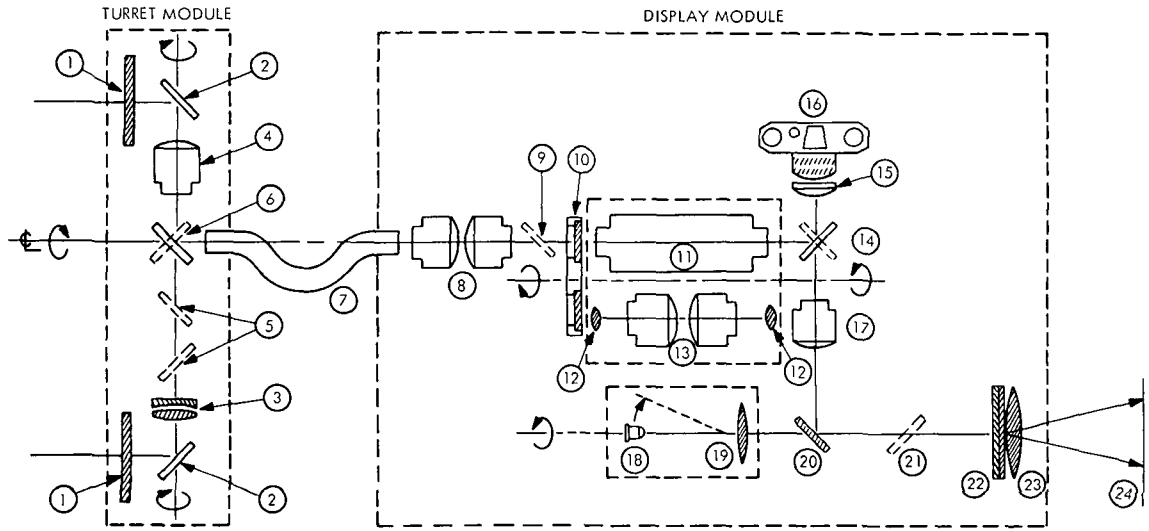

1. TURRET WINDOWS
2. TURRET TURNING MIRRORS
3. 21-in. FOCAL LENGTH OBJECTIVE
4. 3-in. FOCAL LENGTH OBJECTIVE
5. TURRET FOLDING MIRRORS
6. TURRET SWITCHING MIRROR
7. FIBER OPTICS ROPE
8. RELAY LENS PAIR No. 1
9. DISPLAY TURNING MIRROR No. 1
10. FILTER WHEEL
11. IMAGE INTENSIFIER
12. FIELD LENSES
13. RELAY LENS PAIR No. 2
14. DISPLAY SWITCHING MIRROR
15. CLOSE FOCUS ATTACHMENT LENS
16. 35-mm STILL CAMERA
17. PROJECTION LENS
18. LIGHT EMITTING DIODE
19. POSITION INDICATOR PROJECTION LENS
20. COMBINING MIRROR
21. DISPLAY FOLDING MIRROR
22. PUPIL SPLITTER
23. VIEWING FIELD LENS
24. EXIT PUPIL PLANE

Fig. 1. Optical schematic

Objective lens (4) was an 85-mm, f/1.8 Takumar lens normally supplied on an amateur 35-mm camera. The lens was found to have excellent imaging in both the near-infrared and visible regions, although a slight change in focal distance existed between the two.

The turret turning mirrors (2) and the larger one of the two folding mirrors (5) were large Pyrex blanks that were weight relieved by hot pressing a waffle configuration into the back of the blank. Weight-relief factors of 35% (65% remaining) were achieved with the larger mirrors.

The fiber optics bundle (7) was an adaptation of an imaging bundle developed for the U. S. military helicopter-born INFANT[1] Visual Aid System. The bundle is solid at each end and flexible in between. It consisted of approximately 800,000 optical conduits, each 10 μm in diameter, grouped into larger fibers consisting of a 6 by 6 matrix of the individual clad fibers fused together. The bundle was 4 ft in length and sheathed in plastic links and foam rubber.

The fiber optics bundle served a number of purposes. In addition to transmitting an intact image - visible or infrared - from the turret to the display without transmitting mechanical motions from one to the other, the bundle had adequate flexibility to allow its solid end at the turret to be twisted nearly a full turn each way. By twisting the bundle, image rotations, which would otherwise be introduced by the turret azimuth and elevation scan rotations, were removed from the image that was presented to the display unit.

The first relay lens pair, item 8 in the display module, was two f/1.5 military Starlight Scope objective lenses mounted face to face. The function of this relay lens pair was to collect the visible or infrared light from the fiber optics bundle and reform the image either at the photocathode of the image intensifier (11), or at the field lens (12) for further relay through the display module. The Starlight Scope objectives were the only candidate shelf optics and were deemed good enough to prove feasibility in a breadboard demonstration. However, some aberrations were undesirably large in the pair, and a very significant light loss occurred due to an effective f/3.4 solid angle as seen from the image.

The filter wheel (10) contained, in one position, a multilayer filter to pass near-infrared and exclude visible light and, in a second position, a clear piece of glass of an appropriate thickness to correct the visible light focal length of the first relay lens pair (8).

The image intensifier (11) was a cascaded three-stage, electrostatically imaged intensifier with an S-20 extended-red photocathode, and a P-20 phosphor screen. The photocathode and the phosphor screen were each 40 mm in diameter. The tube was developed under contract to the Army Night Vision Laboratories for use in military applications. The tube is nominally

[1] INFANT: Iroquois Night Fighter and Night Tracker

rated as having a total light-output-to-light-input gain of 35,000; however, production units typically have gains of 100,000.

Relay lens pair (13) was mounted in a turret with the image intensifier and could be rotated into position to relay a visible image from the first relay pair (8). Schneider-Xenotar, 100-mm-focal-length, f/2.8 photographic lenses were chosen for this application. Two were used, mounted face to face. Field lenses (12) were located at the input and exit image locations to minimize vignetting, which is the principle drawback to this configuration, approximately 30% at the field edge.

Display switching mirror (14) had two operating positions: one directed light from the image intensifier or second relay lens to a 35-mm recording camera (16), and the other to a projection lens (17), which forms the final image at the viewer end of the display.

The projection lens (17) was selected to be an f/2.9, 152-mm-focal-length Dallmeyer Pentac. The lens was designed for infinity correction, but was used here at a magnification of 4.4 to provide a display image 6.7 in. in diameter at the viewing field lens (23).

The viewing field lens (23) and pupil splitter (22) provided a pair of exit pupils imaged approximately 16 in. beyond the viewing field lens. The exit pupils were approximately 1 in. in diameter and spaced on center by an average human adult interpupillary separation of a little less than 3 in. It was at this location that an observer positioned his eyes to look into the display.

Items 18 and 19 are a light emitting diode (LED) and a projection lens, respectively, which are incorporated into a position indicator. The LED was mounted onto a torquer-driven assembly that was gimballed to allow reproducing the azimuth and elevation angles of the turret assembly.

The combining mirror (20) incorporated a multilayer coating that reflected virtually all of the visible light and presented a bright scene image to the display, yet transmitted about half of the LED illumination. Projection lens (19) then formed an image of the LED emitter area at the pupil splitter and viewing field lens. The red position dot was seen with both eyes superimposed upon the presented scene.

Optical Turret

The major functions of the optical turret illustrated in Fig. 2 were to provide azimuth and elevation scanning for the objective lenses; focusing of the optics; selection of magnification; a mechanization to maintain the horizon level at the display; image motion stabilization; support structure to maintain alignment of the elements; and a housing to provide a protective enclosure against environmental conditions.

Servo-driven, the turret rotated in azimuth through 180°, from straight forward clockwise to straight backward. In elevation, the pointing limits of 0° (horizontal) to 75° below the horizon were achieved. The skew rate of the turret was measured to be 22.5°/s in azimuth and 26.0°/s in elevation.

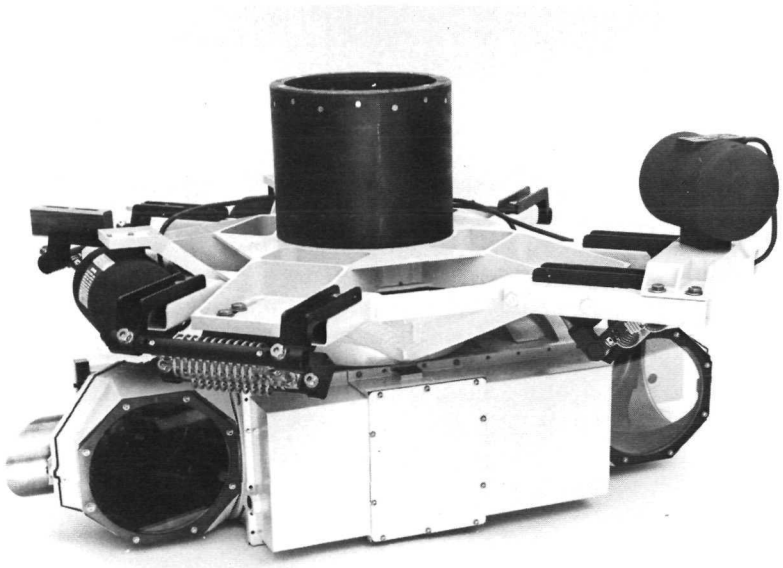

Fig. 2. Turret module, full assembly

The details of image motion stabilization combined three techniques. First, vibration isolators were used between the helicopter and the suspended portion of the turret. Second, large stabilizing gyros were added to the isolated member to increase the rotational inertia. Third, rate gyros were mounted on the turret to sense angular motion, and through the control system, the elevation and azimuth servos were driven to directly compensate for that motion.

Magnification changes were accomplished by rotating a diagonal mirror to direct the optical axis from a one-power (1×) objective lens to the seven power (7×) objective lens. Accurate indexing was achieved through a motor-driven Geneva mechanism.

One feature that is familiar to us is the level horizon at the top of a scene whatever direction we may turn our head. To help maintain orientation, it was decided to present a display with the horizon at the top, which would be fixed with respect to the observer even though the helicopter should roll and pitch. The concept used in the turret utilized rotating mirrors for scanning and as a result caused unwanted image and horizon rotation that required compensation. This was achieved through rotation of the fiber optics rope in response to each of these turret functions.

The mechanization was accomplished by utilizing a geared differential and motor-driven follow-up mechanism, which summed inputs from

elevation and azimuth axes and the switching mirror position (1× or 7×) and provided the proper rotational position for the fiber optics rope end.

Optical Display

Several functions were provided in the display module. These were, principally, display of the image (day or night), conversion of infrared to visible light (night), intensification of the visible or infrared image (night), and display of the turret-pointing position indicator (day or night). Certain ancillary functions were mechanized: a filter wheel for selection of either infrared only or full visible; a camera for recording the scene in the display unit; reticle illumination (night) and display tilt to accommodate the sitting height of the various observers.

Figure 3 shows the display module mounted on a supporting stand prior to installation on the helicopter. The upright drum housed the day-night turret. The knob visible above the camera allowed rotation of the turret after pulling the detent plunger knob located on the side of the drum below the camera. The similar knob on the bottom of the drum housing provided

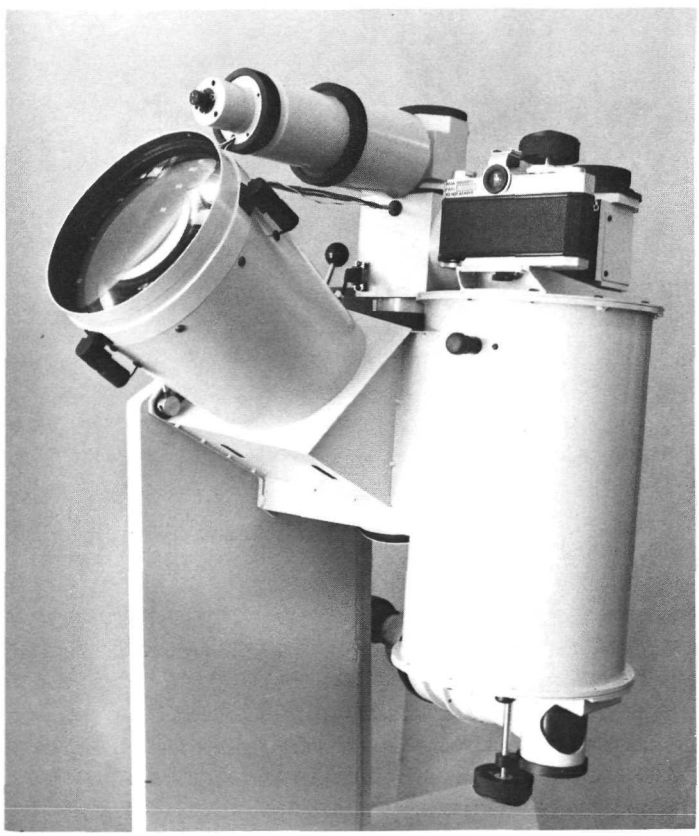

Fig. 3. Display module

for rotation of the filter wheel. The fiber optics rope entered the display module from bottom far side as seen in this photograph.

Searchlight

The searchlight used for the breadboard Visual Aid System was the commercially available SX-16 "Nightsun" manufactured by Spectrolab of Sylmar, California. The light is in wide use by law enforcement agencies for nighttime airborne search and tactical operations. It has a 1600-W xenon short arc lamp that supplies about 20,000 lm in a beam that may be controllably varied in flight from 4° to 10° in diameter. It is servo-driven and slaved to the look vector of the optical turret.

In addition to providing a very powerful visible beam, the xenon searchlight had an equally powerful infrared beam. Approximately 70 W of radiation were emitted in the wavelength interval of 800 to 900 nm – approximately the same as was emitted in the visible interval of 450 to 650 nm.

As procured from Spectrolab, the searchlight had either of two windows mounted in a light-baffled, air-ducted shell (Fig. 4). One was a clear window

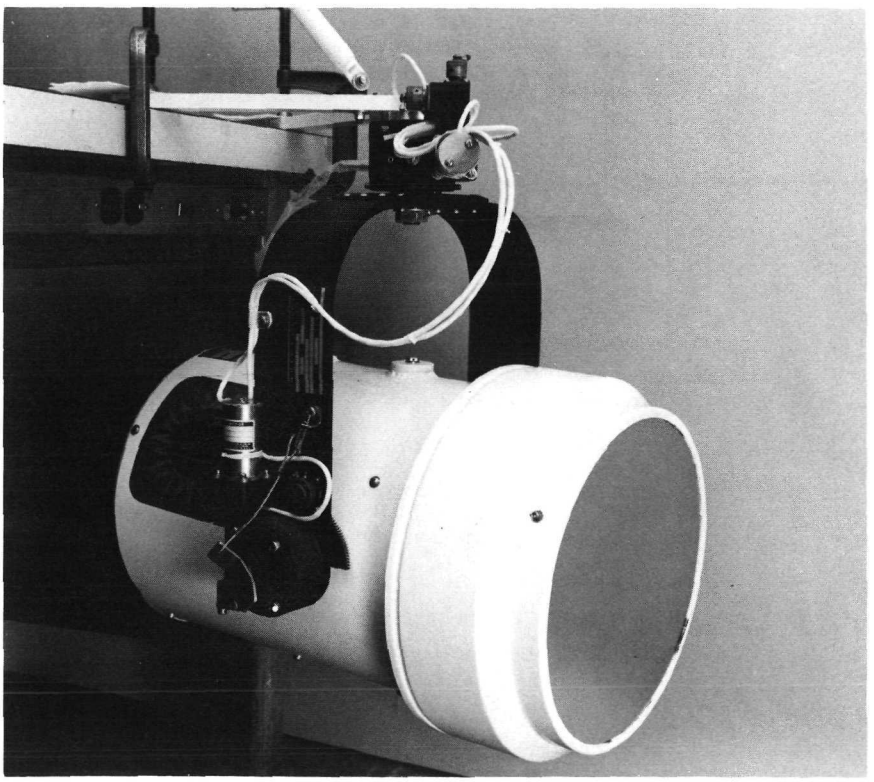

Fig. 4. Searchlight

that passed essentially all visible and near-infrared radiation. The other had a multilayer interference filter that passed the near-infrared, but reflected essentially all visible radiation back to the bulb. The 10% and 90% points on the transmission curve were 775 and 840 nm, respectively. This transmission characteristic reduced the visibility of the direct searchlight beam to an appearance similar to that of the helicopter running lights when viewed from a distance. However, at distances of 1000 ft or so, the large angle subtended by the searchlight reflector distinguished it from running lights.

Control Console

Figure 5 is a photograph of the control console in its breadboard configuration. It was located between the pilot and observer, in a position where the controls were conveniently operated by the observer's left hand.

It provided control over the system as indicated by the functions on the control panel. Pointing of the turret look vector was accomplished by a control stick mounted to a floor pedestal in front of the observer. A rate

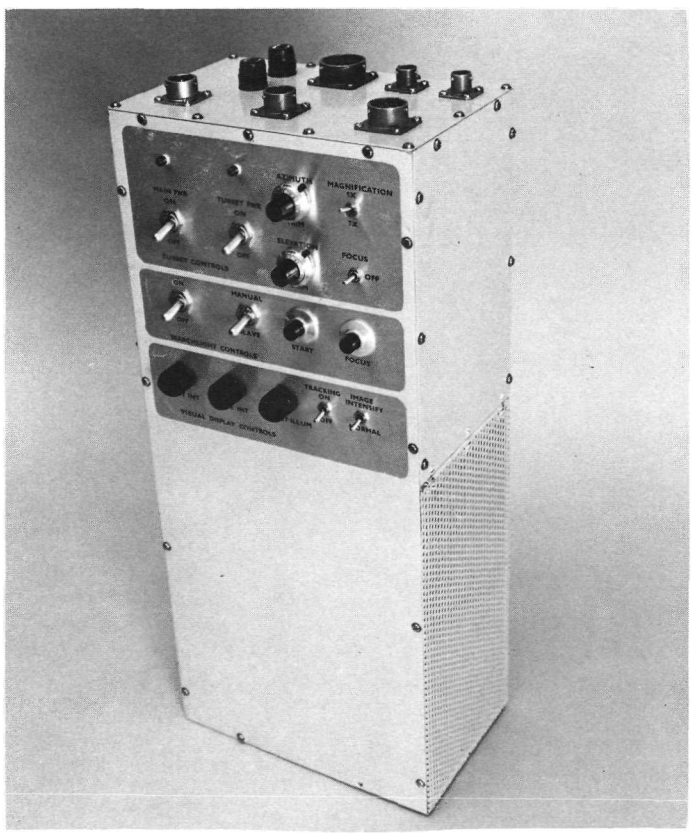

Fig. 5. Control box

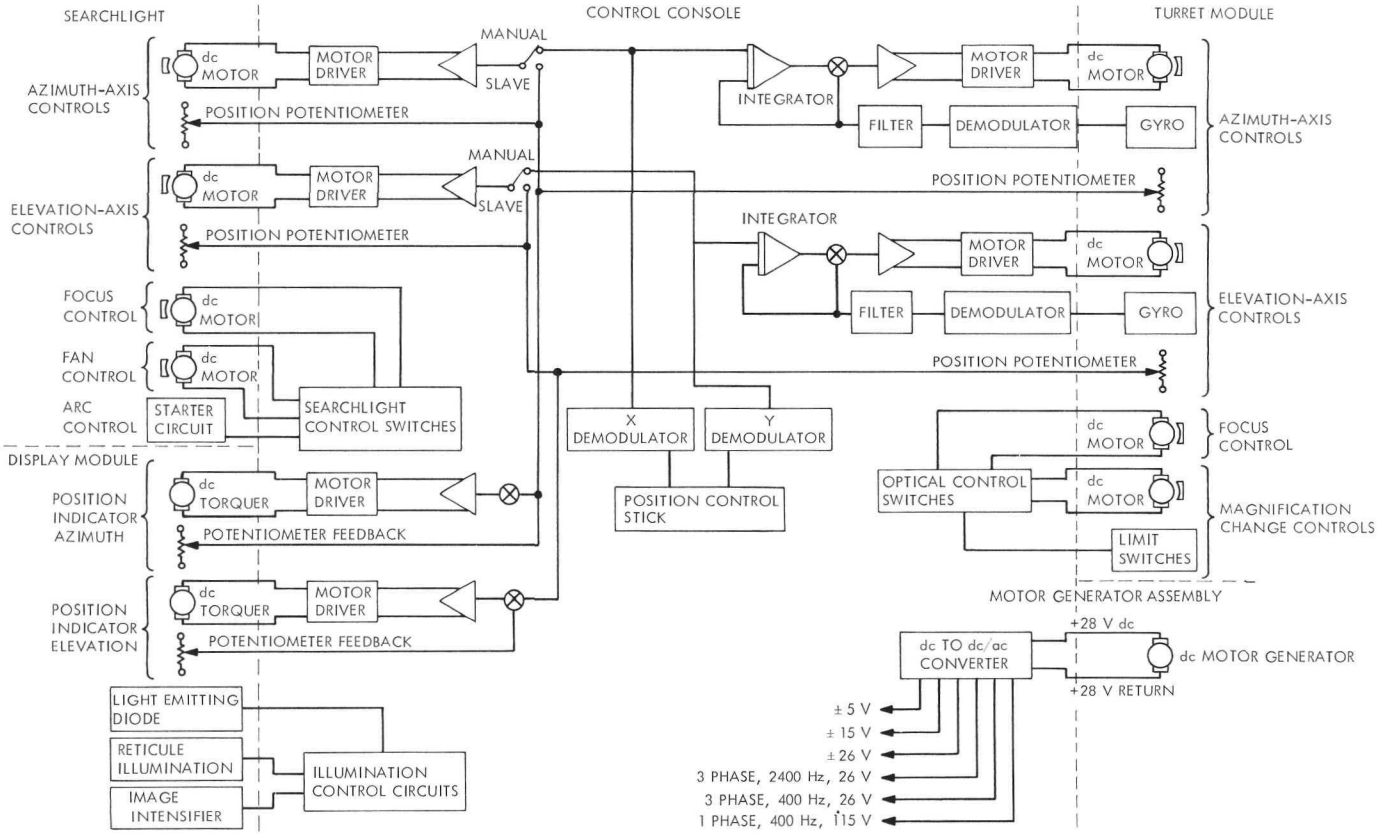

Fig. 6. Electronic control and power conversion

control stick mechanization was selected for the human interface with the turret drives, largely because of the results of a previous study that had shown superior pointing accuracy of an airborne payload by an operator using this type of control. The rate stick provided a plus and minus voltage output proportional to the force vector applied for each of two orthogonal directions. The stick had an appearance similar to an aircraft control stick, except that it did not significantly deflect in response to manual control pressure.

Figure 6 is a functional block diagram illustrating the approach taken for electronic control and power conversion. The control console is shown inside dotted lines in the center of the diagram and the functional interconnections with the other modules of the helicopter Visual Aid System are shown. Interconnections with the turret module, the searchlight module, the display module, and the generator assembly are shown in sufficient detail to make clear the type of control used for positioning and controlling the various parts of the Visual Aid System.

Helicopter Installation

Installation of the Visual Aid into the police helicopter (Bell 47G-5) is illustrated in Fig. 7.

Fig. 7. Completed helicopter installation

Test Program

The purpose of the test program was to determine the feasibility of the system and to evaluate its technical behavior. Criteria were established to guide the determination of system feasibility. The criteria by which feasibility was measured consisted of two basic requirements: the satisfaction of image quality and certain human factors specifications. It was required that these criteria either be met or that a high probability of success in meeting them in subsequent phase be demonstrated. These criteria along with corresponding results are listed in Tables 1 and 2.

Of the 23 criteria listed, 21 were successfully met with a rating of "fair" to "excellent". In two areas the results were judged "poor" by the criteria. These were: linear image motion (1) and camera implementation (13).

The selected approach to image stabilization was a compromise resulting from hardware availability and program constraints. It was anticipated that a stability problem would arise resulting from this decision to use servo-driven gear trains rather than direct-coupled torquers, but that feasibility could be proven with this alternative approach. The test program confirmed the existence of the stability problem and isolated the cause and the effects.

Table 1. Test results — image quality

Criteria No.	Item	Requirement	Performance
		Stability	
1	Linear image motion	Linear vibration, 10 μrad p-p ≥2 Hz	~1000 μrad p-p at ~5 Hz (poor)
2	Rotational image motion	Rotational vibration, 1° p-p ≥2 Hz	None detectable (excellent)
		Day/night resolution (static)	
3	Day	Visible, 50 μrad (7×)	110 μrad (7×) (fair)
4	Night	Infrared, 250 μrad (7×)	170 μrad (7×) (good)
		Brightness/glare	
5	Daylight system transmission	5%	4% (good)
6	Night image intensification	330 ×	27 × (fair)
7	Night display brightness	1 to 10 ft-L	1.1 ft-L (good)
8	Glare, day	Subjective	Fair to good
9	Glare, night	Subjective	Excellent

Table 2. Test results — human factors

Criteria No.	Item	Requirement	Performance
		Stability	
10	Control console	Subjective	Fair, needs human factor engineering
11	Rate stick	Subjective	Fair to good
12	Position indicator	Subjective	Excellent
13	Camera control	Subjective	Poor, needs automation
		Optical display interface	
14	Exit pupil spread	60 to 76 mm	59 to 76 mm (excellent)
15	Exit pupil, night	18 mm	37 mm (excellent)
16	Exit pupil, day	18 mm	1×, 36 mm; 7×, 28 mm; (excellent)
17	Magnification	1×, 7×	1.1×, 6.9× (good)
18	Field of view	1× 19° 7× 2.7°	1×, 17°; 7×, 2.7°; (excellent)
19	View sector	Azimuth 0° to 90° Elevation 0° to −45°	Azimuth 0° to 180°; elevation 0° to −75°; (good)
20	Position indicator	Subjective	Excellent
		Comfort/fatigue factors	
21	Sitting position	Subjective	Fair, should be 4 to 6 in. closer
22	Left arm position	Subjective	Good
23	Eyestrain	Subjective	Good

It is felt that the general approach to the mechanization was proper and that with the use of torquers, the control system deadband would be significantly reduced and the stability problem would be alleviated. The problem and its solution are not new and unique, but have been encountered several times in other applications with success.

Except for exposure control, the camera for the breadboard model was intended to be manual. Remote film advance drive and automatic reflex/shutter operation from a control button were judged to be unnecessary for a breadboard demonstration. The camera was adequate for ground test data recording; however, the camera was located just out of reach for an observer restrained by a seat belt and a shoulder harness. In addition, the time required in flight to manually operate the camera resulted in loss of target in the field of view. Consequently, the camera was useless in flight testing.

A prototype model Visual Aid System would see a fully automatic implementation, with camera control located on the rate stick. This would eliminate the usage problems that were encountered.

Conclusions

This task has demonstrated that the visual aid concept can provide improved daytime visual capability, greatly improved nighttime capability, surveillance from greater distances and/or altitudes, covert operation at night through the use of the IR Searchlight, and a photographic recording of the scene being viewed.

The anticipated problem area, that of image stability, was present but not to such an extent as to detract from feasibility demonstration. It resulted from a decision to limit the full implementation of the control system and it affected performance in the manner predicted, but not to the extent anticipated.

Reference

1. Baisley, R. L., *Helicopter Visual Aid System, Vols. I and II.* Document 650-155, Jet Propulsion Laboratory, Pasadena, Calif., in press. (Internal Document.)

JPL Quarterly Technical Review Volume 2, Number 4 January 1973

Index: computer applications and equipment, management systems

The Mesa Arizona Pupil Tracking System

D. L. Wright

Data Systems Division

A computer-based Pupil Tracking/Teacher Monitoring System was designed for Mesa Public Schools, Mesa, Arizona. The established objectives of the system were to:

(1) Facilitate the economical collection and storage of student performance data necessary to objectively evaluate the relative effectiveness of teachers, instructional methods, materials, and applied concepts.

(2) Identify, on a daily basis, those students requiring special attention in specific subject areas.

The system encompasses computer hardware/software and integrated curricula progression/administration devices. It provides daily evaluation and monitoring of performance as students progress at class or individualized rates. In the process, it notifies the student and collects information necessary to validate or invalidate subject presentation devices, methods, materials, and measurement devices in terms of direct benefit to the students. The system utilizes a small-scale computer (e.g., IBM 1130) to assure low-cost replicability, and may be used for many subjects of instruction.

Introduction

Many educators have long desired to thoroughly evaluate the relative effectiveness of teachers, instructional methods, materials, and applied concepts in terms of their direct benefit to the individual student. The major obstacle to such evaluation has been the manpower and effort necessary to continuously collect and process student achievement data. In fact, only with a certain degree of difficulty are many schools able to collect data sufficient to grossly recognize "problem" learning situations and generally identify student progress.

The staff of Mesa Schools wished not to just re-evaluate the traditional education process, but to establish a dynamic "closed-loop" system that would provide data and facts sufficient to pinpoint deficiencies in any resources of a total educational system. Resources here include teachers, presentation methods, instructional techniques, course curricula, applied

concepts, and measurement devices. The focal point of the "closed-loop" system is the individual student and his rate of progress in attaining discrete knowledge/performance objectives.

In support of the concept, the Mesa educators developed and "field tested" curricula software including definition of learning objectives, logical progression, presentation methods/devices, and measurement instruments. Their reasoning was that the curricula software, in concert with a high-speed computer plus properly designed storage files, computer programs, and supporting procedures, would in fact constitute an initial closed-loop system. The Jet Propulsion Laboratory was contacted to assess the feasibility and cost considerations of the desired computer system.

Following determination that the system was indeed possible and also practical within existing Mesa resource constraints, detailed systems analysis and design were initiated. During a period of four months, the design was refined as the result of extensive contact with Mesa personnel at all levels and reflected in a final design/specification document. The document became the basis for selection of computer hardware and software via a competitive bid process, and refinement/elaboration of the curricula software by the Mesa staff.

A small scale (IBM 1130) computer was selected, and Fremont Junior High School was chosen as the most representative test site. The 800 math students of that school were divided into three equal groups to determine the validity of the devised Pupil Tracking System during most of the 1972 Spring term. One was a control group, instructed within the "traditional" class framework; another was monitored by the computer-based system; the third was monitored by manual devices similar to those of the computer-based systems. The results of that four-month trial were interpreted by Mesa as sufficiently successful to warrant expansion of the Pupil Tracking System to all math students of the school, plus those in select reading classes. The basic reasons for this decision were that the system in fact:

(1) Allowed students to progress at their best rate while consistently identifying learning problems as they occurred.

(2) Collected sufficient information to permit analysis, and facilitate evaluation, of education resources in the context of benefit to the student.

System Components

The components of the Pupil Tracking System are described below (Fig. 1).

(1) A definition of the discrete learning objectives to be attained by students, their sequential relationship, and normative time intervals for each. This information was defined by Mesa educators and retained within the computer files.

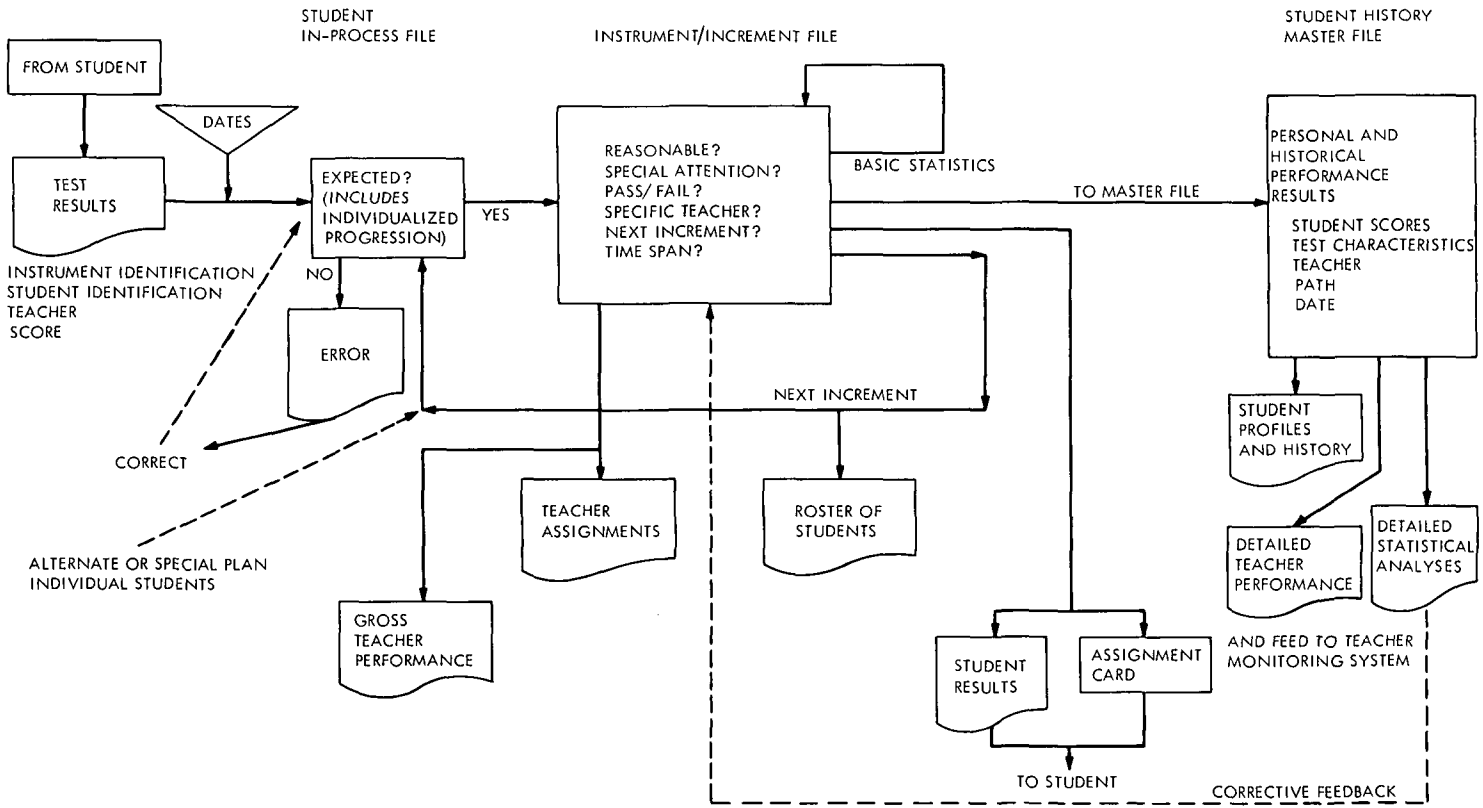

Fig. 1. Arizona Mesa Pupil Tracking System, Information and Logic Schematic

(2) Instruments (tests) that reliably and validly determine whether each learning objective is achieved. Such instruments were devised by the Mesa educators, and keyed to the appropriate objective(s). To permit computer scoring, analysis, and score retention, the correct test responses were recorded as masks within the computer file.

(3) The definition of texts, presentations, and reference media that efficiently assist students in attaining the learning objectives. As established by the Mesa staff, this definition is retained in the computer files and utilized to offer students a choice of learning activities.

(4) Computer files that store the directive, historical, and current status information. Items 1 to 3 above are classified as "directive" because they define objective interrelations, paths of progression, and criteria against which progress may be measured. Historical performance results are retained to permit detailed analysis by instrument, objective, student, or several other perspectives. Current status information is stored within the computer by student name index and "cycled" to detect nonperformance. The three basic computer files are the Student In-Process File (Current Status), the Instrument/Increment File (Directive and Analytical), and the Student History Master File (Historical).

(5) Media by which the Mesa staff and students can successfully communicate with the computer system and vise versa. Special punched cards are used by students to directly enter their answers to objective mastery tests, while concise reports are generated to indicate performance, status, and analyses.

(6) A computer, in this case an IBM 1130 with card reader/punch, printer, one disk drive, and 8192 words of storage capacity.

(7) Computer programs that update the necessary files in accordance with the directive file entries and provide the appropriate reports. All Pupil Tracking System programs are written in the 1130 RPG language, and may be executed (with minor modifications) on larger IBM computers.

(8) Operational procedures that assure consistency and safeguard the contents of valuable files.

System Operation

To initiate the tracking system, students are "enrolled" through entry in the Student In-Process and Student History Master Files, and all initial study increments are defined in the Instrument/Increment File. Special or individual progression paths may also be defined within the Student In-Process File.

The system produces an increment in-process student roster on a daily basis for grouping of instruction and to alert the teacher of potential

problems. The roster lists the students by the increment "in process", indicating the number of days they have been in the increment, the number of times they have attempted the performance test, their final score result, and days on the previous increment plus the next group of increments in which the student will be enrolled. Optionally, the student roster lists only those students who require individual attention because they have exceeded the standard time or number of attempts allowed.

In addition to producing reports describing the increments by title, various limits, objectives, learning activities, and test answers, the system collects and lists the frequency of failing by the number of attempts, the frequency of passing or acceleration, the number of days, and the frequency of participation in each activity by result (fail, pass, or accelerate).

Inquiries into a student's progress or master records are also possible. The Progress inquiry provides the student's current status as well as a complete description of his individual progression path. Inquiries into the Student History Master File can provide a simple plot of up to 15 selected scores or a list of selected semiquantitive, narrative, and/or measurement elements based upon types of data and date limits specified. These items are intended for the student or parent conferences.

A list of students who participated in a given increment within the date, score, and/or time intervals specified can be produced from the Student History Master File for grouping purposes. The information listed includes each student's passing score, number of attempts, total time, time above or below standard, and learning activities utilized. A comparison of the scores of any top increments for all students who participated in the increments can also be produced.

Normal Processing Cycle

During daily operations, the student determines if he is prepared to answer questions determining his mastery of the study objective, or if he needs to perform an additional learning activity. If the student decides to perform a learning activity, he chooses the activity from a list provided by the system upon completion of his last increment. When prepared to test his mastery, the student refers to a set of questions designated by a prepunched "assignment card", which was generated by the system upon completion of his last study increment. He circles the appropriate answers on the assignment card and punches those answers into the card with a "porta punch". This operation requires only a few seconds, and affords computer entry via a completely machine-readable document; student and increment identities are entered in the assignment card when it is created by the system.

Upon receiving the card, in either an individual or batch mode of operation, the system verifies the student/increment data by accessing the Student In-Process and Instrument/Increment Files. If no error is found, the test is scored and a result (fail, teacher decision, pass, accelerate) is

determined. The result (and optionally the score) is accepted and recorded by the system, while a report of the student's test result plus his next assignment card are prepared for him.

The new assignment card and printed report are provided to the student, who reads the assignment and its objectives and chooses a learning activity from those listed. After choosing an activity, he notes its number by circling the proper positions on his assignment card. Upon completing the activity, the student again determines if he is prepared to take the test or needs to participate in another activity.

The test scores and assignments are used to update the frequency statistics maintained in the Instrument/Increment File, and to create measurement records for the Student History Master File.

Results

Based upon one semester of experience with the system, the Mesa School District Administrators and the Fremont Staff concluded that it warranted expansion in the following semester to all math students at Fremont, plus select reading groups. The system is under consideration for expansion to other Mesa schools for both its intended function (daily monitoring) plus long-term monitoring required for a district-wide federally funded program of career education.

Bibliography of Current Reporting

Author Index With Abstracts

ACHESON, D.

A01 **DSN Progress Report for September–October 1972: Improved RF Calibration Techniques: Commercial Precision IF Attenuator Evaluation**

C. Stelzried, B. L. Seidel, M. Franco, and D. Acheson

Technical Report 32-1526, Vol. XII, pp. 74–82, December 15, 1972

For abstract, see Stelzried, C.

AMOROSE, R. J.

A02 **DSN Progress Report for July–August 1972: Network Operations Control**

R. J. Amorose

Technical Report 32-1526, Vol. XI, pp. 157–160, October 15, 1972

The DSN Operations Control Team controls and operates the DSN in real-time to support flight project operations. DSN Operational Control, a mission-independent organization, is headed by the DSN Operations Chief, who is supported by the Deep Space Instrumentation Facility Operations Chief, Ground Communications Facility Operations Chief, Network Operations Analysis Chief, and Network Operations Support Chief. The real-time operation is supported by two non-real-time functions, with liaison provided by: (1) the DSN Operations Representative, who represents the DSN organization to the DSN Manager and flight project Chief of Mission Operations, and (2) the DSN Scheduling Representative, who schedules DSN resources for flight projects.

ANDERSON, T. O.

A03 DSN Progress Report for September–October 1972: Two-Station Interferometer Analog Input Channel

T. O. Anderson

Technical Report 32-1526, Vol. XII, pp. 112–123, December 15, 1972

A signal-sampling system, used for the DSN Venus two-station radar experiment, intended to demonstrate hydrogen maser compatibility in two-station spacecraft tracking with planetary round-trip times, has been implemented. This article describes in detail one sampling channel. Four such channels, one for the sine and one for the cosine signal from each of two antennas, are used in the demonstration interferometer system. Each channel contains two multiplexed subchannels, and each subchannel consists of an integrating circuit, a track-and-hold circuit, and an analog-to-digital converter. All components of the subchannels are multiplexed and the output is derived from a digital multiplexing circuit which puts out digital data in parallel to line drivers for computer connection. Part of the four-channel system, a special-purpose test and calibration system, is also described.

ARMS, J. T.

A04 Heat-Sterilized Silver Oxide–Zinc Cells: Cycle Life Studies

J. T. Arms

Technical Memorandum 33-581, January 1, 1973

This memorandum presents the results of a JPL study to evaluate the cell design parameters that contribute to the cycle life of sealed, heat-sterilized silver-oxide–zinc cells. Test cells having a rated capacity of 4.2 A-h were fabricated using zinc-oxide electrodes prepared by the sintered Teflon process developed at JPL, silver electrodes purchased from ESB, Inc., and separators produced by Southwest Research Institute under NASA contract. Two separator variations were evaluated, one having acrylic acid and the other having methacrylic acid grafted to irradiated polyethylene film.

All cycle-life tests were conducted at ambient temperature on a 24-h cycle consisting of 3-h discharge through a fixed resistance and 21-h charge by modified constant potential having a current limit. Cells were tested as 6-cell batteries. The depth of cycle was approximately 50% of nominal. (The nominal rating was based on the value of 0.25 A-h/g of silver.)

Significant results of this study include the following: (1) Cycle life in excess of 300 cycles was attained; (2) a zinc-oxide–silver stoichiometric ratio of 1.5:1 resulted in a greater cycle life than a ratio of 1.1:1 and a cycle life similar to that for a ratio of 2:1; (3) cells having methacrylic-acid-grafted separators suffered somewhat less in capacity loss due to zinc-electrode shape change than cells having acrylic-acid-type separators; (4) acrylic-acid-grafted separators were slightly superior to methacrylic-acid-type separators with respect to silver penetration; and (5) the inclusion of a layer of potassium titanate paper adjacent to the zinc electrodes resulted in cells that achieved a higher cycle life before any failure than that reached by cells of any other construction.

ARNETT, J. C.

A05 Development of Automatic Through-Insulation Welding for Microelectronic Interconnections

J. C. Arnett

Technical Memorandum 33-544, December 15, 1972

The capability of automatically route, remove insulation from, and weld small-diameter solid conductor (magnet) wire would facilitate the economical small-quantity production of complex, miniature electronic assemblies. JPL has developed and evaluated an engineering model of equipment having this capability. Whereas early work in the use of welded magnet-wire interconnections concentrated on opposed-electrode systems and generally used heat to melt the wire insulation, the present method is based on a concentric-electrode system (patented as "Through Insulation Welding System") and a wire feed system (patent on "Wire Feed System" pending) which splits the insulation by application of pressure prior to welding. (The "Through Insulation Welding System" is the subject of U.S. Patent 3,596,044, and the "Wire Feed System" is the subject of a pending U.S. patent application. Both are licensed exclusively under terms which require that sublicenses be granted. Information regarding these inventions may be obtained from: Patent Officer, 1201 East California Blvd., Pasadena, California 91109.)

The work described in this memorandum deals with the design, fabrication, and evaluation testing of an improved version of this concentric-electrode system. Two different approaches for feeding the wire to the concentric electrodes were investigated. It was concluded that the process described is feasible for the interconnection of complex, miniature electronic assemblies. Recommendations for further work are presented.

BACK, L. H.

B01 *Influence of Contraction Section Shape and Inlet Flow Direction on Supersonic Nozzle Flow and Performance*

L. H. Back, R. F. Cuffel, and P. F. Massier

J. Spacecraft Rockets, Vol. 9, No. 6, pp. 420–427, June 1972

This article presents wall static pressure measurements and performance parameters for axisymmetric supersonic nozzles with relatively steep convergent sections and comparatively small radius-of-curvature throats. The nozzle walls were essentially adiabatic. These results are compared with those obtained in other nozzles tested previously to appraise the influence of contraction shape on performance. Both the flow coefficient and the thrust were less than the corresponding values for one-dimensional, isentropic, plane flow for both the axial and radial inflow nozzles considered; but the specific impules, the most important performance parameter, was found to be relatively unchanged. The thrust decrement for the axial inflow nozzles was established primarily by the shape of the contraction section and could be estimated reasonably well from a conical sink flow consideration. The radial inflow nozzle has a potential advantage from a cooling point of view if used in a rocket engine.

BALL, J. E.

B02 A Summary of the Pioneer 10 Maneuver Strategy

R. B. Frauenholz and J. E. Ball

JPL Quarterly Technical Review, Vol. 2, No. 3, pp. 46–62, October 1972

For abstract, see Frauenholz, R. B.

BARKER, B. J.

B03 Dynamic Measurement of Bulk Modulus of Dielectric Materials Using a Microwave Phase Shift Technique

B. J. Barker and L. D. Strand

Technical Memorandum 33-577, November 15, 1972

This memorandum discusses a microwave doppler-shift technique which has been developed for measuring the dynamic bulk modulus of dielectric materials such as solid propellants. The system has a demonstrated time resolution on the order of milliseconds and a theoretical spatial resolution of a few microns. Accuracy of the

technique is dependent on an accurate knowledge of the wavelength of the microwave in the sample being tested. Preliminary tests with two solid propellants, one non-aluminized and one containing 16% aluminum, yielded reasonable, reproducible results. It was concluded that, with refinements, the technique holds promise as a practical means for obtaining accurate dynamic-bulk-modulus data over a variety of transient conditions.

BATHKER, D. A.

B04 DSN Progress Report for July–August 1972: Dual Carrier Preparations for Viking

D. A. Bathker and D. W. Brown

Technical Report 32-1526, Vol. XI, pp. 146–149, October 15, 1972

Multiple spacecraft vehicles for the Viking mission require simultaneous transmission of two S-band carriers from a single deep space station. Past experience in high-power diplexing, coupled with dual carriers, has shown that, in addition to controlled uplink-intermodulation products, a complex form of receive-band interference will be generated within the ground station. Recent efforts to define and minimize these effects are being supplemented with additional resources including reconfiguration of the Venus Deep Space Station (DSS 13) for dual-carrier diplexed operation with the objective of assuring DSN capability in the Viking mode.

BERLEKAMP, E. R.

B05 DSN Progress Report for July–August 1972: Decoding the Golay Code

E. R. Berlekamp

Technical Report 32-1526, Vol. XI, pp. 81–85, October 15, 1972

This article describes a procedure for correcting all patterns of three or fewer errors with the (23,12) or (24,12) Golay code. The procedure decodes any 24-bit word in about 26 "steps," each of which consists of only a few simple operations such as counting the number of ones in a 12-bit word. The procedure is based on the circulant view-point introduced by Karlin (1969). In addition it is shown how the (24,12) Golay code can be used to correct certain patterns of more than three errors.

BERMAN, P. A.

B06 Photovoltaic Solar Array Technology Required for Three Wide-Scale Generating Systems for Terrestrial Applications: Rooftop, Solar Farm, and Satellite

P. A. Berman

Technical Report 32-1573, October 15, 1972

This report presents three major options for wide-scale generation of photovoltaic energy for terrestrial use: (1) Rooftop Array, (2) Solar Farm, and (3) Satellite Station. The rooftop Array would use solar-cell arrays on the roofs of residential or commercial buildings; the Solar Farm would consist of large ground-based arrays, probably in arid areas with high insolation; and the Satellite Station would consist of an orbiting solar array, many square kilometers in area.

The Technology Advancement Requirements necessary for each option are discussed, including cost reduction of solar cells and arrays, weight reduction, resistance to environmental factors, reliability, and fabrication capability, including the availability of raw materials. The majority of the Technology Advancement Requirements are applicable to all three options, making possible a flexible basic approach regardless of the options that may eventually be chosen. No conclusions are drawn as to which option is most advantageous, since the feasibility of each option depends on the success achieved in the Technology Advancement Requirements specified.

B07 Development of Lithium-Doped Radiation-Resistant Solar Cells

P. A. Berman

Technical Report 32-1574, November 15, 1972

In the middle 1960s, it was discovered that the addition of lithium to *n*-base silicon solar cells resulted in what appeared to be annealing of radiation-induced defects. For the past five years, JPL has been involved in an effort to exploit this phenomenon in order to develop a highly-radiation-resistant, high-efficiency silicon solar cell. This paper discusses the results of the investigations which represent major achievements for attaining this goal. Lithium-doped solar cells have now been fabricated with initial lot efficiencies averaging 11.9% in an air-mass-zero solar simulator and a maximum observed efficiency of 12.8%. The best lithium-doped solar cells are approximately 15% higher in maximum power than state-of-the-art *n–p* cells after moderate-to-high fluences of 1-MeV electrons and after 6–7 months exposure to low-flux (approximately 10^{12}-electrons/cm^2/day) irradiation by a strontium-90 beta source,

which approximates the electron spectrum and flux associated with near-Earth space. Furthermore, lithium-doped cells were found to degrade at a rate only one-tenth that of state-of-the-art n–p cells under 28-MeV electron irradiation.

Excellent progress has been made in quantitative predictions of post-irradiation current–voltage characteristics as a function of cell design by means of capacitance–voltage measurements, and this information has been used to achieve further improvements in lithium-doped cell design. Major improvements in cell processing have also been achieved, resulting in higher cell efficiency and greater reproducibility.

BJORKLUND, R. A.

B08 Trajectory Correction Propulsion for TOPS

H. R. Long and R. A. Bjorklund

Technical Report 32-1571, November 15, 1972

For abstract, see Long, H. R.

BLINN III, J. C.

B09 Microwave Emission From Geological Materials: Observations of Interference Effects

J. C. Blinn III, J. E. Conel, and J. G. Quade (University of Nevada)

J. Geophys. Res., Vol. 77, No. 23, pp. 4366–4378, August 10, 1972

Microwave radiometric field observations were conducted at wavelengths of 21, 2.8, and 0.95 cm to determine the microwave penetration depth of a number of sands and gravels as a function of particle size and moisture content. Observations of a reflecting plate covered with varying thicknesses of test material exhibit a pronounced oscillatory behavior that is consistent with established electromagnetic theory for plane-parallel layered mediums. Utilization of this interference effect is proposed as a microwave radiometric technique for determining the bulk electrical properties of geologic materials, snow, ice, and other materials readily adapted to layering experiments. Extension of the technique could lead to a method for remotely determining layer thickness in certain naturally layered systems such as sea ice.

BOGGS, D. H.

B10 A Partial-Step Algorithm for the Nonlinear Estimation Problem

D. H. Boggs

AIAA J., Vol. 10, No. 5, pp. 675–679, May 1972

The "normal equations" solution to the weighted least-squares estimation problem is recast in terms of singular-value decomposition of the equations-of-condition matrix, A. The superior convergence properties of rank-deficient, pseudoinverse solutions in the presence of nonlinearities and ill-conditionedness of the normal matrix A^TA are examined. An extension of this, partial-step technique, which makes use of part of the information contained along "eigen-directions" associated with singular values previously ignored in the standard rank-deficient solution, is presented. Results are given showing the relative convergence powers of the methods in obtaining a solution to the orbit-determination problem for a simulated Martian orbiter trajectory. These results indicate that the extended partial-step method will be of value during the orbit phase of the Mariner Mars 1971 mission.

BOOTH, R. W. D.

B11 DSN Progress Report for July–August 1972: Preliminary Analysis of the Microwave Weather

M. S. Reid and R. W. D. Booth

Technical Report 32-1526, Vol. XI, pp. 111–120, October 15, 1972

For abstract, see Reid, M. S.

BROWN, D. W.

B12 DSN Progress Report for July–August 1972: Dual Carrier Preparations for Viking

D. A. Bathker and D. W. Brown

Technical Report 32-1526, Vol. XI, pp. 146–149, October 15, 1972

For abstract, see Bathker, D. A.

BUCHANAN, H. R.

B13 DSN Progress Report for September–October 1972: X-Band Uplink Microwave Components

H. R. Buchanan

Technical Report 32-1526, Vol. XII, pp. 22–25, December 15, 1972

Waveguide components for use in the 400-kW X-band radar system will be electrically stressed to a considerably greater extent than previous Deep Space Instrumentation Facility equipment. The electrical characteristics of several possible waveguide sizes have been investigated. A size has been selected which offers an adequate safety margin for X-band radar and other possible X-band uplink applications.

CANNOVA, R. D.

C01 Development and In-Flight Performance of the Mariner 9 Spacecraft Propulsion System

D. D. Evans, R. D. Cannova, and M. J. Cork

Technical Memorandum 33-574, November 1, 1972

For abstract, see Evans, D. D.

CARON, L. G.

C02 Quantum Crystals in the Single-Particle Picture

L. G. Caron

Phys. Rev., Pt. B: Solid State, Vol. 6, No. 4, pp. 1081–1090, August 15, 1972

This article presents a low-temperature formalism for quantum crystals based on the localized-single-particle picture. A proposed transcription to a quasiparticle space provides the basis for an easily accessible thermal analysis and yields correlation and lifetime information. The excitations are shown to be the same as Werthamer's. The effect of wave-function overlap and its impact on magnetism are discussed and the defect crystal is examined.

CHAN, S. I.

C03 Electron Paramagnetic Resonance of Radiation Damage in a Lunar Rock

F.-D. Tsay, S. I. Chan, and S. L. Manatt

Nature Phys. Sci., Vol. 237, No. 77, pp. 121–122, June 19, 1972

For abstract, see Tsay, F.-D.

CLAUSS, R.

C04 DSN Progress Report for July–August 1972: Low Noise Receivers: Microwave Maser Development

R. Clauss, E. Wiebe, and R. Quinn

Technical Report 32-1526, Vol. XI, pp. 71–80, October 15, 1972

A traveling-wave maser, tunable from 7750 to 8750 MHz, has been completed and tested in the laboratory. The maser is ready for installation on the 64-m-diameter antenna at the Deep Space Communications Complex at Goldstone, California. Gain, phase, and group-delay stability were measured as a function of magnetic field, refrigerator temperature, power-supply voltages, and large interfering signals. Several features have been included in this maser to improve the stability performance. A superconducting magnet provides a very stable magnetic field. Push-push pumping results in complete pump saturation and reduced pump frequency-stability requirements. Low-pass filters at a temperature of 4.5 K reduce pump power radiation in signal waveguides.

The maser has a 45-dB net gain and a 17-MHz, 3-dB bandwidth with an equivalent input noise temperature of 6.5 K at 8415 MHz and 8.5 K at 7850 MHz. Simultaneous operation at two frequencies, separated by up to 500 MHz, is available at reduced gain.

CLAUSS, R. C.

C05 DSN Progress Report for September–October 1972: Improved RF Calibration Techniques—A Practical Technique for Accurate Determination of Microwave Surface Resistivity

R. C. Clauss and P. D. Potter

Technical Report 32-1526, Vol. XII, pp. 59–67, December 15, 1972

This article describes a surface-loss measurement technique using a TE_{011}-mode circular-waveguide cavity resonator. A novel feature of this technique is the use of a standard cavity, with a test sample (a flat plate) forming one of the end walls of the cavity. The unique properties of this cavity eliminate the need for intimate contact between the test surface and the rest of the cavity; a surface contact problem is thereby avoided.

Precision Q-measurement equipment is required for this technique. Formulas for the surface resistivity of the sample as a function of the measured cavity Q are derived. Preliminary test data are presented and compared with predicted values, where available. The method described in this article appears to have a wide range of applicability.

CONEL, J. E.

C06 Microwave Emission From Geological Materials: Observations of Interference Effects

J. C. Blinn III, J. E. Conel, and J. G. Quade (University of Nevada)

J. Geophys. Res., Vol. 77, No. 23, pp. 4366–4378, August 10, 1972

For abstract, see Blinn III, J. C.

CONSTENLA, L. C.

C07 DSN Progress Report for September–October 1972: Complex Mixer System

L. C. Constenla

Technical Report 32-1526, Vol. XII, pp. 189–194, December 15, 1972

The complex-mixer system is a signal preconditioner for a Fast-Fourier-Transform power-spectrum analyzer. It generates a complex time-series output of the real-valued time series fed to its input. Two complex mixers have been constructed and installed at the Mars Deep Space Station (DSS 14). They have processed signals received from the Mariner 1971 spacecraft to investigate induced cross polarization of signals passing close to the solar corona.

COOPER, B. M.

C08 DSN Progress Report for July–August 1972: NASTRAN Data Generation and Management Using Interactive Graphics

M. S. Katow and B. M. Cooper

Technical Report 32-1526, Vol. XI, pp. 104–110, October 15, 1972

For abstract, see Katow, M. S.

CORK, M. J.

C09 Development and In-Flight Performance of the Mariner 9 Spacecraft Propulsion System

D. D. Evans, R. D. Cannova, and M. J. Cork

Technical Memorandum 33-574, November 1, 1972

For abstract, see Evans, D. D.

CUFFEL, R. F.

C10 Influence of Contraction Section Shape and Inlet Flow Direction on Supersonic Nozzle Flow and Performance

L. H. Back, R. F. Cuffel, and P. F. Massier

J. Spacecraft Rockets, Vol. 9, No. 6, pp. 420–427, June 1972

For abstract, see Back, L. H.

DALLAS, S. S.

D01 DSN Progress Report for July–August 1972: A Comparison of Cowell's Method and a Variation-of-Parameters Method for the Computation of Precision Satellite Orbits: Phase Three Results

S. S. Dallas and E. A. Rinderle

Technical Report 32-1526, Vol. XI, pp. 30–35, October 15, 1972

Additional test cases were run using a precision special-perturbations program employing either Cowell's method or a variation-of-parameters method to compute a nearly circular, nearly equatorial orbit using two different perturbative accelerations. The results obtained again indicate that the variation-of-parameters method with a predict-only integrator and Cowell's method with a predict–partial-correct integrator are equally efficient, and both are significantly more efficient than Cowell's method with a predict-correct integrator.

DAVIS, E. K.

D02 DSN Progress Report for September–October 1972: Mariner Venus–Mercury 1973 Mission Support

E. K. Davis

Technical Report 32-1526, Vol. XII, pp. 10–13, December 15, 1972

Major planning and design activities and associated reviews and documentation have been completed for the Mariner Venus–Mercury 1973 Project. This article summarizes achievements of the past year as the DSN fully enters the implementation and test phase.

DE WINTER, F.

D03 Xenon-Filled Silicon Germanium Thermoelectric Generators

F. de Winter

JPL Quarterly Technical Review, Vol. 2, No. 3, pp. 22–31, October 1972

This article presents an analysis that shows the desirability and feasibility of using a xenon fill in the initial stages of operation of a silicon-germanium radioisotope thermoelectric generator to be used in outer-planetary exploration. The xenon cover gas offers protection against oxidation and against material sublimation, and allows the generator to deliver required power throughout the prelaunch and launch phases. The protective mechanisms afforded by the xenon cover gas and the mechanization of a xenon supply system are also discussed.

EDELSON, R. E.

E01 Telecommunications Systems Design Techniques Handbook

R. E. Edelson

Technical Memorandum 33-571, July 15, 1972

The DSN, managed by JPL for NASA, increasingly supports deep space missions sponsored and managed by organizations without long experience in DSN design and operation. This memorandum is intended as a textbook for those DSN users inexperienced in the design and specification of a DSN-compatible spacecraft telecommunications system. For experienced DSN users, the memorandum provides a reference source of telecommunication information which summarizes knowledge previously available only in a multitude of sources. Extensive references are quoted for those who wish to explore specific areas more deeply.

EISENBERGER, I.

E02 DSN Progress Report for September–October 1972: An Inventory and Procurement Policy for the Deep Space Network

I. Eisenberger, F. R. Maiocco, and G. Lorden (California Institute of Technology)

Technical Report 32-1526, Vol. XII, pp. 131–148, December 15, 1972

This article presents a technical description of a proposed inventory and procurement policy for ordering and allocating maintenance and operating supplies throughout the DSN. This policy differs from the conventional economic lot-size procurement policy in that the reorder point for the Network Supply Depot (NSD) depends upon the stockage levels at all area, station, or Complex Supply Facilities (CSF), as well as on the level at the NSD. Thus, by basing reorder decisions upon the state of the inventory supplies throughout the entire DSN, an efficient cost-minimizing policy is possible. Safe minimum inventory levels are established for each CSF by means of statistical decision-theory techniques which require NSD to reorder whenever one or more of the CSFs reaches its prescribed minimum. Some results of a statistical study of the effect of this policy are included.

ELACHI, C.

E03 Cerenkov and Transition Radiation in Space–Time Periodic Media

C. Elachi

J. Appl. Phys., Vol. 43, No. 9, pp. 3719–3723, September 1972

The solution to the problem of determining the radiation emitted by a uniformly moving charged particle in a sinusoidally space-time periodic medium is obtained. The space-time periodicity can be considered as due to a strong pump wave and is expressed as a traveling-wave-type change in the dielectric constant or the plasma density. The solution covers also the limiting case of sinusoidally stratified media. The expression and spectrum of the radiated electromagnetic field are determined for different media: dielectric, isotropic and uniaxial plasma. Depending on the nature of the medium and the velocity of the particle, the radiated field is of the Cerenkov and/or transition type. The Brillouin diagram is used extensively in understanding and determining the nature, extent, and spectrum of the different modes of radiation, and a focusing effect is also studied.

ERPENBACH, H.

E04 DSN Progress Report for September–October 1972: Frequency Generation and Control: Atomic Hydrogen Dissociator

H. Erpenbach and D. Norris

Technical Report 32-1526, Vol. XII, pp. 56–58, December 15, 1972

This article describes a long-life hydrogen gas discharge source for the JPL hydrogen maser. The lifetime of this source has been extended from approximately 6 months to 2 years or more by changing the geometry of the RF power coupling mechanism. Other improvements over the older type source are: (1) the gas discharge may be started without increasing hydrogen pressure, and (2) an acceptable impedance match to the RF power generator can be achieved over a broader range of operating hydrogen pressures.

ESCOBAL, P. R.

E05 3-D Multilateration: A Precision Geodetic Measurement System

P. R. Escobal, H. F. Fliegel, R. M. Jaffe, P. M. Muller, K. M. Ong, O. H. von Roos, and M. S. Shumate

JPL Quarterly Technical Review, Vol. 2, No. 3, pp. 1–11, October 1972

The assessment of earthquake hazards, indication of probable locations for earthquakes, and the eventual possibility of earthquake prediction or premonitory warning have become an important part of the NASA Earth Physics Applications Program. The key to moving toward these goals is believed to be precision monitoring of the near- and far-field strain buildup and release within a few hundred kilometers of active fault zones such as the San Andreas. A system with the capability of determining station positions in three dimensions with 1-cm accuracy has been designed using pulsed-laser Earth-satellite tracking stations coupled with strictly geometric data reduction.

ESPOSITO, P. B.

E06 Geocentric Gravitational Constant Determined From Mariner 9 Radio Tracking Data

P. B. Esposito and S. K. Wong

Preprint of paper presented at International Symposium on Earth Gravity Models and Related Problems (Sponsored by the American Geophysical Union, NASA), St. Louis, Missouri, August 16–18, 1972

Several days of the Mariner 9 near-Earth radio tracking data have been analyzed to determine the Earth's gravitational constant. The doppler data distribution is essentially continuous as five deep space network stations have been receiving data. All basic forces influencing the spacecraft's motion have been modeled and a typical analysis of the data yields doppler residuals within ±0.004 Hz which amounts to ±0.3 mm s^{-1} in range-rate. During this interval, the spacecraft's range-rate varied from 5.6 to 3.2 km s^{-1}.

The value of the Earth's gravitational constant and associated standard deviation deduced from this preliminary analysis is GM = 398600.8 ± 0.4 km^3 s^{-2}. Additional analysis, which includes refining the model for the attitude-control perturbations, incorporating an ionospheric model, and extending the data arc, should improve both the value and uncertainty of this constant. The major source of error is due to perturbative accelerations caused by the attitude-control subsystem on the spacecraft. A comparison of this result with independent determinations deduced from analyses of previous spacecraft data is also presented.

EVANS, D. D.

E07 Development and In-Flight Performance of the Mariner 9 Spacecraft Propulsion System

D. D. Evans, R. D. Cannova, and M. J. Cork

Technical Memorandum 33-574, November 1, 1972

On November 14, 1971, Mariner 9 was decelerated into orbit about Mars by a 1334-N (300-lbf) liquid-bipropellant propulsion system. This memorandum describes and summarizes the development and in-flight performance of this pressure-fed, nitrogen tetroxide/monomethyl hydrazine bipropellant system. The design of all Mariner propulsion subsystems has been predicated upon the premise that simplicity of approach, coupled with thorough qualification and margin-limits testing, is the key to cost-effective reliability. The Mariner 9 subsystem design illustrates this approach in that little functional redundancy is employed. This memorandum summarizes the design and test rationale employed in the Mariner 9 design and development program.

The qualification test program and analytical modeling are also discussed. Since the propulsion subsystem is modular in nature, it was completely checked, serviced, and tested independent of the

spacecraft. Proper prediction of in-flight performance required the development of three significant modeling tools to predict and account for nitrogen saturation of the propellant during the 6-month coast period and to predict and statistically analyze in-flight data. The flight performance of the subsystem was excellent, as were the performance-prediction correlations, which are presented.

FARRAR, J. W.

F01 Development and Testing of the Ultraviolet Spectrometer for the Mariner Mars 1971 Spacecraft

J. W. Farrar

Technical Memorandum 33-569, October 15, 1972

The Mariner Mars 1971 ultraviolet spectrometer is an Ebert-Fastie type of the same basic design as the Mariner Mars 1969 instrument. Light enters the instrument and is split into component wavelengths by a scanning reflection diffraction grating. Two monochrometer exit slits allow the use of two independent photomultiplier-tube sensors. Channel 1 has a spectral range of 1100 to 1692 Å with a fixed gain, while Channel 2 has a spectral range of 1450 to 3528 Å with an automatic step gain control, providing a dynamic range over the expected atmosphere and surface brightness of Mars.

This memorandum describes the scientific objectives, basic operation, design, testing, and calibration for the Mariner Mars 1971 ultraviolet spectrometer. The design discussion includes those modifications that were necessary to extend the lifetime of the instrument in order to accomplish the Mariner Mars 1971 mission objectives.

FEDORS, R. F.

F02 A Molecular Theory of Elastomer Deformation and Rupture

R. F. Landel and R. F. Fedors

Mechanical Behavior of Materials: Proceedings of the 1971 International Conference on Mechanical Behavior of Materials (Sponsored by the Society of Materials Science), Kyoto, Japan, August 1971, Vol. III, pp. 496-507

For abstract, see Landel, R. F.

FINNEGAN, E. J.

F03 DSN Progress Report for September–October 1972: A Dual-Ignitron Crowbar

E. J. Finnegan

Technical Report 32-1526, Vol. XII, pp. 205–208, December 15, 1972

This article describes a high-voltage protective device (crowbar) that is capable of operating at 100,000 V. This device has two ignitrons in series, with the appropriate electronics to trigger the tubes to a conducting state when desired. The crowbar is needed to increase the reliability of the transmitter, as the present tubes have difficulty operating at over 60,000 V. A new photon generator was designed and tested using light-emitting diodes and infrared-detecting pin diodes in conjunction with fiber optics for transmitting a pulse to the high-voltage deck and triggering the ignitron crowbar.

FJELDBO, G.

F04 Bistatic Radar Measurements of the Surface of Mars With Mariner 1969

G. Fjeldbo, A. J. Kliore, and B. L. Seidel

Icarus, Vol. 16, No. 3, pp. 502–508, June 1972

This article describes the detection of echoes produced by oblique reflection of the radio frequency (2300 MHz) spacecraft carrier from the Martian surface as Mariners 6 and 7 flew behind Mars in 1969. Changes in echo center frequency and bandwidth are utilized to study the radius and roughness of the surface along a quasi-specular radar track that led from an optically dark and densely cratered region of Meridiani Sinus over into a smoother and brighter looking area of Thymiamata. A 3 to 1 decrease in surface roughness of large size compared to the wavelength (13 cm) was observed as the reflecting zone moved across the boundary between these two regions. The average radius obtained along the track was 3393 ± 3 km. Due to large angles of incidence (86 to 90°), and surface shadowing, the data are not suitable for mapping the reflection coefficient of the surface material.

FLEISCHER, G. E.

F05 Large-Deformation Modal Coordinates for Nonrigid Vehicle Dynamics

P. W. Likins and G. E. Fleischer

Technical Report 32-1565, November 1, 1972

For abstract, see Likins, P. W.

FLIEGEL, H. F.

F06 DSN Progress Report for July–August 1972: Use of Doppler Determinations of Polar Motion Using Artificial Satellites to Support JPL Planetary Missions

H. F. Fliegel

Technical Report 32-1526, Vol. XI, pp. 36–41, October 15, 1972

Standard deviations and systematic differences are calculated between the U.S. Navy Weapons Laboratory (USNWL) determination of the X and Y coordinates of the pole using artificial satellites, and the smoothed 5-day means published by the Bureau International de l'Heure (BIH). The results indicate slowly varying errors of about 1 m in the conventionally obtained optical data of the BIH, which are presently used by JPL. Although current values of polar coordinates should be based upon the BIH Rapid Service, values for previous months might be improved with the help of USNWL doppler data.

F07 3-D Multilateration: A Precision Geodetic Measurement System

P. R. Escobal, H. F. Fliegel, R. M. Jaffe, P. M. Muller, K. M. Ong, O. H. von Roos, and M. S. Shumate

JPL Quarterly Technical Review, Vol. 2, No. 3, pp. 1–11, October 1972

For abstract, see Escobal, P. R.

FOSTER, C. F.

F08 DSN Progress Report for July–August 1972: Wideband Distribution Amplifier for Coherent Reference Generator

C. F. Foster

Technical Report 32-1526, Vol. XI, pp. 140–145, October 15, 1972

A wideband (0.1- to 100-MHz) frequency-distribution module has been designed to have high output-to-output isolation, low phase shift with temperature, no RF tuning, and internal means to detect module performance that can be monitored by a computer. The amplifier and its use with a coherent reference generator are described in this article.

FRANCO, M.

F09 DSN Progress Report for September–October 1972: Improved RF Calibration Techniques: Commercial Precision IF Attenuator Evaluation

C. Stelzried, B. L. Seidel, M. Franco, and D. Acheson

Technical Report 32-1526, Vol. XII, pp. 74–82, December 15, 1972

For abstract, see Stelzried, C.

FRANK, J.

F10 A Study on Heavy/Light Atom Discrimination in Bright-Field Electron Microscopy Using the Computer

J. Frank (Cornell University)

Biophys. J., Vol. 12, No. 5, pp. 484–511, May 1972

The Z dependence of the phase angle of the complex atomic scattering amplitude can be used to separate the image due to the heavy atoms from that due to the light atoms of the object structure. The linear theory of image formation applied to a focus series of bright-field images leads to Schiske's formula for the calculation of the structure factor. A program system is described which uses this algorithm for computing both images from a set of digitized electron micrographs of a focus series of uranyl-stained DNA on a thin carbon film.

FRAUENHOLZ, R. B.

F11 A Summary of the Pioneer 10 Maneuver Strategy

R. B. Frauenholz and J. E. Ball

JPL Quarterly Technical Review, Vol. 2, No. 3, pp. 46–62, October 1972

The Pioneer Project placed a number of interesting and precise requirements on the navigation of the Pioneer 10 flyby mission to Jupiter during 1972–1973. To satisfy these requirements the Pioneer Navigation Team employed a number of versatile computer programs to evaluate the strategies and maneuver sequences required to execute midcourse corrections. This article summarizes the Pioneer 10 mission objectives and the midcourse strategies used to satisfy these objectives.

GARDNER, J. A.

G01 Solar Electric Propulsion System Integration Technology (SEPSIT) Final Report: Encke Rendezvous Mission and Space Vehicle Functional Description

J. A. Gardner

Technical Memorandum 33-583, Vol. II, November 15, 1972

This memorandum is the final report on the Solar Electric Propulsion System Integration Technology study conducted at JPL. This volume describes in detail the solar electric propulsion (SEP) space vehicle and the mission to which it is applied. It includes a detailed functional description of the SEP thrust subsystem along with its technical specifications and requirements as are known at this time.

Detailed analyses that were performed in support of the SEP module thrust subsystem functional description are contained in Volume III of this memorandum series. Volume I contains a technical summary of the work documented in Volumes II and III.

G02 Solar Electric Propulsion System Integration Technology (SEPSIT) Final Report: Supporting Analyses

J. A. Gardner

Technical Memorandum 33-583, Vol. III,
November 15, 1972

This memorandum is the final report on the Solar Electric Propulsion System Integration Technology study conducted at JPL. This volume contains detailed analyses that were performed in support of the solar electric propulsion (SEP) module thrust subsystem functional description that is presented in Volume II of this memorandum series.

Volume II describes in detail the SEP space vehicle and the mission to which it is applied. A technical summary of the work documented in Volumes II and III is presented in Volume I.

GELLER, E. N.

G03 Nature of Two-Particle Correlations in Atoms

E. N. Geller and M. Geller

J. Chem. Phys., Vol. 57, No. 4, p. 1814, August 15, 1972

This article presents an analytical evaluation of radial integrals of the form

$$I_n(Z') = \int_0^\infty \int_0^\infty \exp\left[-2Z'(r_1 + r_2)\right]$$

$$\times \frac{r_1^{n+1} r_2^{n+1}}{(r_1^2 + r_2^2)^{n-0.5}} dr_1\, dr_2$$

The first few integrals are given as well as a recurrence relation for successive integrals.

GELLER, M.

G04 Nature of Two-Particle Correlations in Atoms

E. N. Geller and M. Geller

J. Chem. Phys., Vol. 57, No. 4, p. 1814, August 15, 1972

For abstract, see Geller, E. N.

GEORGEVIC, R. M.

G05 The Solar Radiation Pressure on the Mariner 9 Mars Orbiter

R. M. Georgevic

Technical Memorandum 33-582, December 15, 1972

The refined mathematical model of the force created by the light pressure of the Sun has been used to compute the solar-radiation pressure force acting on the Mariner 9 (Mariner Mars 1971) spacecraft, taking into account the reflectivity characteristics of all its components. As demonstrated in this memorandum, the results have been compared with values obtained from Mariner 9 observations during the cruise phase and found to be in agreement within 0.1% of the experimental values.

GILLESPIE, A. R.

G06 An Orthographic Photomap of the South Pole of Mars From Mariners 6 and 7

A. R. Gillespie and J. M. Soha

Icarus, Vol. 16, No. 3, pp. 522–527, June 1972

Television pictures of the south polar regions of Mars obtained by the Mariner 6 and 7 spacecraft in 1969 are rectified to a standard

mapping projection using computer image processing techniques. Mosaicking of these pictures produces the first photomap of the entire south polar cap.

GINGO, P. J.

G07 Neutron Radiation Characteristics of Plutonium Dioxide Fuel

M. Taherzadeh and P. J. Gingo (Akron State University)

Nucl. Technol., Vol. 15, No. 3, pp. 396–410, September 1972

For abstract, see Taherzadeh, M.

GOODWIN, P. S.

G08 DSN Progress Report for September–October 1972: Helios Mission Support

P. S. Goodwin

Technical Report 32-1526, Vol. XII, pp. 5–9, December 15, 1972

Project Helios is a joint deep space project of the Federal Republic of West Germany and the United States. Two solar orbiting spacecraft are planned, the first to be launched in mid-1974 and the second in late 1975. The spacecraft will have a perihelion of approximately 0.25 AU and an aphelion of 1.0 AU. These spacecraft with their highly elliptical orbits will come closer to the Sun than any previous or planned spacecraft.

Prior articles of this series described the history and organization of this program, the spacecraft configuration and trajectory, its telecommunications system, and the results of the semi-annual Helios Joint Working Group Meetings which are held alternately in the United States and the Federal Republic of West Germany. This article deals with DSN activities since the Sixth Helios Joint Working Group Meeting, which was held at JPL in April–May 1972.

GOSLINE, R. M.

G09 DSN Progress Report for July–August 1972: DSN Research and Technology Support

R. M. Gosline

Technical Report 32-1526, Vol. XI, pp. 132–134, October 15, 1972

This article summarizes the activities of the Development Support Group for the 2-month period ending August 15, 1972. The activities are arranged according to whether they were performed at the Venus Deep Space Station (DSS 13) or at the Microwave Test Facility, and are further subdivided as to the section receiving support. Activities include operational clock synchronization, precision antenna-gain measurements, weak-source observations, pulsar observations, planetary radar, and Mars Deep Space Station (DSS 14) 400-kW transmitter support.

GREEN, W. B.

G10 Recent Developments in Digital Image Processing at the Image Processing Laboratory at the Jet Propulsion Laboratory

D. A. O'Handley and W. B. Green

Proc. IEEE, Vol. 60, No. 7, pp. 821–828, July 1972

For abstract, see O'Handley, D. A.

GREENWOOD, R. F.

G11 Results of the 1970 Balloon Flight Solar Cell Standardization Program

R. F. Greenwood and R. L. Mueller

Technical Report 32-1575, December 1, 1972

For the eighth consecutive year, high-altitude calibration of solar cells was accomplished with the aid of free-flight balloons. Flights were conducted to an altitude of 36,576 m (120,000 ft), which is above 99.5% of the Earth's atmosphere where all water vapor and significant ozone bands are absent. Solar cells calibrated in this manner are recovered and used as intensity references in solar simulators and in terrestrial sunlight. Balloon-calibrated solar cells were made available by JPL to NASA centers and other government agencies through a cooperative effort. An attempt to fly radiometers to measure the solar constant was aborted because of a balloon failure at launch. This report discusses the method employed for high-altitude balloon flight solar-cell calibration. Also presented are the data collected on 52 standard solar cells on two flights conducted during July and August 1970. Solar cells flown repeatedly on successive flights have shown correlation of better than ±1.0%.

GULKIS, S.

G12 **Jupiter: New Evidence of Long-Term Variations of Its Decimeter Flux Density**

M. J. Klein, S. Gulkis, and C. T. Stelzried

Astrophys. J., Vol. 176, No. 2, Pt. 2, pp. L85–L88, September 1, 1972

For abstract, see Klein, M. J.

GUPTA, K. K.

G13 **Dynamic Response Analysis of Geometrically Non-linear Structures Subjected to High Impact**

K. K. Gupta

Int. J. Numer. Methods Eng., Vol. 4, No. 2, pp. 163–174, March–April 1972

This article presents an efficient digital computer method for the determination of propagation of elastic stresses and deformations in certain geometrically non-linear structures subjected to high-impact loading. The finite-element matrix displacement approach utilizing curved quadrilateral shell elements in conjunction with a nodewise predictor–corrector method employing Runge–Kutta extrapolation techniques has been adopted for the present solution.

The related computer program written in FORTRAN V for the UNIVAC 1108 computer has proved to be effective for the solution of a range of practical problems including rectangular and cylindrical panels. Numerical results are presented for a relevant structure, the cell container and the negative electrode of an impact-reisitant battery subjected to high impact, simulating its free landing on a planetary surface.

G14 **Solution of Eigenvalue Problems by Sturm Sequence Method**

K. K. Gupta

Int. J. Numer. Methods Eng., Vol. 4, No. 3, pp. 379–404, May–June 1972

This article presents a generalized eigenvalue algorithm along with the complete listing of the associated computer program which may be conveniently utilized for the efficient solution of certain broad classes of eigenvalue problems. Extensive applications of the procedure are envisaged in the analysis of many important engineering problems, such as stability and natural frequency analysis of practical discrete structural systems, idealized by the finite-element technique. The procedure based on the Sturm sequence

method is accurate and fast, possessing several significant advantages over other known methods of such analysis. Numerical results are also presented for two representative structural engineering problems.

HALL, J. R.

H01 DSN Progress Report for July–August 1972: Network Control System

J. R. Hall

Technical Report 32-1526, Vol. XI, pp. 5–11, October 15, 1972

This article provides: (1) background material describing the philosophy leading to a Network Control System (NCS) function using data-processing equipment separate from that used by flight projects, (2) key characteristics of the NCS, (3) a listing of the functional requirements for each NCS subsystem, (4) a generic subsystem data-flow description, and (5) an overall NCS data-flow description.

HARDY, J. P.

H02 Rapid Determination of Twenty Amino Acids by Gas Chromatography

J. P. Hardy and S. L. Kerrin

Anal. Chem., Vol. 44, No. 8, pp. 1497–1499, July 1972

Determination of amino acids by gas chromatographic separation of appropriate volatile derivatives has been described in numerous literature reports. For all methods, the limiting step in analyses of multiple samples is the gas chromatographic determination time, since preparation of volatile derivatives of several samples may be carried along in parallel, but each gas chromatographic analysis must be performed sequentially.

This article presents a method for the preparation of volatile *N*-trimethylsilyl-*O*-*n*-butyl ester (TMSi-butyl) derivatives of 20 amino acids and the conditions under which they can be separated, in less than 35 minutes, on a lightly-loaded textured-glass-bead gas chromatographic column.

HARPER, L. H.

H03 DSN Progress Report for July–August 1972: Reducing the Complexity of Calculating Syndromes for Error-Correcting Codes

L. H. Harper and J. E. Savage

Technical Report 32-1526, Vol. XI, pp. 89–91, October 15, 1972

The calculation of the syndrome—the first step performed by all decoders of linear codes—can require a number of logical operations which grows faster than the square of block length. This article shows that the complexity of syndrome calculation can be reduced for many linear codes by a factor of log of the code block length and that Hamming codes can be decoded with combinational machines having a number of logic elements which is linear with block length.

HARSTAD, K. G.

H04 Review of Laser–Solid Interaction and Its Possibilities for Space Propulsion

K. G. Harstad

Technical Memorandum 33-578, November 15, 1972

This memorandum surveys the literature on laser–solid-matter interaction and delineates the important regimes of this process. This information is used to discuss the possibility of a laser-induced ablation thruster. It is concluded that such a thruster may be feasible if a sufficiently high-intensity, high-frequency laser beam is available and that further study of laser–solid-matter interaction is needed.

H05 Rational Approximation for the Voigt Line Profile

K. G. Harstad

J. Opt. Soc. Am., Vol. 62, No. 6, pp. 827–828, June 1972

For many problems of calculating radiative transfer or curves of growth for a line, the Voigt profile is used. This article presents an accurate approximation for this profile in cases where the ratio of the Lorentz semi-half-width to doppler width is not small.

HELTON, M. R.

H06 Mariner Mars 1971 Television Picture Catalog: Sequence Design and Picture Coverage

P. E. Koskela, M. R. Helton, L. N. Seeley, and S. J. Zawacki

Technical Memorandum 33-585, Vol. II, December 15, 1972

For abstract, see Koskela, P. E.

HIGA, W. H.

H07 Time Synchronization via Lunar Radar

W. H. Higa

Proc. IEEE, Vol. 60, No. 5, pp. 552–557, May 1972

The advent of round-trip radar measurements has permitted the determination of the ranges to the nearby planets with greater precision than was previously possible. When the distances to the planets are known with high precision, the propagation delay for electromagnetic waves reflected by the planets may be calculated and used to synchronize remotely located clocks. Details basic to the operation of a lunar radar indicate a capability for clock synchronization to ±20 μs. One of the design goals for this system was to achieve a simple semiautomatic receiver for remotely located tracking stations.

The lunar radar system is in operational use for deep space tracking at JPL and synchronizes five world-wide tracking stations with a master clock at Goldstone, Calif. Computers are programmed to correct the Goldstone transmissions for transit time delay and doppler shifts so as to be received on time at the tracking stations; this dictates that only one station can be synchronized at a given time period and that the moon must be simultaneously visible to both the transmitter and receiver for a minimum time of 10 min. Both advantages and limitations of the system are given. Finally, an experiment is described which has detected the effects of lunar topography and libration on radar results; a monthly cyclic effect in time synchronization of about ±6 μs is shown.

HOLMES, J. K.

H08 DSN Progress Report for September–October 1972: Optimum Noncoherent Receiver at Low Signal-to-Noise Ratio for Unknown Doppler Shifted Signals

J. K. Holmes

Technical Report 32-1526, Vol. XII, pp. 88–91, December 15, 1972

This article derives an optimum, low-signal-to-noise-ratio receiver for the case when the received signal has unknown phase and an unknown doppler shift. This receiver appears to be new and is quite similar in form to the wideband frequency-shift-keyed receiver.

HUGHES, R. S.

H09 The Mariner Mars 1971 Radio Frequency Subsystem

R. S. Hughes

Technical Memorandum 33-573, December 1, 1972

This memorandum describes the radio frequency subsystem (RFS) for the Mariner Mars 1971 spacecraft. The Mariner Mars 1969 RFS was used as the baseline design for the Mariner Mars 1971 RFS, and the memorandum describes design changes made to the Mariner Mars 1969 RFS for use on Mariner Mars 1971. The memorandum also notes various problems encountered during the fabrication and testing of the RFS as well as the types of tests the RFS was subjected to. In areas where significant problems were encountered, a detailed description of the problem and its solution is presented. In addition, the memorandum recommends some modifications to the RFS and to the test techniques for future programs.

HUNT, G. E.

H10 The Infrared Spectrum of Jupiter: Structure and Radiative Properties of the Clouds

F. W. Taylor and G. E. Hunt

Proceedings of the Conference on Atmospheric Radiation, Fort Collins, Colorado, August 7–9, 1972, pp. 100–102

For abstract, see Taylor, F. W.

HUNTRESS, W. T., JR.

H11 Hydrogen Atom Scrambling in Ion–Molecule Reactions of Methane and Ethylene

W. T. Huntress, Jr.

J. Chem. Phys., Vol. 56, No. 10, pp. 5111–5120, May 15, 1972

The product distribution for the reactions $CH_4^+ + CD_4$, $CH_3^+ + CD_4$, $C_2H_4^+ + C_2D_4$, and their isotopic complements are determined as a function of reactant-ion kinetic energy over the range from thermal energies to 10 eV. The reaction of CH_4^+ with the parent neutral proceeds both via proton transfer and hydrogen atom abstraction accompanied by approximately 10% hydrogen atom exchange during reaction. The reactions $CH_3^+ + CD_4$ and $C_2H_4^+ + C_2D_4$ are shown to proceed with isotopic scrambling of the hydrogen atoms over the entire kinetic energy range from thermal energies to 10 eV. Several endothermic channels are observed at high kinetic energies for the reaction $C_2H_4^+ + C_2H_4$ including the production of $C_2H_2^+$, $C_2H_3^+$, $C_2H_5^+$, and $C_3H_3^+$ ions.

HURD, W. J.

H12 DSN Progress Report for July–August 1972: Efficient Generation of Statistically Good Pseudonoise by Linearly Interconnected Shift Registers

W. J. Hurd

Technical Report 32-1526, Vol. XI, pp. 92–103, October 15, 1972

This article presents some new algorithms for generating pseudorandom noise utilizing binary maximal-length recursive sequences of high degree and with many nonzero terms. The ability to efficiently implement high-degree recursions is important because the number of consecutive bits which can be guaranteed to be both linearly and statistically independent is equal to the degree of the recursion. The implementations are by interconnection of several short shift registers in a linear manner in such a way that different widely spaced phase shifts of the same pseudonoise sequence appear in the stages of the several registers. This is efficient both in hardware and in software. Several specific algorithms are subjected to extensive statistical evaluation, with no evidence found to distinguish the sequences from purely random binary sequences.

H13 DSN Progress Report for September–October 1972: A Demonstration of DSN Clock Synchronization by VLBI

W. J. Hurd

Technical Report 32-1526, Vol. XII, pp. 149–160, December 15, 1972

A prototype of a semi-real-time system for synchronizing the DSN station clocks by radio interferometry was successfully demonstrated on August 30, 1972. Synchronization accuracies as good as 100 ns rms were achieved between the Pioneer Deep Space Station (DSS 11) and the Echo Deep Space Station (DSS 12), both at Goldstone. The accuracy can be improved by increasing the system bandwidth until the fundamental limitations due to baseline and source-position uncertainties and atmospheric effects are reached. These limitations are about 10 ns for transcontinental baselines.

JACKSON, E. B.

J01 DSN Progress Report for September–October 1972: DSN Research and Technology Support

E. B. Jackson and R. B. Kolbly

Technical Report 32-1526, Vol. XII, pp. 124–130, December 15, 1972

This article presents the activities of the Development Support Group in operating the Venus Deep Space Station (DSS 13) and the Microwave Test Facility for the period August 16–October 15, 1972, categorized by the JPL technical section supported. Major activities include a strong planetary-radar and pulsar-observation program for the Communications Systems Research Section, extensive precision-antenna-gain measurements for the Communications Elements Research Section, and a major installation and modification effort for dual-carrier experimentation for the RF Systems Development Section. Preliminary activity in measuring the sidelobe patterns of the 26-m-diameter antenna at the Venus Deep Space Station is described, and the cessation of clock synchronization transmissions (due to nonavailability of polynomial predicts) is noted.

JAFFE, R. M.

J02 3-D Multilateration: A Precision Geodetic Measurement System

P. R. Escobal, H. F. Fliegel, R. M. Jaffe, P. M. Muller, K. M. Ong, O. H. von Roos, and M. S. Shumate

JPL Quarterly Technical Review, Vol. 2, No. 3, pp. 1–11, October 1972

For abstract, see Escobal, P. R.

JUVINALL, G. L.

J03 Gravitational Effects on Electrochemical Batteries

R. E. Meredith (Oregon State University),
G. L. Juvinall, and A. A. Uchiyama

Technical Report 32-1570, November 15, 1972

For abstract, see Meredith, R. E.

KALFAYAN, S. H.

K01 Long-Term Aging of Elastomers: Chemorheology of Viton B Fluorocarbon Elastomer

S. H. Kalfayan, R. H. Silver, A. A. Mazzeo, and S. T. Liu

JPL Quarterly Technical Review, Vol. 2, No. 3, pp. 32–39, October 1972

Elastomers have extensive aerospace applications. They are used as bladder materials for liquid-propellant expulsion systems, propellant binders, and fuel-tank sealants for high-speed aircraft. Predicting the long-term behavior of these materials is of primary importance. This article is a continuation of a study to ascertain the nature, extent, and rate of chemical changes that take place in certain selected elastomers. Under discussion is Viton B, regarded as a temperature- and fuel-resistant fluorocarbon rubber. The kinetic analysis of the chemical stress relaxation, and infrared and gel-permeation chromatography analysis results are discussed.

KATOW, M. S.

K02 DSN Progress Report for July–August 1972: NASTRAN Data Generation and Management Using Interactive Graphics

M. S. Katow and B. M. Cooper

Technical Report 32-1526, Vol. XI, pp. 104–110, October 15, 1972

For effective use of the NASA Structural Analysis computer system, the input bulk data must accurately model the structure to be analyzed with a minimum expenditure of time and money. This article describes a method of using an interactive graphics device to generate a large portion of the input bulk data with visual checks of the structure and the card images. The generation starts from GRID and PBAR cards. The visual checks result from a three-dimensional display of the model in any rotated position. By detailing the steps, the time saving and cost effectiveness of this

method may be judged, and its potential as a useful tool for the structural analyst may be established.

KERRIN, S. L.

K03 Rapid Determination of Twenty Amino Acids by Gas Chromatography

J. P. Hardy and S. L. Kerrin

Anal. Chem., Vol. 44, No. 8, pp. 1497–1499, July 1972

For abstract, see Hardy, J. P.

KLEIN, M. J.

K04 Jupiter: New Evidence of Long-Term Variations of Its Decimeter Flux Density

M. J. Klein, S. Gulkis, and C. T. Stelzried

Astrophys. J., Vol. 176, No. 2, Pt. 2, pp. L85–L88, September 1, 1972

Jupiter's flux density at 12.6 cm was measured at weekly intervals from May through October 1971. When compared with previous decimetric measurements, these data indicate that Jupiter's total flux density has decreased approximately 20% since 1964. No short-term variations greater than a few percent were observed.

KLIMASAUSKAS, C. C.

K05 DSN Progress Report for September–October 1972: An Execution Analyzer for the Sigma 5 Computer

C. C. Klimasauskas

Technical Report 32-1526, Vol. XII, pp. 176–188, December 15, 1972

Since many different computers on the market today claim to perform the same class of tasks, and no uniform criterion has been established to aid the decision-making process, the problem of how to select the "best" computer for a particular job mix becomes almost a matter of personal preference and chance. One technique for evaluating the performance of a central processing unit is based on the frequency of usage of the various machine instructions. This technique is particularly applicable to machines used in a dedicated process-control activity such as those of the deep space stations. This article describes a program which has been

written for the Sigma 5 computer to gather data on the dynamic usage of computer instructions in various tasks.

KLIORE, A. J.

K06 Bistatic Radar Measurements of the Surface of Mars With Mariner 1969

G. Fjeldbo, A. J. Kliore, and B. L. Seidel

Icarus, Vol. 16, No. 3, pp. 502–508, June 1972

For abstract, see Fjeldbo, G.

KOLBLY, R. B.

K07 DSN Progress Report for September–October 1972: DSN Research and Technology Support

E. B. Jackson and R. B. Kolbly

Technical Report 32-1526, Vol. XII, pp. 124–130, December 15, 1972

For abstract, see Jackson, E. B.

KOSKELA, P. E.

K08 Mariner Mars 1971 Television Picture Catalog: Sequence Design and Picture Coverage

P. E. Koskela, M. R. Helton, L. N. Seeley, and S. J. Zawacki

Technical Memorandum 33-585, Vol. II, December 15, 1972

This memorandum contains a collection of data relating to the Mariner 9 television pictures. The data are arranged to offer speedy identification of what took place during entire science cycles, on individual revolutions, and during individual science links or sequences.

Summary tables present the nominal design for each of the major picture-taking cycles, along with the sequences actually taken on each revolution. These tables enable one to identify, at a glance, all television sequences and the corresponding individual pictures for the first 262 revolutions (the primary mission). A list of television pictures, categorized according to their latitude and longitude, is also provided. The bulk of the memorandum consists of orthographic and/or mercator plots for all pictures, along with pertinent numerical data for their center points. Other tables and plots of interest are also included. This memorandum is based upon data

contained in the Supplementary Experiment Data Record (SEDR) files as of August 21, 1972.

KUSHIDA, R.

K09 Effect on Supersonic Jet Noise of Nozzle Plenum Pressure Fluctuations

R. Kushida and J. H. Rupe

AIAA J., Vol. 10, No. 7, pp. 946-948, July 1972

The proportion of the total engine noise which is attributable to the jet plume in a jet propulsion device increases markedly as the exhaust velocity increases. When the jet velocity is nearly sonic or supersonic, then the jet noise can overwhelm other noise sources. In this preliminary study it is found that the interaction of upstream disturbance with a supersonic jet plume causes an increase in the total noise. It is expected that this added insight into jet noise sources will be useful in devising improved methods of noise reduction in future jet engines.

LAM, C.

L01 DSN Progress Report for September–October 1972: On the Weight Enumerators of Quadratic Residue Codes

J. Mykkeltveit (California Institute of Technology), C. Lam (California Institute of Technology), and R. J. McEliece

Technical Report 32-1526, Vol. XII, pp. 161-166, December 15, 1972

For abstract, see Mykkeltveit, J.

LANDEL, R. F.

L02 Stored Energy Function of Rubberlike Materials Derived From Simple Tensile Data

T. J. Peng and R. F. Landel

J. Appl. Phys., Vol. 43, No. 7, pp. 3064-3067, July 1972

For abstract, see Peng, T. J.

L03 A Molecular Theory of Elastomer Deformation and Rupture

R. F. Landel and R. F. Fedors

Mechanical Behavior of Materials: Proceedings of the 1971 International Conference on Mechanical Behavior of Materials (Sponsored by the Society of Materials Science), Kyoto, Japan, August 1971, Vol. III, pp. 496–507

The mechanical properties of elastomers, including rupture and its time dependence, can be semi-quantitatively predicted from nine molecular parameters which are characteristic for a given species, from the initial molecular weight of a sample before crosslinking, and from the effective chain concentration (which must still be determined for each vulcanizate). Only two empirical quantities are involved—the Plazek retardation function $\psi(a_x)$ for entanglement slippage and a related constant which serves to locate $\psi(a_x)$ on the time scale. The theory leads to a new method of estimating fatigue lifetimes from short-time data.

LAYLAND, J. W.

L04 DSN Progress Report for September–October 1972: Sequential Decoding With a Noisy Carrier Reference

J. W. Layland

Technical Report 32-1526, Vol. XII, pp. 167–175, December 15, 1972

This article presents an approximate analysis of the effect of a noisy carrier reference on the performance of sequential decoding. The limitations of the analysis are discussed, and steps that could be taken to extend the performance region over which the model used produces accurate, rather than merely bounding, results are described.

L05 DSN Progress Report for September–October 1972: A Multicomputer Communications System

J. W. Layland and W. A. Lushbaugh

Technical Report 32-1526, Vol. XII, pp. 195–199, December 15, 1972

This article gives a general description of the requirements for, and one proposal for the provision of, the multicomputer communications facility needed in a multiple-minicomputer system, such as the anticipated tracking-station computer network of the DSN. The main features are: (1) a basically high-speed point-to-point link whose rate adapts without data loss to the capabilities of the computers with which it interfaces; and (2) a very-wide-bandwidth transmission control unit (TCU) which provides a functional path from each computer to every other computer, while requiring only one physical link between each computer and the TCU.

LESH, J. R.

L06 DSN Progress Report for July–August 1972: Accuracy of the Signal-to-Noise Ratio Estimator: A Comment on the Derivation of the Estimator Mean

J. R. Lesh

Technical Report 32-1526, Vol. XI, pp. 164–166, October 15, 1972

The mean of the signal-to-noise ratio estimator used with the symbol-synchronizer assembly is derived without assuming independence of the sample mean and sample variance errors. The resulting expression is found to differ only slightly from a previous expression determined by assuming independence.

L07 DSN Progress Report for September–October 1972: Spectrum of an Asynchronously Biphase Modulated Square Wave

J. R. Lesh

Technical Report 32-1526, Vol. XII, pp. 226–230, December 15, 1972

This article presents an exact closed-form expression for the power spectrum of a square-wave carrier (or subcarrier) which is biphase modulated by a random binary data stream. The resulting expression is valid for any carrier frequency and data bit rate, provided that the two sources are not phase-coherently related. Also presented is an approximate expression which can be used to alleviate some computational difficulties of the exact expression at low spectral frequencies.

LEVITT, B. K.

L08 DSN Progress Report for September–October 1972: Optimum Frame Sync Acquisition for Biorthogonally Coded Telemetry

B. K. Levitt

Technical Report 32-1526, Vol. XII, pp. 92–99, December 15, 1972

This article describes an optimum frame-sync algorithm for biorthogonally coded telemetry. This algorithm takes the coding into account and therefore performs significantly better than algorithms derived for uncoded telemetry, with only a slight increase in implementation complexity.

LEVY, R.

L09 **DSN Progress Report for September–October 1972: PARADES Structural Design System Capabilities**

R. Levy and R. Melosh (Virginia Polytechnic Institute and State University)

Technical Report 32-1526, Vol. XII, pp. 68–73, December 15, 1972

This article outlines design approaches, program capabilities, problem formulation, and user options for the Parabolic Reflector Analysis and Design Subsystem (PARADES) program. PARADES is a new computer program for the analysis and design of parabolic antenna-reflector structures.

L10 **DSN Progress Report for September–October 1972: Iterative Design of Antenna Structures**

R. Levy

Technical Report 32-1526, Vol. XII, pp. 100–111, December 15, 1972

This article describes a new procedure for the design of antenna-reflector structures for improved performance when subjected to operational gravity loading. The design objective is to reduce the difference in pathlength of the RF energy beam that is reflected from the deformed surface with respect to the pathlength of the beam from a perfect paraboloidal surface. A virtual-work formulation is used to state this objective in terms of the bar areas that compose the structure. These bar areas become the design variables. A special application of the Lagrange-multiplier technique defines preferential redistributions of the design variables to improve performance. Improvements are developed subject to a primary constraint on total structure weight and additional practical side constraints. Design examples show efficient and effective applications of the described procedure.

LIKINS, P. W.

L11 **Large-Deformation Modal Coordinates for Nonrigid Vehicle Dynamics**

P. W. Likins and G. E. Fleischer

Technical Report 32-1565, November 1, 1972

This report documents the derivation of minimum-dimension sets of discrete-coordinate and hybrid-coordinate equations of motion for a system consisting of an arbitrary number of hinge-connected

rigid bodies assembled in tree topology. These equations are useful for the simulation of dynamic systems that can be idealized as tree-like arrangements of substructures, with each substructure consisting of either a rigid body or a collection of elastically interconnected rigid bodies restricted to small relative rotations at each connection. Thus, some of the substructures represent elastic bodies subjected to small strains or local deformations, but possibly large gross deformations; in the hybrid formulation, distributed coordinates, herein referred to as large-deformation modal coordinates, are used for the deformations of these substructures. The equations are in a form suitable for incorporation into one or more computer programs for use as multipurpose tools in the simulation of spacecraft and other complex electromechanical systems.

LINNES, K. W.

L12 DSN Progress Report for July–August 1972: Radio Science Support

K. W. Linnes

Technical Report 32-1526, Vol. XI, pp. 26–29, October 15, 1972

Since 1967, radio scientists have used the DSN 26- and 64-m-diameter antenna stations to investigate pulsars, to study the effect of solar corona on radio signals, and to observe radio emissions from X-ray sources. More recently, very-long-baseline interferometry (VLBI) techniques have been used for high-resolution studies of quasars. During the reporting period, VLBI observations were made of quasars and pulsars. Support was also provided by the 64-m-diameter antenna for the measurement of cosmic background noise and weak radio sources to search for interstellar molecules and for the observation of radiation from Jupiter.

LIPSIUS, P.

L13 DSN Progress Report for July–August 1972: Performance of the 64-Meter-Diameter Antenna Servo

P. Lipsius

Technical Report 32-1526, Vol. XI, pp. 153–156, October 15, 1972

A 64-m-diameter antenna has been installed and tested at the Tidbinbilla Deep Space Station in Australia. Part of the final acceptance testing was demonstration of antenna servo performance. This report summarizes the major tests and the resulting data.

LIU, S. T.

L14 Long-Term Aging of Elastomers: Chemorheology of Viton B Fluorocarbon Elastomer

S. H. Kalfayan, R. H. Silver, A. A. Mazzeo, and S. T. Liu

JPL Quarterly Technical Review, Vol. 2, No. 3, pp. 32-39, October 1972

For abstract, see Kalfayan, S. H.

LIVERMORE, R. W.

L15 DSN Progress Report for July-August 1972: High-Speed Data Communication: A Description of Software Techniques

R. W. Livermore

Technical Report 32-1526, Vol. XI, pp. 161-163, October 15, 1972

This article describes some methods of using the high-speed data assembly of the Ground Communications Facility operating at 4.8 kbps and the Xerox Data Systems 920 computers for keeping the deep space stations supplied with up-to-date programs and documentation. The present method for transmitting this information employs magnetic tapes, punched tapes, and hardcopy documentation transmitted by mail or air freight.

LONG, H. R.

L16 Trajectory Correction Propulsion for TOPS

H. R. Long and R. A. Bjorklund

Technical Report 32-1571, November 15, 1972

A blowdown-pressurized hydrazine propulsion subsystem was selected to provide trajectory-correction impulse for outer-planet flyby spacecraft as the result of cost/mass/reliability tradeoff analyses. Present hydrazine component and system technology and component designs were evaluated for application to the Thermoelectric Outer-Planet Spacecraft (TOPS). While general hydrazine technology was adequate, component design changes were deemed necessary for TOPS-type missions. A prototype hydrazine propulsion subsystem was fabricated and fired nine times for a total of 1600 s to demonstrate the operation and performance of the TOPS propulsion subsystem configuration. A flight-weight trajectory-correction propulsion subsystem was designed for the TOPS based on actual and estimated advanced components.

LORDEN, G.

L17 DSN Progress Report for September–October 1972: An Inventory and Procurement Policy for the Deep Space Network

I. Eisenberger, F. R. Maiocco, and G. Lorden (California Institute of Technology)

Technical Report 32-1526, Vol. XII, pp. 131–148, December 15, 1972

For abstract, see Eisenberger, I.

LUSHBAUGH, W. A.

L18 DSN Progress Report for September–October 1972: A Multicomputer Communications System

J. W. Layland and W. A. Lushbaugh

Technical Report 32-1526, Vol. XII, pp. 195–199, December 15, 1972

For abstract, see Layland, J. W.

LUTES, G.

L19 DSN Progress Report for September–October 1972: Phase-Stable, Low-Phase-Noise Filters for Reference Signals

G. Lutes

Technical Report 32-1526, Vol. XII, pp. 44–46, December 15, 1972

This article describes a phase-locking filter which filters reference signals by locking the phase of the output signal to the phase of the input signal. A very small phase drift may be achieved over a large temperature range without the use of temperature-controlled ovens, which are bulky and costly.

MacCLELLAN, R. N.

M01 DSN Progress Report for September–October 1972: Digital Frequency Shifter

R. N. MacClellan

Technical Report 32-1526, Vol. XII, pp. 209–213, December 15, 1972

Digital techniques applied to the development of frequency shifters yield a circuit that exhibits both wide bandwidth and exceptionally low phase noise while requiring no alignment.

MacDORAN, P. F.

M02 DSN Progress Report for September–October 1972: Very Long Baseline Interferometry (VLBI) Possibilities for Lunar Study

M. A. Slade, P. F. MacDoran, and J. B. Thomas

Technical Report 32-1526, Vol. XII, pp. 35–39, December 15, 1972

For abstract, see Slade, M. A.

MAIOCCO, F. R.

M03 DSN Progress Report for September–October 1972: An Inventory and Procurement Policy for the Deep Space Network

I. Eisenberger, F. R. Maiocco, and G. Lorden (California Institute of Technology)

Technical Report 32-1526, Vol. XII, pp. 131–148, December 15, 1972

For abstract, see Eisenberger, I.

MANATT, S. L.

M04 Electron Paramagnetic Resonance of Radiation Damage in a Lunar Rock

F.-D. Tsay, S. I. Chan, and S. L. Manatt

Nature Phys. Sci., Vol. 237, No. 77, pp. 121–122, June 19, 1972

For abstract, see Tsay, F.-D.

MARTIN, D. P.

M05 A Combined Radar–Radiometer With Variable Polarization

D. P. Martin

Technical Memorandum 33-570, October 15, 1972

This memorandum describes an instrument that provides both radar and radiometer data at the same time. The antenna and receiver are time shared for the two sensor functions. The antenna polarization can be electronically scanned at rates up to 5000 changes/s for both the transmit and receive signal paths. The purpose of the equipment is to investigate target signatures for remote sensing applications. The function of the equipment is described, and the results for observations of asphalt, grass, and gravel surfaces are presented.

MASSIER, P. F.

M06 Influence of Contraction Section Shape and Inlet Flow Direction on Supersonic Nozzle Flow and Performance

L. H. Back, R. F. Cuffel, and P. F. Massier

J. Spacecraft Rockets, Vol. 9, No. 6, pp. 420–427, June 1972

For abstract, see Back, L. H.

MATHUR, F. P.

M07 A Survey of and an Introduction to Fault Diagnosis Algorithms

F. P. Mathur

Technical Memorandum 33-567, October 1, 1972

This memorandum surveys the field of fault diagnosis and introduces the reader to some of the key algorithms and heuristics currently in use. Fault diagnosis is an important and rapidly growing discipline. This is important to JPL's research efforts in the design of self-repairable computers because the present diagnosis resolution of its fault-tolerant computer is limited to a functional unit or processor. Better resolution is necessary before failed units can become partially reuseable. The approach that holds the greatest promise is that of resident microdiagnostics; however, that presupposes a microprogrammable architecture for the computer being self-diagnosed. The presentation here is tutorial and contains examples. An extensive bibliography of some 220 entries is included.

MAXWORTHY, T.

M08 Comments on "A Mechanism for Jupiter's Equatorial Acceleration"

T. Maxworthy

J. Atmos. Sci., Vol. 29, No. 5, pp. 1007–1008, July 1972

The mechanism proposed by Gierasch and Stone (1968) to account for the equatorial jet found high in the Jovian atmosphere has recently been criticized by Hide (1969, 1970). This article presents one more comment which casts further doubt on the validity of the Gierasch–Stone picture. It is based more directly on the fluid dynamical processes invoked by Gierasch and Stone and less on general considerations, as presented by Hide.

MAZZEO, A. A.

M09 Long-Term Aging of Elastomers: Chemorheology of Viton B Fluorocarbon Elastomer

S. H. Kalfayan, R. H. Silver, A. A. Mazzeo, and S. T. Liu

JPL Quarterly Technical Review, Vol. 2, No. 3, pp. 32–39, October 1972

For abstract, see Kalfayan, S. H.

McCLURE, J. P.

M10 DSN Progress Report for July–August 1972: Ground Communications Facility Functional Design for 1973–1974

J. P. McClure

Technical Report 32-1526, Vol. XI, pp. 124–131, October 15, 1972

This article describes the Ground Communications Facility (GCF) 1973–1974 capability that will be used to support Pioneer, Mariner Venus–Mercury 1973, and Helios operations, plus the early development and testing associated with the 1975 Viking Project. The design includes a full spectrum of GCF capabilities for the overseas 64-m-diameter antenna stations. The wideband data system will be enlarged to cover all 64-m-diameter antenna stations, plus the Compatibility Test Area (CTA 21) at JPL and the Compatibility Test Station (DSS 71) at Cape Kennedy. The standard wideband rate will be 28.5 kbps with limited use of 50 and 230 kbps for special purposes. The wide-band block length will be increased to 2400 bits after Mariner Venus–Mercury 1973 operations. The number of teletype circuits will be reduced in keeping with the

DSN policy of eliminating this medium for computer-to-computer data transfer.

McELIECE, R. J.

M11 DSN Progress Report for July–August 1972: Weights Modulo 8 in Binary Cyclic Codes

R. J. McEliece

Technical Report 32-1526, Vol. XI, pp. 86–88, October 15, 1972

This article presents a new technique for computing the weights modulo 8 in binary cyclic codes. These codes have proved to be the most important ones for Ground Communications Facility error detection/correction, and the method described will frequently aid in the detailed analysis of such codes.

M12 DSN Progress Report for September–October 1972: On the Weight Enumerators of Quadratic Residue Codes

J. Mykkeltveit (California Institute of Technology), C. Lam (California Institute of Technology), and R. J. McEliece

Technical Report 32-1526, Vol. XII, pp. 161–166, December 15, 1972

For abstract, see Mykkeltveit, J.

McGINNESS, H.

M13 DSN Progress Report for July–August 1972: Salvaging an Expensive Shaft by Brush Electroplating

H. McGinness

Technical Report 32-1526, Vol. XI, pp. 150–152, October 15, 1972

An expensive shaft was salvaged by depositing nickel on an undersized bearing journal. The shaft is a component in the Master Equatorial instrument, required for the 64-m-diameter antenna of the DSN. In special cases, this electroplating process could be considered part of the fabrication method rather than a salvage process.

M14 DSN Progress Report for September–October 1972: Excessive Shaft Friction Variation Corrected by Lubricant Change

H. McGinness

Technical Report 32-1526, Vol. XII, pp. 51–55, December 15, 1972

During testing of the Master Equatorial for the 64-m-diameter antenna under construction in Australia, a drag-torque variation ratio as large as 5:1 was observed on a shaft supported by two angular-contact ball bearings. A change in the grease lubricant reduced the ratio to 1.1:1.0.

MELOSH, R.

M15 DSN Progress Report for September–October 1972: PARADES Structural Design System Capabilities

R. Levy and R. Melosh (Virginia Polytechnic Institute and State University)

Technical Report 32-1526, Vol. XII, pp. 68–73, December 15, 1972

For abstract, see Levy, R.

MEREDITH, R. E.

M16 Gravitational Effects on Electrochemical Batteries

R. E. Meredith (Oregon State University), G. L. Juvinall, and A. A. Uchiyama

Technical Report 32-1570, November 15, 1972

This report summarizes the existing work on gravitational effects on electrochemical batteries and makes recommendations for future activities in this field. Theoretical evaluations of the problem have met with only limited success; theories based upon a treatment of natural convection have fallen short of the mark, partly because the mass transfer involved in the power-producing electrochemical reactions in a battery is not completely due to convection, and partly because a battery is far removed from the idealized models necessarily employed in the development of the theory. The latter point is best illustrated by the fact that, although theory generally predicts that the limiting current density will vary with the 1/4 power of the acceleration constant, the experimental data falls in the range of a 1/3 to 1/5 power dependence because of differences in the way the cell is constructed.

The effects of sustained high-g environments on cycled silver–zinc and nickel–cadmium cells have been evaluated over four complete cycles in the region of 10 to 75 g. Although no effects on high current-discharge performances or on ampere-hour capacity were noted, severe zinc migration and sloughing of active material from

the zinc electrode were observed. This latter effect constitutes real damage and, over a long period of time, would result in loss of capacity.

The work of Arcand, based upon smooth zinc electrodes, predicted a limiting current density of 7 mA/cm^2. However, the Mariner 7 battery easily provided a current density of 10.5 mA/cm^2 in deep space. Fundamental battery studies performed at zero g are necessary to resolve the conflict. To this end, experiments have been planned, and a breadboard model of an in-flight battery test unit has been designed and fabricated. It is recommended that a zero-g battery experiment be implemented. Both an orbiting-satellite and a sounding-rocket approach are being considered.

MOYNIHAN, P. I.

M17 Attitude Propulsion Technology for TOPS

P. I. Moynihan

Technical Report 32-1560, November 1, 1972

This report summarizes the JPL Thermoelectric Outer Planet Spacecraft (TOPS) attitude-propulsion subsystem (APS) effort. It includes the tradeoff rationale that went into the selection of an anhydrous-hydrazine baseline system, followed by a discussion of the 0.22-N (0.05-lbf) JPL-developed thruster and its integration into a portable, self-contained propulsion module that was designed, developed, and 'man-rated' to support the TOPS single-axis attitude control tests in the JPL Celestarium.

The results of a cold-start feasibility demonstration with a modified JPL thruster are presented. A description of three types of 0.44-N (0.1lbf) thrusters that were procured for in-house evaluation is included along with the results of the test program. This is followed by a description of the APS feed system components, their evaluations, and a discussion of an evaluation of elastomeric material for valve seat seals. The report concludes with a list of new-technology items which will be of value for application to future systems of this type.

MUDGWAY, D. J.

M18 DSN Progress Report for July–August 1972: Viking Mission Support

D. J. Mudgway

Technical Report 32-1526, Vol. XI, pp. 19–22, October 15, 1972

The DSN support for Viking continues to move from the completion of the planning and negotiating phase into the implementation phase in accordance with established schedules. Most documents reflecting this activity have been completed, and a major Project review of the ground data system design for Viking has been supported. A problem associated with the Viking requirement for simultaneous dual-carrier operation is being investigated.

M19 DSN Progress Report for September–October 1972: Viking Mission Support

D. J. Mudgway

Technical Report 32-1526, Vol. XII, pp. 14–18, December 15, 1972

DSN support for Viking continues to move forward into the implementation phase in accordance with new schedules developed to meet a new Viking requirement for advanced deep-space-station readiness dates. This article discusses network configurations for the DSN Tracking System, DSN/Viking interfaces, and schedule revisions and describes the continued investigation of the downlink interference effects caused by a dual-carrier environment at the Venus Deep Space Station (DSS 13).

MUELLER, R. L.

M20 Results of the 1970 Balloon Flight Solar Cell Standardization Program

R. F. Greenwood and R. L. Mueller

Technical Report 32-1575, December 1, 1972

For abstract, see Greenwood, R. F.

MULHALL, B. D.

M21 DSN Progress Report for July–August 1972: An Evaluation of Charged Particle Calibration by a Two-Way Dual-Frequency Technique and Alternatives to This Technique

O. H. von Roos and B. D. Mulhall

Technical Report 32-1526, Vol. XI, pp. 42–52, October 15, 1972

For abstract, see von Roos, O. H.

M22 **DSN Progress Report for September–October 1972: Determination of the Helios Spacecraft Attitude by Polarization Measurement**

B. D. Mulhall

Technical Report 32-1526, Vol. XII, pp. 40–43, December 15, 1972

This article describes the possibility of determining the attitude or orientation of the Helios spacecraft by means of polarization measurements of the spacecraft radio signal. One principal error source is the Faraday rotation of the S-band radio signal by Earth's ionosphere. If this effect can be removed by independent measurements of the ionosphere, then the orientation of the spacecraft in two dimensions perpendicular to the spacecraft line-of-sight can be determined to better than 0.5 deg.

MULLER, P. M.

M23 **3-D Multilateration: A Precision Geodetic Measurement System**

P. R. Escobal, H. F. Fliegel, R. M. Jaffe, P. M. Muller, K. M. Ong, O. H. von Roos, and M. S. Shumate

JPL Quarterly Technical Review, Vol. 2, No. 3, pp. 1–11, October 1972

For abstract, see Escobal, P. R.

M24 **Apollo 15 Gravity Analysis From the S-Band Transponder Experiment**

W. L. Sjogren, P. M. Muller, and W. R. Wollenhaupt (Manned Spaceflight Center)

Proceedings of the Conference on Lunar Geophysics, Lunar Science Institute, Houston, Texas, October 18–21, 1971, pp. 411–418

For abstract, see Sjogren, W. L.

MYKKELTVEIT, J.

M25 **DSN Progress Report for September–October 1972: On the Weight Enumerators of Quadratic Residue Codes**

J. Mykkeltveit (California Institute of Technology), C. Lam (California Institute of Technology), and R. J. McEliece

Technical Report 32-1526, Vol. XII, pp. 161–166, December 15, 1972

Binary quadratic-residue codes, some of which are currently being studied for use in the Mariner Jupiter–Saturn 1977 mission, are among the most powerful known block codes. They are, however, notoriously difficult to analyze. In this article, a method is developed for obtaining information about the weights of these codes by exploiting the fact that they are left invariant by the linear fractional group.

NISHIMURA, H. G.

N01 DSN Progress Report for July–August 1972: Coaxial Switch Evaluation

H. G. Nishimura

Technical Report 32-1526, Vol. XI, pp. 135–139, October 15, 1972

Miniature coaxial transfer switches from various manufacturers were tested for the purpose of finding an acceptable replacement for the larger switch now used in the Deep Space Instrumentation Facility. The switches, which are planned for use in the S- through X-bands, were tested to determine both their mechanical and electrical properties. Two units were considered acceptable. These switches will reduce the size and cost of future microwave equipment and will meet increasing performance demands.

NISHIMURA, T.

N02 Spectral Factorization in Periodically Time-Varying Systems and Application to Navigation Problems

T. Nishimura

J. Spacecraft Rockets, Vol. 9, No. 7, pp. 540–546, July 1972

Spectral factorization is a powerful tool in deriving the steady-state solution of Kalman filtering equations. It is an algebraic, nonrecursive method and, therefore, economical in terms of computing cost when compared with the conventional iterative algorithm. In this paper the technique is extended to time-varying systems having periodic coefficient matrices for both discrete and continuous systems. The tracking of low-thrust spacecraft from an Earth-based station is used as an example and a sensitivity study is performed using a computer program incorporating the algorithm.

NORRIS, D.

N03 DSN Progress Report for September–October 1972: Frequency Generation and Control: Atomic Hydrogen Dissociator

H. Erpenbach and D. Norris

Technical Report 32-1526, Vol. XII, pp. 56–58, December 15, 1972

For abstract, see Erpenbach, H.

O'HANDLEY, D. A.

001 Recent Developments in Digital Image Processing at the Image Processing Laboratory at the Jet Propulsion Laboratory

D. A. O'Handley and W. B. Green

Proc. IEEE, Vol. 60, No. 7, pp. 821–828, July 1972

Image processing of spacecraft images has been carried on at JPL since 1964. The most recent advances in removal of geometric distortion and residual image effects along with various types of mapping projections are covered, and the recent applications of image processing to the areas of biomedicine, forensic sciences, and astronomy are discussed. These treatments are of a tutorial nature and should serve as a guide to more complete discussions on the subjects.

ONDRASIK, V. J.

002 DSN Progress Report for July–August 1972: Topics in the Implementation and Application of Two-Station Tracking Data Types

K. H. Rourke and V. J. Ondrasik

Technical Report 32-1526, Vol. XI, pp. 62–70, October 15, 1972

For abstract, see Rourke, K. H.

ONG, K. M.

003 3-D Multilateration: A Precision Geodetic Measurement System

P. R. Escobal, H. F. Fliegel, R. M. Jaffe, P. M. Muller, K. M. Ong, O. H. von Roos, and M. S. Shumate

JPL Quarterly Technical Review, Vol. 2, No. 3, pp. 1–11, October 1972

For abstract, see Escobal, P. R.

OTOSHI, T. Y.

004 DSN Progress Report for September–October 1972: RF Properties of the 64-m-Diameter Antenna Mesh Material as a Function of Frequency

T. Y. Otoshi

Technical Report 32-1526, Vol. XII, pp. 26–31, December 15, 1972

This article presents some accurate theoretical data on the RF properties of the perforated panels presently used as reflector surface material on the 64-m-diameter antenna. The properties are given for the frequency range of 1.0 to 30 GHz.

PENG, T. J.

P01 Extensional Flow of Bulk Polymers

T. J. Peng

JPL Quarterly Technical Review, Vol. 2, No. 3, pp. 40–45, October 1972

This article presents a study of the behavior of polyisobutylene under motion at a constant stretch history for both strip-biaxial extensional flow and simple extensional flow. Steady-state non-Newtonian viscosities were observed at various constant-stretch histories. Newtonian viscosities for both strip-biaxial and simple extensional flow were found to be in agreement with the classical theory. The results of this study provide an essential part of the experimental background necessary for the development of a new general stress–strain–time relation for uncrosslinked and lightly crosslinked polymers.

P02 Stored Energy Function of Rubberlike Materials Derived From Simple Tensile Data

T. J. Peng and R. F. Landel

J. Appl. Phys., Vol. 43, No. 7, pp. 3064–3067, July 1972

This article develops an explicit formulation to obtain the stored energy function W from simple tension experiments alone, based on the Valanis–Landel separable, symmetric, stored-energy function

$$W(\lambda_1,\lambda_2,\lambda_3) = w(\lambda_1) + w(\lambda_2) + w(\lambda_3)$$

For a simple extension stress–strain law of the form $\lambda\sigma = E\epsilon$ the analytical formula of W in the limited range $1 \leqslant \lambda \leqslant 2.5$ is found to be

$$W = E\sum_{i=1}^{3}\left[\lambda_i - 1 - \ln\lambda_i - \frac{1}{6}(\ln\lambda_i)^2 + \frac{1}{18}(\ln\lambda_i)^3 - \frac{1}{216}(\ln\lambda_i)^4\right]$$

where the limitation originates with the stress–strain law. The expression is used to verify for validity of the Valanis–Landel postulation through prediction of the stress–strain behavior in multiaxial deformations.

PHILLIPS, H. P.

P03 DSN Progress Report for September–October 1972: Hydrostatic Bearing Runner Leveling at Overseas 64-m-Diameter Antenna

H. P. Phillips

Technical Report 32-1526, Vol. XII, pp. 214–219, December 15, 1972

The hydrostatic-bearing runners on the DSN 64-m-diameter antennas must be set to flatness tolerances which represent a major field-alignment problem. A new method was successfully employed in setting the runners for the new 64-m-diameter antennas at the Ballima Deep Space Station (DSS 43) in Australia and the Robledo Deep Space Station (DSS 63) in Spain. The method, based on the use of an electronic level, is described in this article.

PHILLIPS, R. J.

P04 The Lunar Conductivity Profile and the Nonuniqueness of Electromagnetic Data Inversion

R. J. Phillips

Icarus, Vol. 17, No. 1, pp. 88–103, August 1972

This article presents a review of the theory for the electromagnetic functional used to date to determine the lunar conductivity

profile from spectral analyses of lunar magnetometer data. The use of the spectral data in conjunction with the functional to find a least squares conductivity profile is examined from the point of view of the nonuniqueness of nonlinear estimation.

Of the models generated, those that best fit the data all have a conductivity peak at a depth of 240 km. However, all of these models are quite distinct elsewhere in the profile. It is shown how such models are dependent on both the nature of the functional as well as the initial guess in the least squares procedure.

A correlation analysis shows that the only resolvable features from this type of model are a low conductivity crust, a high conductivity peak of limited radial extent, and a low conductivity zone beneath the peak. It is also concluded that the two-layer model of Kuckes (1971) is equally as valid as the peaked models, and the totality of "equally valid" models derived from the spectral data place no reasonable constraint on the electrical conductivity below a depth of 350 km.

POTTER, P. D.

P05 DSN Progress Report for September–October 1972: Improved RF Calibration Techniques—A Practical Technique for Accurate Determination of Microwave Surface Resistivity

R. C. Clauss and P. D. Potter

Technical Report 32-1526, Vol. XII, pp. 59–67, December 15, 1972

For abstract, see Clauss, R. C.

QUADE, J. G.

Q01 Microwave Emission From Geological Materials: Observations of Interference Effects

J. C. Blinn III, J. E. Conel, and J. G. Quade (University of Nevada)

J. Geophys. Res., Vol. 77, No. 23, pp. 4366–4378, August 10, 1972

For abstract, see Blinn III, J. C.

QUINN, R.

Q02 DSN Progress Report for July–August 1972: Low Noise Receivers: Microwave Maser Development

R. Clauss, E. Wiebe, and R. Quinn

Technical Report 32-1526, Vol. XI, pp. 71–80, October 15, 1972

For abstract, see Clauss, R.

REEDY, G. K.

R01 Determination of Solid-Propellant Transient Regression Rates Using a Microwave Doppler Shift Technique

L. D. Strand, A. L. Schultz, and G. K. Reedy

Technical Report 32-1569, October 15, 1972

For abstract, see Strand, L. D.

REID, M. S.

R02 DSN Progress Report for July–August 1972: Preliminary Analysis of the Microwave Weather

M. S. Reid and R. W. D. Booth

Technical Report 32-1526, Vol. XI, pp. 111–120, October 15, 1972

The Weather Project forms part of an overall Radio Systems Development Project which seeks to optimize the spacecraft-to-ground communications link. Statistical correlations of weather and communications capability at X- and K-bands are needed to provide practical predictions of link performance. Thus the objective of the Weather Project is the statistical prediction of the performance of the DSN at X-band and, in the future, at K-band. A previous article discussed the general approach of the Weather Project, the measurements, calibrations, equipment, and methods. Problems encountered were also discussed as well as proposed future work.

This article reports on a preliminary analysis of the Weather Project data for calendar year 1971. These results are presented in tabular form. Cumulative frequency distributions of percentages of excess system temperature are tabulated as a function of time (whole year and quarterly periods) and of antenna elevation angle (four elevation ranges and all elevation angles). Averages, standard deviations, and confidence limits are tabulated, and the experimen-

tal results are compared with the data from a theoretical study based on estimated and observed cloud-cover effects.

R03 **DSN Progress Report for September–October 1972: An Analysis of System Performance Under the Severe Weather Conditions at Goldstone, December 1971**

M. S. Reid

Technical Report 32-1526, Vol. XII, pp. 32–34, December 15, 1972

Adverse weather conditions, unusual for the area in their severity, were experienced at Goldstone Deep Space Communications Complex in California in December 1971. This article summarizes an analysis of the system performance under these conditions and reports subsequent conclusions. The results of a brief study of cloud-cover characteristics in the southwestern United States to a distance of several hundred miles from Goldstone are also presented.

R04 **DSN Progress Report for September–October 1972: Improved RF Calibration Techniques: System Operating Noise Temperature Calibrations**

M. S. Reid

Technical Report 32-1526, Vol. XII, pp. 83–87, December 15, 1972

This article reports the system operating-noise-temperature performance and other calibration data of the low-noise research cones at the Goldstone Deep Space Communications Complex for June 1, 1972 through September 30, 1972. The performance of the following cones is presented for this reporting period: the S-band radar operational cone at the Venus Deep Space Station (DSS 13), the S-band megawatt transmit cone at the Mars Deep Space Station (DSS 14), and the polarization diversity S-band cone at DSS 14. In addition to the above S-band calibration data, elevation profile measurements were made at fixed azimuth at 8415 MHz on the multifrequency X- and K-band cone.

RENZETTI, N. A.

R05 **DSN Progress Report for July–August 1972: DSN Functions and Facilities**

N. A. Renzetti

Technical Report 32-1526, Vol. XI, pp. 1–4,
October 15, 1972

The Deep Space Network (DSN), established by the NASA Office of Tracking and Data Acquisition and under the system management and technical direction of JPL, is designed for two-way communications with unmanned spacecraft traveling approximately 16,000 km (10,000 mi) from Earth to planetary distances. The objectives, functions, and organization of the DSN are summarized, and its three facilities—the Deep Space Instrumentation Facility, the Ground Communications Facility, and the Space Flight Operations Facility—are described.

R06 DSN Progress Report for September–October 1972: DSN Functions and Facilities

N. A. Renzetti

Technical Report 32-1526, Vol. XII, pp. 1–4,
December 15, 1972

The Deep Space Network (DSN), established by the NASA Office of Tracking and Data Acquisition and under the system management and technical direction of JPL, is designed for two-way communications with unmanned spacecraft traveling approximately 16,000 km (10,000 mi) from Earth to planetary distances. The objectives, functions, and organization of the DSN are summarized, and its three facilities—the Deep Space Instrumentation Facility, the Ground Communications Facility, and the Space Flight Operations Facility—are described.

RINDERLE, E. A.

R07 DSN Progress Report for July–August 1972: A Comparison of Cowell's Method and a Variation-of-Parameters Method for the Computation of Precision Satellite Orbits: Phase Three Results

S. S. Dallas and E. A. Rinderle

Technical Report 32-1526, Vol. XI, pp. 30–35,
October 15, 1972

For abstract, see Dallas, S. S.

ROBINSON, E. Y.

R08 A Brief Survey of Carbon–Carbon Refractory Composites at the Jet Propulsion Laboratory

E. Y. Robinson

Technical Memorandum 33-579, December 1, 1972

Refractory composites of carbon–carbon material are being considered for application in: (a) rocket-motor nozzles and skirts, (b) a unique integrated propulsion structure, and (c) planetary-atmosphere-entry shells. The first application is intended for radiation-cooled nozzles and skirts which, with presently available materials, can meet operational requirements of deep space missions at substantially lower weights. The second application requires very high structural performance as well as refractory capability, and is feasible only if high-strength graphite filaments are efficiently incorporated into a carbon-matrix composite. The third application is comparable in many respects to Earth-entry aeroshells and heat shields; however, planetary atmospheres may pose new gas-dynamic and corrosion problems. Furthermore, the entry shell is likely to be an integral structural element which is not jettisoned, and to which critical hard-point attachment must be made. This memorandum describes technical developments and plans in each of these areas.

R09 Estimating Weibull Parameters for Materials

E. Y. Robinson

Technical Memorandum 33-580, December 15, 1972

This memorandum deals with the statistical analysis of strength and fracture of materials in general with application to fiber composites. The "weakest link" model is considered in a fairly general form, and the resulting equations are demonstrated by using a Weibull distribution for flaws. This distribution appears naturally in a variety of problems, and therefore additional attention is devoted to analysis and statistical estimation connected with this distribution. Special working charts are included to facilitate interpretation of observed data and estimation of parameters. Implications of the size effect are considered for various kinds of flaw distributions.

The memorandum describes failure and damage in a fiber-reinforced system. Some useful graphs are included for predicting the strength of such a system. Recent data on organic-fiber (PRD 49) composite material is analyzed by the Weibull distribution with the methods presented here. This memorandum should serve as a useful handbook for data characterization and statistical fracture analysis.

ROSS, R. G., JR.

R10 An Algorithm for Synthesizing Mass and Stiffness Matrices From Experimental Vibration Modes

R. G. Ross, Jr.

JPL Quarterly Technical Review, Vol. 2, No. 3, pp. 12–21, October 1972

It is sometimes desirable to derive a dynamic model of highly complex structures from experimental vibration data. This article presents an algorithm for synthesizing the mass and stiffness matrices from experimentally derived modal data in a way that preserves the physical significance of the individual mass and stiffness elements. The mass and stiffness matrices are derived for a rollup-solar-array example, and are then used to define the modal response of a modified array.

ROURKE, K. H.

R11 DSN Progress Report for July–August 1972: Topics in the Implementation and Application of Two-Station Tracking Data Types

K. H. Rourke and V. J. Ondrasik

Technical Report 32-1526, Vol. XI, pp. 62–70, October 15, 1972

Two proposed two-station-tracking data-processing techniques, direct data filtering and differenced data filtering, are analyzed using advanced orbit-determination filtering methods. Both techniques are shown to perform comparably, yet direct filtering methods prove to be more sensitive to error-model assumptions. Two-station tracking data are shown to be potentially superior to conventional tracking data in determining deep space station locations.

RUPE, J. H.

R12 Effect on Supersonic Jet Noise of Nozzle Plenum Pressure Fluctuations

R. Kushida and J. H. Rupe

AIAA J., Vol. 10, No. 7, pp. 946–948, July 1972

For abstract, see Kushida, R.

SAVAGE, J. E.

S01 **DSN Progress Report for July–August 1972: Reducing the Complexity of Calculating Syndromes for Error-Correcting Codes**

L. H. Harper and J. E. Savage

Technical Report 32-1526, Vol. XI, pp. 89–91, October 15, 1972

For abstract, see Harper, L. H.

SCHULTZ, A. L.

S02 **Determination of Solid-Propellant Transient Regression Rates Using a Microwave Doppler Shift Technique**

L. D. Strand, A. L. Schultz, and G. K. Reedy

Technical Report 32-1569, October 15, 1972

For abstract, see Strand, L. D.

SEELEY, L. N.

S03 **Mariner Mars 1971 Television Picture Catalog: Sequence Design and Picture Coverage**

P. E. Koskela, M. R. Helton, L. N. Seeley, and S. J. Zawacki

Technical Memorandum 33-585, Vol. II, December 15, 1972

For abstract, see Koskela, P. E.

SEIDEL, B. L.

S04 **DSN Progress Report for September–October 1972: Improved RF Calibration Techniques: Commercial Precision IF Attenuator Evaluation**

C. Stelzried, B. L. Seidel, M. Franco, and D. Acheson

Technical Report 32-1526, Vol. XII, pp. 74–82, December 15, 1972

For abstract, see Stelzried, C.

S05 **Bistatic Radar Measurements of the Surface of Mars With Mariner 1969**

G. Fjeldbo, A. J. Kliore, and B. L. Seidel

Icarus, Vol. 16, No. 3, pp. 502–508, June 1972

For abstract, see Fjeldbo, G.

SHIRLEY, D. L.

S06 Mariner Venus–Mercury 1973 Encounter Strategy

D. L. Shirley

AIAA Preprint 72-942, AIAA (American Institute of Aeronautics and Astronautics)/AAS (American Astronautical Society) Astrodynamics Conference, Palo Alto, California, September 11–12, 1972

This paper describes the selection of launch and arrival conditions and Venus and Mercury encounter aiming zones to maximize the science return from the Mariner Venus–Mercury mission. A single Mariner spacecraft will be launched in November 1973, fly by Venus in early February 1974, and encounter Mercury (the primary target) in late March 1974. Mercury aiming points will provide: (a) Sun and Earth occultation, (b) 1000-km periapsis altitude, and (c) return to Mercury after 176 days (two Mercury years). The selected Mercury arrival dates allow high-contrast television imaging. Aiming points at Venus allow gravity assist to Mercury and also permit Earth occultation.

SHUMATE, M. S.

S07 3-D Multilateration: A Precision Geodetic Measurement System

P. R. Escobal, H. F. Fliegel, R. M. Jaffe, P. M. Muller, K. M. Ong, O. H. von Roos, and M. S. Shumate

JPL Quarterly Technical Review, Vol. 2, No. 3, pp. 1–11, October 1972

For abstract, see Escobal, P. R.

SIEGMETH, A. J.

S08 DSN Progress Report for July–August 1972: Pioneers 6–9 Mission Support

A. J. Siegmeth

Technical Report 32-1526, Vol. XI, pp. 12–13, October 15, 1972

During July and August 1972, the DSN supported a radial experiment requiring simultaneous signals of Pioneers 9 and 10. The Pioneer principal investigators plan to establish the distribution of

fields and particle gradients. The DSN demonstrated a Mark III-system-type station software which can transmit Pioneers 6,7,8, and 9 telemetry data by high-speed data lines.

S09 **DSN Progress Report for July–August 1972: Pioneers 10 and G Mission Support**

A. J. Siegmeth

Technical Report 32-1526, Vol. XI, pp. 14–18, October 15, 1972

The DSN has already completed 6 months of continuous telemetry data acquisition, command, and radio metric tracking support for Pioneer 10, which was launched on March 4, 1972. The Pioneer 10 spacecraft, on the way to the giant planet Jupiter, crossed the orbit of Mars during the first part of May and entered the asteroid belt in the middle of July 1972. This article presents a summary of extended-mission support capabilities.

S10 **DSN Progress Report for July–August 1972: Pioneer Venus Mission Support**

A. J. Siegmeth

Technical Report 32-1526, Vol. XI, pp. 23–25, October 15, 1972

This article presents a summary of the history of the Pioneer Venus missions, as well as the characteristics of the 1976/1977 probe missions. The Pioneer Project is investigating a preliminary plan to develop a cooperative agreement on the Venus Orbiter mission with the European Space Research Organization.

SILVER, R. H.

S11 **Long-Term Aging of Elastomers: Chemorheology of Viton B Fluorocarbon Elastomer**

S. H. Kalfayan, R. H. Silver, A. A. Mazzeo, and S. T. Liu

JPL Quarterly Technical Review, Vol. 2, No. 3, pp. 32–39, October 1972

For abstract, see Kalfayan, S. H.

SIMMONDS, P. G.

S12 **Novel Type of Hydrogenator**

P. G. Simmonds and C. F. Smith

Anal. Chem., Vol. 44, No. 8, pp. 1548–1550, July 1972

This article describes the investigation of a palladium–silver tube as a catalytic reactor for the vapor phase hydrogenation of unsaturated carbon–carbon bonds in a variety of organic compounds. The device is simple to construct from an appropriate length of palladium–silver tubing and may be used for both continuous and batch hydrogenations. Furthermore, in contrast to other hydrogenation techniques, the palladium-tube device does not cause hydrogenolysis of sensitive aldehyde groups.

SJOGREN, W. L.

S13 Apollo 15 Gravity Analysis From the S-Band Transponder Experiment

W. L. Sjogren, P. M. Muller, and
W. R. Wollenhaupt (Manned Spaceflight Center)

Proceedings of the Conference on Lunar Geophysics, Lunar Science Institute, Houston, Texas, October 18–21, 1971, pp. 411–418

The S-band transponder experiment used precision doppler tracking data of the command and service module, the lunar module and the subsatellite to provide detailed information about the near-side lunar gravity field. No special instruments are required other than the existing S-band transponder used for real-time navigation. The data consists of variations in the spacecraft speed as measured by the Earth-based radio tracking system, which has a resolution of 0.65 mm/s.

Initial data reduction, which has been concentrated on the low altitude (≈20 km) command and service module data, provides new detailed gravity profiles of the Serenitatis and Crisium mascons. The results are in good agreement with Apollo 14 analysis and strongly suggest that the mascons are near-surface features with a mass distribution per unit area of approximately 800 kg/cm^2. The Apennines reveal themselves as a local gravity high of 85 mgal and Marius Hills likewise have a gravity high of 62 mgal.

The subsatellite data is too sparse at present to definitely determine new gravity-anomaly locations. The spacecraft is functioning well and a dense data block is being obtained, which will provide a new gravity map from ±95° longitude to ±30° latitude. Since periapsis altitudes are relatively close to predicted altitudes, it seems fairly safe at this point to believe the subsatellite lifetime will be at least one yr.

SLADE, M. A.

S14 DSN Progress Report for September–October 1972: Very Long Baseline Interferometry (VLBI) Possibilities for Lunar Study

M. A. Slade, P. F. MacDoran, and J. B. Thomas

Technical Report 32-1526, Vol. XII, pp. 35–39, December 15, 1972

The availability of several channels for transmissions from the lunar surface and lunar-orbiting vehicles presents opportunities for demonstrating the utility of radio-interferometric tracking. The expected accuracy of such very-long-baseline-interferometry (VLBI) tracking is expected to be equivalent to 50 cm (transverse to the line of sight) at the moon's distance, affording significant opportunities for studies of lunar dynamics and selenodesy. In addition to direct applicability to lunar study, VLBI tracking of these several lunar-based signals provides an opportunity to evaluate simultaneous multiprobe tracking techniques which could significantly enhance the Viking 1975 and Pioneer Venus 1977 missions, where multiprobe tracking is imperative.

SMITH, C. F.

S15 Novel Type of Hydrogenator

P. G. Simmonds and C. F. Smith

Anal. Chem., Vol. 44, No. 8, pp. 1548–1550, July 1972

For abstract, see Simmonds, P. G.

SMITH, R. H.

S16 DSN Progress Report for September–October 1972: Dual Carrier

R. H. Smith

Technical Report 32-1526, Vol. XII, pp. 200–204, December 15, 1972

Two simultaneous (dual) uplink carriers from a single DSN 64-m-diameter antenna site are required to support the Viking 1975 project. A prototype dual-carrier exciter has been built and tested. The dual-carrier exciter amplifies and combines two standard DSN exciter signals, which are used to drive a high-power klystron operating in a linear mode (10% of normal power). The measured intermodulation products were at least 20 dB below the carrier's power.

SOHA, J. M.

S17 **An Orthographic Photomap of the South Pole of Mars From Mariners 6 and 7**

A. R. Gillespie and J. M. Soha

Icarus, Vol. 16, No. 3, pp. 522–527, June 1972

For abstract, see Gillespie, A. R.

STELZRIED, C.

S18 **DSN Progress Report for September–October 1972: Improved RF Calibration Techniques: Commercial Precision IF Attenuator Evaluation**

C. Stelzried, B. L. Seidel, M. Franco, and D. Acheson

Technical Report 32-1526, Vol. XII, pp. 74–82, December 15, 1972

The intermediate frequency (IF) attenuator normally used for system-noise temperature calibrations is the largest single contributor to measurement inaccuracy. Various IF attenuators have been evaluated and calibrated using a National Bureau of Standards IF precision standard. This article describes the measurement techniques used and presents measurement results. It is noted that there is a wide spread in accuracy among various manufacturers and also in the same model type from a particular manufacturer. Excessive use appears to be an important factor in accuracy degradation.

STELZRIED, C. T.

S19 **Jupiter: New Evidence of Long-Term Variations of Its Decimeter Flux Density**

M. J. Klein, S. Gulkis, and C. T. Stelzried

Astrophys. J., Vol. 176, No. 2, Pt. 2, pp. L85–L88, September 1, 1972

For abstract, see Klein, M. J.

STIRN, R. J.

S20 **Comment on "Temperature Dependence of Hole Velocity in p GaAs"**

R. J. Stirn

J. Appl. Phys., Vol. 43, No. 5, pp. 2484–2485, May 1972

A comparison of magnetoresistance mobility values and their temperature dependence with theoretical values of the conductivity mobility was made in a recent publication. In this article, reasons are discussed as to why such a comparison is unwarranted, particularly when multiple-carrier conduction is present.

STRAND, L. D.

S21 Determination of Solid-Propellant Transient Regression Rates Using a Microwave Doppler Shift Technique

L. D. Strand, A. L. Schultz, and G. K. Reedy

Technical Report 32-1569, October 15, 1972

A microwave doppler-shift system, with increased resolution over earlier microwave techniques, was developed for the purpose of measuring the regression rates of solid propellants during rapid pressure transients (10^4–10^5 N/cm^2-s). A continuous microwave beam is transmitted to the base of a burning propellant sample cast in a metal waveguide tube. A portion of the wave is reflected from the regressing propellant–flame-zone interface. The phase-angle difference between the incident and reflected signals and its time differential are continuously measured using a high-resolution microwave network analyzer and related instrumentation. The apparent propellant regression rate is directly proportional to this latter differential measurement.

Experiments were conducted to verify the (1) spatial and time resolution of the system, (2) effect of propellant surface irregularities and compressibility on the measurements, and (3) accuracy of the system for quasi-steady-state regression-rate measurements. The microwave system was also used in two different transient combustion experiments: in a rapid-depressurization bomb, and in the high-frequency acoustic pressure environment of a T-burner. Polyether-polyurethane, hydroxy-terminated polybutadiene, and carboxyl-terminated polybutadiene/ammonium perchlorate composite propellants were tested.

In the rapid-depressurization tests the measured apparent regression rates generally fell near or below the steady-state rate at the corresponding pressure and exhibited oscillations in tests near the critical depressurization rates for extinguishment. The results seem to reinforce the description of rapid-depressurization extinction presented by Steinz and Selzer. Comparisons with the only other known transient data, that of Yin and Hermance, yielded both points of agreement and disagreement.

Unreasonably high oscillatory regression rates were obtained in the T-burner experiments. A set of parametric calculations were carried out, the results of which predict that flame-ionization effects could be of sufficient magnitude to account for these high-response results.

A direct comparison of the analytical predictions and experimental results yielded the conclusion that flame-ionization effects probably produced some errors in the absolute values, but not the general characteristics, of the rapid-depressurization regression-rate measurements.

S22 Dynamic Measurement of Bulk Modulus of Dielectric Materials Using a Microwave Phase Shift Technique

B. J. Barker and L. D. Strand

Technical Memorandum 33-577, November 15, 1972

For abstract, see Barker, B. J.

SWANSON, J.

S23 Accelerated Life Testing of Spacecraft Subsystems

D. Wiksten and J. Swanson

Technical Memorandum 33-575, November 1, 1972

For abstract, see Wiksten, D.

SZEJN, R. M.

S24 Theoretical Determination of Cesiated Work Functions

R. M. Szejn

Technical Memorandum 33-565, September 15, 1972

A computer program based on the theoretical work of Gyftopoulos, Steiner, and Levine on bimetallic systems and using a modified version of Wilkins' SIMCON subroutine SURFAS has been written for the UNIVAC 1108 computer. This program, WFGSL, accepts the operating conditions and the physical parameters pertinent to the substrate and adsorbate and outputs the field-free work function, electron current (Richardson equation), ion current (Saha equation), and fractional substrate coverage by the adsorbate. This memorandum presents a brief description of the theory together with a program description and listing. An application of the program to a bimetallic system of cesium (adsorbate) and rhenium (substrate) is also described.

TAHERZADEH, M.

T01 Neutron Radiation Characteristics of Plutonium Dioxide Fuel

M. Taherzadeh

Technical Report 32-1555, Rev. 1, December 1, 1972

This report considers in detail the major sources of neutrons from plutonium-dioxide nuclear fuel. These sources include spontaneous fission of several of the Pu isotopes, (α,n) reactions with low-Z impurities in the fuel, and (α,n) reactions with oxygen 18. For spontaneous fission neutrons, a value of $(1.95 \pm 0.07) \times 10^3$ n/s/g PuO_2 is obtained. The neutron yield from (α,n) reactions with oxygen is calculated by integrating the reaction-rate equation over all α-particle energies and all center-of-mass angles. The results indicate a neutron emission rate of $(1.42 \pm 0.32) \times 10^4$ n/s/g PuO_2.

The neutron yield from (α,n) reactions with low-Z impurities in the fuel is presented in tabular form for one part per million of each impurity. The total neutron yield due to the combined effects of all the impurities depends upon the fractional weight concentration of each impurity. The total neutron flux emitted from a particular fuel geometry is estimated by adding the neutron yield due to the induced fission to that of the other neutron sources.

T02 Neutron Radiation Characteristics of Plutonium Dioxide Fuel

M. Taherzadeh and P. J. Gingo (Akron State University)

Nucl. Technol., Vol. 15, No. 3, pp. 396–410, September 1972

The major sources of neutrons from plutonium-dioxide nuclear fuel are considered in detail. These sources include spontaneous fission of several of the plutonium isotopes, (α,n) reactions with low Z impurities in the fuel, and (α,n) reactions with oxygen 18. For spontaneous fission neutrons a value of $(1.95 \pm 0.07 \times 10^3$ n/s/g PuO_2 is used.

The neutron yield from (α,n) reactions with oxygen is calculated by integrating the reaction rate equation over all alpha-particle energies and all center-of-mass angles. The results indicate a neutron emission rate of $(1.14 \pm 0.26) \times 10^4$ n/s/g PuO_2.

The neutron yield from (α,n) reactions with low Z impurities in the fuel is presented in tabular form for 1 part per million of each impurity. The total neutron yield due to the combined effects of all the impurities depends on the fractional weight concentration of each impurity. The total neutron flux emitted from a particular fuel geometry is estimated by adding the neutron yield due to the induced fission to that of the other neutron sources.

TAYLOR, F. W.

T03 Temperature Sounding Experiments for the Jovian Planets

F. W. Taylor

J. Atmos. Sci., Vol. 29, No. 5, pp. 950–958, July 1972

The possibilities for vertical temperature sounding experiments by medium-resolution measurements of outgoing radiance are examined for non-scattering models of Jupiter, Saturn, Uranus, and Neptune. It is shown that for Jupiter the widest vertical coverage of the atmosphere results from five or six channels placed in the ν_4 band of methane at 7.5 μm, but energy constraints render this experiment marginal at Saturn and useless at Uranus and Neptune. For the outermost planets, the best experiment is three or four channels located in the long-wavelength half of the pressure-induced S(O) line of hydrogen in the range 25–40 μm with which a limited vertical range of about two scale heights can be covered. Some results of inversion of synthetic data are presented in each case, and the likely effect of clouds on the measurements is discussed.

T04 The Infrared Spectrum of Jupiter: Structure and Radiative Properties of the Clouds

F. W. Taylor and G. E. Hunt

Proceedings of the Conference on Atmospheric Radiation, Fort Collins, Colorado, August 7–9, 1972, pp. 100–102

The interpretation of ground-based observations of Jupiter in terms of the composition and structure of the atmosphere is greatly complicated by clouds and haze which appear to extensively cover the planet. Most observers and theoreticians have attempted to take account of absorption and scattering by clouds in their calculations by simple modeling, but it has been usual to ignore the horizontal and vertical inhomogeneous which are apparently present in the cloud structure. This is a serious shortcoming in models which are used to plan experiments to be carried by spacecraft, when high spatial resolution will be available.

No useful way to approximate the radiative transfer properties of the Jovian clouds at thermal infrared wavelengths has been proposed, except for the dangerous expedient of neglecting cloud effects entirely. As a result, thermal equilibrium models of the planet and temperature structure and composition determinations based on emission measurements will be in error by some unknown amount.

This paper describes a model for the Jovian clouds which is inhomogeneous both vertically and laterally and presents radiative

transfer calculations which include cloud effects to show that the model can account for the available observations at all wavelengths.

THOMAS, J. B.

T05 DSN Progress Report for September–October 1972: Very Long Baseline Interferometry (VLBI) Possibilities for Lunar Study

M. A. Slade, P. F. MacDoran, and J. B. Thomas

Technical Report 32-1526, Vol. XII, pp. 35–39, December 15, 1972

For abstract, see Slade, M. A.

TSAY, F.-D.

T06 Electron Paramagnetic Resonance of Radiation Damage in a Lunar Rock

F.-D. Tsay, S. I. Chan, and S. L. Manatt

Nature Phys. Sci., Vol. 237, No. 77, pp. 121–122, June 19, 1972

Although lunar material has been exposed to radiations from indigenous radioactive atoms, solar wind protons, and cosmic ray particles for a very long time, no electron paramagnetic resonance (EPR) signals attributable to natural radiation damage had been observed in the returned Apollo 11 and 12 samples. This article presents evidence of radiation-induced EPR signals in one of the lunar samples examined.

UCHIYAMA, A. A.

U01 Gravitational Effects on Electrochemical Batteries

R. E. Meredith (Oregon State University), G. L. Juvinall, and A. A. Uchiyama

Technical Report 32-1570, November 15, 1972

For abstract, see Meredith, R. E.

VON ROOS, O. H.

V01 DSN Progress Report for July–August 1972: An Evaluation of Charged Particle Calibration by a Two-Way Dual-Frequency Technique and Alternatives to This Technique

O. H. von Roos and B. D. Mulhall

Technical Report 32-1526, Vol. XI, pp. 42–52, October 15, 1972

This article discusses the accuracy of the three charged-particle calibration methods—differenced range versus integrated doppler, Faraday rotation, and dual frequency—as they apply to the various tracking modes, e.g., one-station tracking, two-station tracking, spacecraft very-long-baseline interferometry. It is found that many calibration schemes are deficient at small Sun–Earth–probe angles (SEPs). Observations of the Sun during its active period between 1967 and 1969 have been used to obtain quantitative information on range degradation at small SEPs. Likewise, range errors at small SEPs during a quiet Sun period (in this case the 1964–1965 solar minimum) have also been computed with the result that, even at times of a comparatively inactive Sun, range errors engendered by plasma clouds are still troublesome inasmuch as they prevent range measurement with an accuracy of less than 1 m.

V02 DSN Progress Report for July–August 1972: Derivation of a General Expression for Ionospheric Range Corrections Valid for Arbitrary Solar Zenith Angles, Azimuths, Elevation Angles and Station Locations

O. H. von Roos and K. W. Yip

Technical Report 32-1526, Vol. XI, pp. 53–61, October 15, 1972

A general expression is derived for the electron-density profile as a function of latitude and longitude for that part of the Earth which is in direct sunlight including dawn and dusk. This expression allows one to determine by standard means the range correction for arbitrary ray-path directions. It is also shown that the naive application of the Chapman ionosphere entails range-correction errors which for low elevation angles (<20 deg) and large solar zenith angles (>40 deg) cannot be tolerated. Numerical calculations are displayed showing the dependence of the range correction on the pertinent parameters.

V03 3-D Multilateration: A Precision Geodetic Measurement System

P. R. Escobal, H. F. Fliegel, R. M. Jaffe, P. M. Muller, K. M. Ong, O. H. von Roos, and M. S. Shumate

JPL Quarterly Technical Review, Vol. 2, No. 3, pp. 1–11, October 1972

For abstract, see Escobal, P. R.

WEETALL, H. H.

W01 Studies of Antigen–Antibody Interaction on Some Specific Solid Adsorbents Derived From Cellulose

N. Weliky and H. H. Weetall

Immunochemistry, Vol. 9, No. 10, pp. 967–978, October 1972

For abstract, see Weliky, N.

WELIKY, N.

W02 Studies of Antigen–Antibody Interaction on Some Specific Solid Adsorbents Derived From Cellulose

N. Weliky and H. H. Weetall

Immunochemistry, Vol. 9, No. 10, pp. 967–978, October 1972

Studies of the dissociation of complexes using specific insoluble complexing agents under specified conditions can yield information concerning the nature of the specific interactions contributing to complex formation. For the case of the interaction of specific antibody with antigen conjugates, data is obtained concerning heterogeneity of apparent equilibrium constants and the influence of antigen and immunoadsorbent structure on protein interaction and antigen–antibody dissociation. Such information can be useful for predicting conditions for antiserum purification or antibody recovery.

For the case of the cellulose adsorbents chosen, it was found that (1) the adsorbent may contribute strongly to the interaction of ionizable haptens with antibody, with a pH dependency typical of acid catalyzed reactions, (2) immunoadsorbent properties can be modified through physical and chemical structural changes, (3) the dissociation of antibody from the haptenic and protein immunoadsorbents showed no significant discontinuities in the acid range, and (4) antibodies to those haptens chosen which do not ionize in the acid range, do not dissociate appreciably from the immunoadsorbent in the acid range but do at sufficiently high pH.

WIEBE, E.

W03 DSN Progress Report for July–August 1972: Low Noise Receivers: Microwave Maser Development

R. Clauss, E. Wiebe, and R. Quinn

Technical Report 32-1526, Vol. XI, pp. 71–80, October 15, 1972

For abstract, see Clauss, R.

WIGGINS, C. P.

W04 DSN Progress Report for September–October 1972: X-Band Radar Development

C. P. Wiggins

Technical Report 32-1526, Vol. XII, pp. 19–21, December 15, 1972

A high-power X-band radar is under development for use on the 64-m-diameter antenna at the Mars Deep Space Station (DSS 14). The 400-kW transmitter will operate at 8.495 GHz. Ground testing of portions of the transmitter will start in early 1973.

WIKSTEN, D.

W05 Accelerated Life Testing of Spacecraft Subsystems

D. Wiksten and J. Swanson

Technical Memorandum 33-575, November 1, 1972

This memorandum presents the results of a study performed to establish the rationale and requirements for conducting accelerated life tests on electronic subsystems of spacecraft. A method for applying data on the reliability and temperature sensitivity of the parts contained in a subsystem to the selection of accelerated life-test parameters is described. Additional considerations affecting the formulation of test requirements are identified, and practical limitations of accelerated aging are described.

WINKELSTEIN, R.

W06 DSN Progress Report for September–October 1972: Complex Mixer Error Analysis

R. Winkelstein

Technical Report 32-1526, Vol. XII, pp. 47–50, December 15, 1972

The complex mixer is composed of two channels. One channel contains the signal mixed with the sine of the reference frequency and the other contains the signal mixed with the cosine of the reference frequency. Errors unique to this system are gain and phase shifts of one channel with respect to the other. When the power spectrum of the mixer's output, considered a complex quantity, is calculated, these errors produce an unwanted image response to each signal component in the true spectrum. This analysis was carried out to ensure that hardware specifications were sufficient to limit these image responses to tolerable levels. Calculations for various gain and phase errors show that image responses in the power spectrum for prototype hardware will be limited to less than 1% of the true signal components.

WOLLENHAUPT, W. R.

W07 Apollo 15 Gravity Analysis From the S-Band Transponder Experiment

W. L. Sjogren, P. M. Muller, and W. R. Wollenhaupt (Manned Spaceflight Center)

Proceedings of the Conference on Lunar Geophysics, Lunar Science Institute, Houston, Texas; October 18–21, 1971, pp. 411–418

For abstract, see Sjogren, W. L.

WONG, S. K.

W08 Geocentric Gravitational Constant Determined From Mariner 9 Radio Tracking Data

P. B. Esposito and S. K. Wong

Preprint of paper presented at International Symposium on Earth Gravity Models and Related Problems (Sponsored by the American Geophysical Union, NASA), St. Louis, Missouri, August 16–18, 1972

For abstract, see Esposito, P. B.

YAMAKAWA, K. A.

Y01 Radiation Effects on Three Low-Power Microcircuits

K. A. Yamakawa

Technical Memorandum 33-576, November 15, 1972

This memorandum gives the results of irradiating several low-power circuit elements with cobalt-60 gamma radiation, low-energy (1.5-MeV) and high-energy (28- to 85-MeV) electrons, and neutrons. The bipolar circuits used were an SE480Q NAND gate and a micropower frequency divider used in electronic wristwatches that is designated ICB-9002. The metal-oxide-semiconductor device used was a dual p-channel metal-oxide semiconductor-field-effect transistor designated 2N4067.

YIP, K. W.

Y02 DSN Progress Report for July–August 1972: Derivation of a General Expression for Ionospheric Range Corrections Valid for Arbitrary Solar Zenith Angles, Azimuths, Elevation Angles and Station Locations

O. H. von Roos and K. W. Yip

Technical Report 32-1526, Vol. XI, pp. 53–61, October 15, 1972

For abstract, see von Roos, O. H.

YOUNGER, H. C.

Y03 DSN Progress Report for September–October 1972: DSS Receiving System Saturation at High Signal Levels

H. C. Younger

Technical Report 32-1526, Vol. XII, pp. 220–225, December 15, 1972

A loss of telemetry data from the Lunar Module occurred at the Mars Deep Space Station (DSS 14) during the Apollo 16 mission. This was caused by saturation of the first mixer in the DSS 14 receiving system by a very strong Command Module signal. Tests have been conducted to determine the saturation characteristics of the major components of the deep space station receiving system. The problem will be avoided during the Apollo 17 mission by using a lower-gain maser as prime maser, and by adding a pad following the high-gain backup maser.

ZAWACKI, S. J.

Z01 Mariner Mars 1971 Television Picture Catalog: Sequence Design and Picture Coverage

P. E. Koskela, M. R. Helton, L. N. Seeley, and S. J. Zawacki

Technical Memorandum 33-585, Vol. II, December 15, 1972

For abstract, see Koskela, P. E.

ZUNDEL, E. F.

Z02 DSN Progress Report for July–August 1972: High-Reliability Microcircuit Procurement in the DSN

E. F. Zundel

Technical Report 32-1526, Vol. XI, pp. 121–123, October 15, 1972

This article discusses the implementation of microelectronic circuits in the DSN together with utilization of an equivalent MIL-STD-883 Class B device, screening tests to be used, and screening philosophy relative to failure-mechanism patterns. The expected costs and the advantages of standardization of device types to increase quantity buys are also discussed.

Subject Index

Subject Categories

Acoustics
Antennas and Transmission Lines
Apollo Project
Atmospheric Entry

Biology

Chemistry
Comets
Computer Applications and Equipment
Computer Programs
Control and Guidance

Earth Atmosphere
Earth Interior
Earth Surface
Electricity and Magnetism
Electronic Components and Circuits
Energy Storage
Environmental Sciences

Facility Engineering
Fluid Mechanics

Helios Project

Industrial Processes and Equipment
Information Distribution and Display
Information Theory
Interplanetary Exploration, Advanced

Lunar Interior
Lunar Surface

Management Systems
Mariner Mars 1969 Project
Mariner Mars 1971 Project
Mariner Venus-Mercury 1973 Project
Masers and Lasers
Materials, Nonmetallic
Mathematical Sciences
Mechanics
Mechanisms

Optics
Orbits and Trajectories

Packaging and Cabling
Particle Physics
Photography
Pioneer Project
Planetary Atmospheres
Planetary Exploration, Advanced
Planetary Surfaces
Plasma Physics
Power Sources
Propulsion, Electric
Propulsion, Liquid
Propulsion, Solid

Quality Assurance and Reliability

Radar
Radio Astronomy
Relativity

Safety Engineering
Scientific Instruments
Soil Sciences
Solar Phenomena
Solid-State Physics
Spectrometry
Standards, Reference
Sterilization
Structural Engineering

Telemetry and Command
Temperature Control
Test Facilities and Equipment
Thermoelectric Outer-Planet Spacecraft (TOPS)
Tracking

Viking Project

Wave Propagation

Subjects

Subject **Entry**

Acoustics
effect on supersonic jet noise of nozzle plenum-pressure fluctuations ... K09

Antennas and Transmission Lines
X-band waveguide components ... B13
DSN precision antenna gain measurements ... G09
J01
PARADES: computer program for structural design of antennas ... L09
iterative design of antenna structures ... L10
testing of 64-m-diameter antenna servo ... L13
brush electroplating of bearing journal on antenna master equatorial shaft ... M13
antenna shaft lubrication ... M14
coaxial switch evaluation ... N01
microwave leakage through perforated flat plates ... O04
64-m-diameter antenna hydrostatic-bearing-runner leveling ... P03
system operating noise temperature calibrations of feed cones ... R04

Apollo Project
analysis of lunar gravity from Apollo 15 radio metric data ... S13
electron paramagnetic resonance of radiation damage in Apollo 11 and 12 lunar rock samples ... T06
loss of telemetry data during Apollo 16 mission due to saturation of DSN system component ... Y03

Subject	Entry
Atmospheric Entry	
JPL carbon–carbon refractory composites for use in entry shells	R08
Biology	
antigen–antibody interaction on specific solid adsorbents derived from cellulose	W02
Chemistry	
rapid determination of amino acids by gas chromatography	H02
hydrogen-atom scrambling in ion–molecule reactions of methane and ethylene	H11
long-term aging of elastomers	K01
molecular theory of elastomer deformation and rupture	L03
newly-designed hydrogenator	S12
antigen–antibody interaction on specific solid adsorbents derived from cellulose	W02
Comets	
proposed solar-electric spacecraft mission to Comet Encke	G01 G02
Computer Applications and Equipment	
bright-field electron microscope with heavy/light atom-discrimination using computer	F10
solar-electric spacecraft on-board computer	G01
computer image-processing techniques used to make orthographic photomap of Martian south pole from Mariner Mars 1969 photographs	G06
use of interactive graphics with NASA structural analysis system (NASTRAN)	K02
computer program for evaluation of computers	K05
multicomputer communications system	L05
computer fault-diagnosis algorithms	M07
JPL digital image-processing development	O01
Computer Programs	
programs for prediction of Mariner 9 propulsion subsystem performance	E07
program for solution of eigenvalue problems by Sturm sequence method	G14
program for evaluation of computers	K05
PARADES: computer program for structural design of antennas	L09
software techniques for high-speed data communication	L15
computer fault-diagnosis algorithms	M07
program for theoretical determination of cesiated work functions	S24

Subject	Entry
Control and Guidance	
solar-electric spacecraft control and guidance	G01, G02
solar radiation pressure on Mariner 9 spacecraft	G05
Thermoelectric Outer-Planet Spacecraft (TOPS) attitude propulsion technology	M17
Earth Atmosphere	
statistical predictions of effect of weather on spacecraft telecommunications link	R02
DSN performance in severe weather	R03
derivation of general expression for ionospheric range corrections	V02
Earth Interior	
Earth-gravity constant determined from Mariner 9 radio metric data	E06
Earth Surface	
use of laser tracking of satellites for precision measurements of Earth surface and possible earthquake prediction	E05
Electricity and Magnetism	
lunar conductivity profile and nonuniqueness of electromagnetic data inversion	P04
Electronic Components and Circuits	
two-station interferometer analog input channel	A03
automatic through-insulation welding of microelectronic interconnections	A05
complex mixer system	C07
dual-ignitron crowbar	F03
wideband distribution amplifier for coherent reference generator	F08
solar-electric spacecraft electronics	G01, G02
derivation of optimum noncoherent receiver for noisy signal with unknown doppler shift	H08
Mariner Mars 1971 radio frequency subsystem	H09
digital frequency shifter	M01
coaxial switch evaluation	N01
dual uplink carriers for support of Viking spacecraft	S16
evaluation of commercial IF attenuators	S18
accelerated life testing of spacecraft electronic subsystems	W05
study of radiation effects on low-power microcircuits	Y01
alterations to DSN masers to prevent saturation	Y03
DSN high-reliability microcircuit procurement	Z02

Subject	Entry
Energy Storage	
cycle-life studies of heat-sterilized silver-oxide-zinc batteries	A04
gravitational effects on electrochemical batteries	M16
Environmental Sciences	
photovoltaic solar-generator technology for terrestrial use	B06
use of laser tracking of satellites for precision measurements of Earth surface and possible earthquake prediction	E05
effect on supersonic jet noise of nozzle plenum-pressure fluctuations	K09
Facility Engineering	
dual-carrier preparations for Viking 1975 mission	B04
upgrading of deep space stations	G09, J01
Ground Communications Facility functional design for 1973–1974	M10
64-m-diameter antenna hydrostatic-bearing-runner leveling	P03
Fluid Mechanics	
influence of contraction-section shape and inlet flow-direction on supersonic-nozzle flow and performance	B01
effect on supersonic jet noise of nozzle plenum-pressure fluctuations	K09
Helios Project	
DSN support	G08
Industrial Processes and Equipment	
automatic through-insulation welding of microelectronic interconnections	A05
brush electroplating of bearing journal on antenna master equatorial shaft	M13
Information Distribution and Display	
use of interactive graphics with NASA structural analysis system (NASTRAN)	K02
multicomputer communications system	L05
software techniques for high-speed data communication	L15
Ground Communications Facility functional design for 1973–1974	M10
Information Theory	
decoding of Golay code	B05
reduction in complexity of calculating syndromes for error-correcting codes	H03
efficient generation of statistically good pseudonoise by linearly interconnected shift registers	H12

Subject	Entry
analysis of effect of noisy carrier reference on sequential decoding	L04
algorithm for optimum frame sync acquisition for biorthogonally coded telemetry	L08
improved method for calculating weights modulo 8 in a binary cyclic code	M11
weight enumerators of quadratic residue codes	M25
analysis of radio metric data processing techniques	R11
Interplanetary Exploration, Advanced	
proposed solar-electric spacecraft mission to Comet Encke	G01 G02
Lunar Interior	
lunar conductivity profile and nonuniqueness of electromagnetic data inversion	P04
analysis of lunar gravity from Apollo 15 radio metric data	S13
Lunar Surface	
tracking by long baseline interferometry for study of Moon	S14
electron paramagnetic resonance of radiation damage in Apollo 11 and 12 lunar rock samples	T06
Management Systems	
DSN organization	A02 E01 R05 R06
DSN inventory policy	E02
DSN Network Control System	H01
Mariner Mars 1969 Project	
Mariner 6 and 7 bistatic radar measurements of Martian surface	F04
Mariner 6 and 7 photographs used for orthographic photomap of Martian south pole	G06
Mariner Mars 1971 Project	
Earth-gravity constant determined from Mariner 9 radio metric data	E06
development and performance of Mariner 9 propulsion subsystem	E07
development and testing of ultraviolet spectrometer	F01
solar radiation pressure on Mariner 9 spacecraft	G05
radio frequency subsystem	H09
Mariner 9 television picture data	K08
Mariner Venus-Mercury 1973 Project	
DSN support	D02

Subject	Entry
encounter strategy	S06
Masers and Lasers	
microwave maser development	C04
new hydrogen source for maser	E04
use of laser tracking of satellites for precision measurements of Earth surface and possible earthquake prediction	E05
detonation of explosives by laser	H04
alterations to DSN masers to prevent saturation	Y03
Materials, Nonmetallic	
long-term aging of elastomers	K01
extensional flow of bulk polymers	P01
stored-energy function of rubberlike materials derived from experimental tensile data	P02
JPL carbon–carbon refractory composites	R08
estimation of Weibull parameters for structural fiber-composite materials	R09
Mathematical Sciences	
decoding of Golay code	B05
partial-step algorithm for nonlinear estimation problem	B10
mathematical model of solar light pressure used to compute forces acting on Mariner 9 spacecraft	G05
dynamic response analysis of geometrically nonlinear structures subjected to high impact	G13
solution of eigenvalue problems by Sturm sequence method	G14
reduction in complexity of calculating syndromes for error-correcting codes	H03
efficient generation of statistically good pseudonoise by linearly interconnected shift registers	H12
analysis of effect of noisy carrier reference on sequential decoding	L04
analysis of signal-to-noise ratio estimator	L06
exact closed-form expression for power spectrum of biphase-modulated squarewave carrier	L07
algorithm for optimum frame sync acquisition for biorthogonally coded telemetry	L08
equations of motion for rigid bodies in tree topology	L11
computer fault-diagnosis algorithms	M07
improved method for calculating weights modulo 8 in a binary cyclic code	M11
weight enumerators of quadratic residue codes	M25
spectral factorization in periodically time-varying systems and application to navigational tracking problems	N02

Subject	Entry
estimation of Weibull parameters for structural fiber-composite materials	R09
algorithm for synthesizing mass and stiffness matrices from experimental vibration modes	R10
analysis of radio metric data processing techniques	R11
derivation of general expression for ionospheric range corrections	V02
error analysis for complex mixer	W06
Mechanics	
dynamic response analysis of geometrically nonlinear structures subjected to high impact	G13
solution of eigenvalue problems by Sturm sequence method	G14
large-deformation modal-coordinates for nonrigid-vehicle dynamics	L11
algorithm for synthesizing mass and stiffness matrices from experimental vibration modes	R10
Mechanisms	
solar-electric spacecraft mechanisms	G01 G02
Optics	
rational approximation for Voigt line profile	H05
Orbits and Trajectories	
partial-step algorithm for nonlinear estimation problem used in determining orbits	B10
comparison of Cowell's method and a variation-of-parameters method for computation of precision satellite orbits	D01
Pioneer 10 maneuver strategy	F11
solar-electric spacecraft low-thrust navigation	G01 G02
spectral factorization in periodically time-varying systems and application to navigational tracking problems	N02
Mariner Venus-Mercury 1973 encounter strategy	S06
Packaging and Cabling	
solar-electric spacecraft packaging and cabling	G01 G02
Particle Physics	
quantum crystals in the single-particle picture	C02
Cerenkov and transition radiation in space-time periodic media	E03
bright-field electron microscope with heavy/light atom-discrimination using computer	F10

Subject	Entry
nature of two-particle correlations in atoms	G03
neutron radiation characteristics of plutonium dioxide fuel	T01 T02
electron paramagnetic resonance of radiation damage in Apollo 11 and 12 lunar rock samples	T06
Photography	
computer image-processing techniques used to make orthographic photomap of Martian south pole from Mariner Mars 1969 photographs	G06
Mariner 9 television picture data	K08
JPL digital image-processing development	O01
Pioneer Project	
Pioneer 10 maneuver strategy	F11
DSN support	S08 S09 S10
Planetary Atmospheres	
measurements of Jupiter RF radiation	K04
mechanism for equatorial acceleration of Jupiter	M08
temperature-sounding experiments for outer-planet spacecraft	T03
model for clouds of Jupiter	T04
Planetary Exploration, Advanced	
temperature-sounding experiments for outer-planet spacecraft	T03
Planetary Surfaces	
Mariner 6 and 7 bistatic radar measurements of Martian surface	F04
orthographic photomap of Martian south pole	G06
Mariner 9 television picture data	K08
Plasma Physics	
Cerenkov and transition radiation in space-time periodic media	E03
Power Sources	
photovoltaic solar-generator technology for terrestrial use	B06
lithium-doped radiation-resistant solar cells	B07
xenon-filled germanium thermoelectric generators	D03
solar-electric spacecraft power subsystem	G01 G02
solar cell standardization tests on high-altitude balloons	G11
algorithm for synthesizing mass and stiffness matrices from experimental vibration modes for rollup solar array	R10
neutron radiation characteristics of plutonium dioxide fuel	T01 T02

Subject	Entry
Propulsion, Electric	
solar-electric propulsion system integration technology	G01, G02
solar-electric spacecraft low-thrust navigation	G01, G02
Propulsion, Liquid	
development and performance of Mariner 9 propulsion subsystem	E07
Thermoelectric Outer-Planet Spacecraft (TOPS) trajectory-correction propulsion subsystem	L16
JPL carbon-carbon refractory composites for use in rocket motors	R08
Propulsion, Solid	
dynamic measurement of bulk modulus of dielectric materials such as solid propellants using a microwave phase-shift technique	B03
detonation of explosives by laser	H04
JPL carbon-carbon refractory composites for use in rocket motors	R08
determination of solid-propellant transient-regression rates using microwave doppler-shift technique	S21
Quality Assurance and Reliability	
cycle-life studies of heat-sterilized silver-oxide-zinc batteries	A04
solar-electric spacecraft redundant systems	G02
accelerated life testing of spacecraft electronic subsystems	W05
study of radiation effects on low-power microcircuits	Y01
DSN high-reliability microcircuit procurement	Z02
Radar	
Mariner 6 and 7 bistatic radar measurements of Martian surface	F04
DSN planetary radar experiments	G09, J01
lunar-radar clock synchronization	H07
combined radar-radiometer with variable polarization	M05
X-band radar development	W04
Radio Astronomy	
DSN radio science support	G09, J01, L12
measurements of Jupiter RF radiation	K04

Subject	Entry
Relativity	
Cerenkov and transition radiation in space-time periodic media	E03
Safety Engineering	
microwave leakage through perforated flat plates	O04
Scientific Instruments	
development and testing of Mariner Mars 1971 ultraviolet spectrometer	F01
bright-field electron microscope with heavy/light atom-discrimination using computer	F10
combined radar–radiometer with variable polarization	M05
Soil Sciences	
interference effects in microwave emission from geological materials	B09
electron paramagnetic resonance of radiation damage in Apollo 11 and 12 lunar rock samples	T06
Solar Phenomena	
solar radiation pressure on Mariner 9 spacecraft	G05
Solid-State Physics	
quantum crystals in the single-particle picture	C02
molecular theory of elastomer deformation and rupture	L03
extensional flow of bulk polymers	P01
stored-energy function of rubberlike materials derived from experimental tensile data	P02
estimation of Weibull parameters for structural fiber-composite materials	R09
algorithm for synthesizing mass and stiffness matrices from experimental vibration modes	R10
temperature dependence of hole velocity in p GaAs	S20
theoretical determination of cesiated work functions	S24
electron paramagnetic resonance of radiation damage in Apollo 11 and 12 lunar rock samples	T06
Spectrometry	
development and testing of Mariner Mars 1971 ultraviolet spectrometer	F01
rational approximation for Voigt line profile	H05
Standards, Reference	
artificial satellite doppler data compared with optical determination of polar motion	F06
DSN clock synchronization transmissions	G09, J01
lunar-radar clock synchronization	H07
DSN clock synchronization by long baseline interferometry	H13

Subject	Entry
phase-stable low-phase-noise filters for reference signals	L19
error analysis for complex mixer	W06
Sterilization	
cycle-life studies of heat-sterilized silver-oxide–zinc batteries	A04
Structural Engineering	
dynamic response analysis of geometrically nonlinear structures subjected to high impact	G13
solution of eigenvalue problems by Sturm sequence method	G14
use of interactive graphics with NASA structural analysis system (NASTRAN)	K02
PARADES: computer program for structural design of antennas	L09
iterative design of antenna structures	L10
large-deformation modal-coordinates for nonrigid-vehicle dynamics	L11
estimation of Weibull parameters for structural fiber-composite materials	R09
algorithm for synthesizing mass and stiffness matrices from experimental vibration modes	R10
Telemetry and Command	
DSN functions and facilities	A02
	E01
	R05
	R06
decoding of Golay code	B05
DSN support of Mariner Venus–Mercury 1973 Project	D02
solar-electric spacecraft telemetry and command	G01
	G02
DSN support of Helios Project	G08
reduction in complexity of calculating syndromes for error-correcting codes	H03
analysis of effect of noisy carrier reference on sequential decoding	L04
algorithm for optimum frame sync acquisition for biorthogonally coded telemetry	L08
improved method for calculating weights modulo 8 in a binary cyclic code	M11
DSN support of Viking Project	M18
	M19
weight enumerators of quadratic residue codes	M25
DSN support of Pioneer Project	S08
	S09
	S10

Subject	Entry
alterations to DSN masers to prevent saturation	Y03
loss of telemetry data during Apollo 16 mission due to saturation of DSN system component	Y03
Temperature Control	
solar-electric spacecraft temperature control	G01, G02
Test Facilities and Equipment	
test equipment for dynamic measurement of bulk modulus of dielectric materials using a microwave phase-shift technique	B03
test waveguide for determination of microwave surface resistivity	C05
newly-designed hydrogenator	S12
apparatus for determination of solid-propellant transient-regression rates by microwave doppler-shift technique	S21
Thermoelectric Outer-Planet Spacecraft (TOPS)	
trajectory-correction propulsion subsystem	L16
spacecraft attitude propulsion technology	M17
Tracking	
DSN functions and facilities	A02, E01, R05, R06
two-station interferometer analog input channel	A03
DSN support of Mariner Venus–Mercury 1973 Project	D02
Earth-gravity constant determined from Mariner 9 radio metric data	E06
DSN support of Helios Project	G08
DSN support of Viking Project	M18, M19
spacecraft-attitude tracking by measurement of signal polarization	M22
spectral factorization in periodically time-varying systems and application to navigational tracking problems	N02
analysis of radio metric data processing techniques	R11
DSN support of Pioneer Project	S08, S09, S10
analysis of lunar gravity from Apollo 15 radio metric data	S13
tracking by long baseline interferometry for study of Moon	S14
evaluation of charged-particle calibration techniques	V01
derivation of general expression for ionospheric range corrections	V02

Subject	Entry
Viking Project	
dual-carrier preparations for Viking 1975 mission	B04
DSN support	M18, M19
dual uplink carriers for support of Viking spacecraft	S16
Wave Propagation	
interference effects in microwave emission from geological materials	B09
technique for determination of microwave surface resistivity	C05
Cerenkov and transition radiation in space-time periodic media	E03
derivation of optimum noncoherent receiver for noisy signal with unknown doppler shift	H08
efficient generation of statistically good pseudonoise by linearly interconnected shift registers	H12
analysis of effect of noisy carrier reference on sequential decoding	L04
analysis of signal-to-noise ratio estimator	L06
exact closed-form expression for power spectrum of biphase-modulated squarewave carrier	L07
PARADES: computer program for structural design of antennas	L09
microwave leakage through perforated flat plates	O04
statistical predictions of effect of weather on spacecraft telecommunications link	R02
DSN performance in severe weather	R03
error analysis for complex mixer	W06
alterations to DSN masers to prevent saturation	Y03
loss of telemetry data during Apollo 16 mission due to saturation of DSN system component	Y03

Publication Index

Technical Reports

Number	Entry
32-1555, Rev. 1	T01
32-1560	M17
32-1565	L11
32-1569	S21
32-1570	M16
32-1571	L16
32-1573	B06
32-1574	B07
32-1575	G11

DSN Progress Reports for July–October 1972 (Technical Report 32-1526, Vols. XI and XII)

JPL Technical Section	Entry
331 Communications Systems Research	A03
	B05
	C07
	E02
	H03
	H08
	H12
	H13
	K05

331 Communications Systems Research (contd) L04
L05
L08
L19
M11
M25
W06

332 DSIF Engineering K02
L09
L10
L13
M13
M14
P03

333 Communications Elements Research B04
C04
C05
E04
O04
R02
R03
R04
S18

335 R. F. Systems Development B04
B13
F03
F08
G09
J01
M01
N01
S16
W04

337 DSIF Operations L06

338 DSIF Digital Systems Development M10
Z02

391 Tracking and Orbit Determination F06
M22
R11
S14
V01
V02

392 Navigation and Mission Design D01

401 DSN Engineering and Operations Office A02

420 DSN Operations Office G08
L12
L15
M18
R05
R06
S08
S09
S10

421 Network Operations L07
Y03

430 DSN Systems Office D02
H01
M19

440 TDA Program Control Office L15

914 Science and Engineering Computing K02

915 Flight Applications Programming D01

Technical Memorandums

Number	Entry
33-544	A05
33-565	S24
33-567	M07
33-569	F01
33-570	M05
33-571	E01
33-573	H09
33-574	E07
33-575	W05
33-576	Y01
33-577	B03
33-578	H04
33-579	R08
33-580	R09

33-581 ..... A04
33-582 ..... G05
33-583, Vol. II G01
33-583, Vol. III G02
33-585, Vol. II K08

JPL Quarterly Technical Review, Vol. 2, No. 3

JPL Technical Division		Entry
330	Telecommunications	E05
340	Guidance and Control	D03
350	Applied Mechanics	R10
380	Propulsion	K01 P01
390	Mission Analysis	E05 F11

Open Literature Reporting

AIAA J. — **Entry**

Vol. 10, No. 5, pp. 675–679 ..... B10
Vol. 10, No. 7, pp. 946–948 ..... K09

AIAA/AAS Astrodynamics Conference, Palo Alto, California, September 11–12, 1972 — **Entry**

AIAA Preprint 72-942 ..... S06

Anal. Chem. — **Entry**

Vol. 44, No. 8, pp. 1497–1499 ..... H02
Vol. 44, No. 8, pp. 1548–1550 ..... S12

Astrophys. J. — **Entry**

Vol. 176, No. 2, Pt. 2, pp. L85–L88 ..... K04

Biophys. J. **Entry**

Vol. 12, No. 5, pp. 484–511 ..... F10

Icarus **Entry**

Vol. 16, No. 3, pp. 502–508 ..... F04

Vol. 16, No. 3, pp. 552–527 ..... G06

Vol. 17, No. 1, pp. 88–103 ..... P04

Immunochemistry **Entry**

Vol. 9, No. 10, pp. 967–978 ..... W02

International Symposium on Earth Gravity Models and Related Problems, St. Louis, Missouri, August 16–18, 1972 **Entry**

Preprint E06

Int. J. Numer. Methods Eng. **Entry**

Vol. 4, No. 2, pp. 163–174 ..... G13

Vol. 4, No. 3, pp. 379–404 ..... G14

J. Appl. Phys. **Entry**

Vol. 43, No. 5, pp. 2484–2485 ..... S20

Vol. 43, No. 7, pp. 3064–3067 ..... P02

Vol. 43, No. 9, pp. 3719–3723 ..... E03

J. Atmos. Sci. **Entry**

Vol. 29, No. 5, pp. 950–958 ..... T03

Vol. 29, No. 5, pp. 1007–1008 ..... M08

J. Chem. Phys. **Entry**

Vol. 56, No. 10, pp. 5111–5120 ..... H11

Vol. 57, No. 4, p. 1814 ..... G03

J. Geophys. Res. **Entry**

Vol. 77, No. 23, pp. 4366–4378 ..... B09

J. Opt. Soc. Am. **Entry**

Vol. 62, No. 6, pp. 827–828 ..... H05

J. Spacecraft Rockets **Entry**

Vol. 9, No. 6, pp. 420–427 ..... B01

Vol. 9, No. 7, pp. 540–546 ..... N02

Mechanical Behavior of Materials: Proceedings of the 1971 International Conference on Mechanical Behavior of Materials **Entry**

pp. 496–507 ..... L03

Nature Phys. Sci. **Entry**

Vol. 237, No. 77, pp. 121–122 ..... T06

Nucl. Technol. **Entry**

Vol. 15, No. 3, pp. 396–410 ..... T02

Phys. Rev., Pt. B: Solid State **Entry**

Vol. 6, No. 4, pp. 1081–1090 ..... C02

Proceedings of the Conference on Atmospheric Radiation, Fort Collins, Colorado, August 7–9, 1972 **Entry**

pp. 100–102 ..... T04

Proceedings of the Conference on Lunar Geophysics, Lunar Science Institute, Houston, Texas, October 18–21, 1971 **Entry**

pp. 411–418 ..... S13

Proc. IEEE **Entry**

Vol. 60, No. 5, pp. 552–557 ..... H07

Vol. 60, No. 7, pp. 821–828 ..... O01

NASA — JPL — Coml., L.A., Calif.